INVESTIGATIONS OF NON-COVALENT BONDING: SYNTHESIS-AIDED CALCULATIONS

By

Laura Kathryn Engerer

Dissertation
Submitted to the Faculty of the
Graduate School of Vanderbilt University
in partial fulfillment of the requirements
for the degree of

DOCTOR OF PHILOSOPHY
in
Chemistry

May, 2017

Nashville, Tennessee

Approved:	Date:
_____	_____
Timothy P. Hanusa, Ph.D., Chair	
_____	_____
Charles M. Lukehart, Ph.D.	
_____	_____
David W. Wright , Ph.D.	
_____	_____
D. Greg Walker, Ph.D.	

to God, with whom all things are possible

ACKNOWLEGEMENTS

This work would not have been possible without the financial support of Vanderbilt University, the National Science Foundation, and the Petroleum Research Fund–ACS. I also am indebted to Dr. Timothy Hanusa who has stuck with me and given me so much help through this whole process. Finally, thanks must be given to the Psychological & Counseling Center of Vanderbilt University who helped me get through my first two years of depression and quickly back on track to finishing this.

Critical to the completion of this document is my sister Carolyn whose editing skills, support, and encouragement to keep on track were more than any sister could hope for. Thanks also to my parents, other sister, friends and family who believed in me.

TABLE OF CONTENTS

LIST OF TABLES

LIST OF FIGURES

Chapter 4

LIST OF ABBREVIATIONS

Ae ..... Group 2 element, alkaline earth

Cp^*_2 ..... pentamethylcyclopentadienyl

Cp ..... cyclopentadienyl

Me ..... methyl group

tmeda ..... tetramethylethylenediamine

18-crown-6 ..... 1,4,7,10,13,16-hexaoxacyclooctadecane

thf ..... tetrahydrofuran

i-Pr ..... isopropyl

t-Bu ..... tertiary-butyl

Cp–M –Cp ..... metal ion bound to two cyclopentadienyl ligands

PES ..... potential energy surface

LUMO ..... lowest unoccupied molecular orbital

HOMO ..... highest occupied molecular orbital

CCDC ..... Cambridge Crystallographic Data Center

A´ ..... the substituted allyl: $[1,3\text{-}(SiMe_3)_2C_3H_3]$

A´´ ..... $[1,1´,3\text{-}(SiMe_3)_3C_3H_2]$

Pz ..... pyrazolyl

μ_{eff} ..... effective magnetic moment

VSEPR ..... Valence Shell Electron Pair Repulsion

SZ/DZ ..... single zeta/double zeta basis set

DZP /TZP ..... valence double zeta, triple zeta basis sets each + 1 polarization function

TZ2P ..... valence triple zeta basis set + 2 polarization functions

QZ4P ..... valence quadruple zeta basis set + 4 polarization functions

ZORA ..... Zeroth Order Regular Approximation

DFT ..... Density Functional Theory

HF ..... Hartree-Fock method

MP2..... Møller-Plesset 2nd order correction

MP3..... Møller-Plesset 3rd order correction

ADF.....Amsterdam Density Functional program package

M06, M06L.....Minnesota class of functionals

APF ..... Austin, Petersson, and Frisch functional

AIM.....Atoms In Molecules

CCSD(T) ..... Coupled Cluster Single Double (Triple)

BP86.....Becke's exchange functional with Perdew's correlation functional

BP86-D3 .....BP86 with dispersion correction by Grimme

PBE ..... The 1996 functional of Perdew, Burke and Ernzerhof

PBE-D3 ..... PBE with dispersion correction by Grimme

BLYP ..... Becke's exchange functional with correlation functional of Lee, Yang, and Parr

BLYP-D3 ..... BLYP with dispersion correction by Grimme

B3LYP .....a hybrid functional based on BLYP

B3LYP-D3 ..... B3LYP with dispersion correction by Grimme

CHAPTER 1

INTRODUCTION

This work contains three separate projects, for which Density Functional Theory (DFT) computations provide a unifying theme. Chapter 2 contains a modified version of a paper published in the *Journal of Organic Chemistry* in 2011 in the first section[1] and the follow-up work to the paper in the second section. Chapter 3 contains work performed with manganese allyls. Chapter 4 contains the computational study of the effect of dispersion-corrected functionals in delicate systems of the unusually bent group 2 metallocenes and of the group 14 metallocenes. This introduction will contain a general introduction to DFT along with a general summary of each chapter.

DFT calculations are used in all three chapters. Density functional theory is known for its low computational requirements relative to model accuracy. Like any theoretical model, it has its weaknesses and deficiencies. Therefore, a brief overview of the nature of this modeling method and shortcomings that likely affected the computations is presented here for better understanding of results in subsequent chapters.

Density Functional Theory proposes the existence of a functional that can be used to describe the chemical and physical properties of a system using its electron density. This approach gives a theoretically sound way to decrease the computational resources needed for a problem compared to high level methods of wave function theory; the computational demands of the latter increase far faster with the size of the system than do those of DFT methods (i.e., DFT scales as N^3 (N = the number of basis functions describing the atoms), whereas coupled cluster methods, for example, scale as N^6 or higher). However, this comes with the inherent problem that, although the exact functional has been proven to exist, it is

not completely known and so all calculations are completed with various approximations. The exact functional has four terms, of which three are known: kinetic energy, nucleus electron potential energy, and the electron–electron repulsion energy. The fourth term, the exchange-correlation functional, is approximated, as the electron exchange is known but the dynamic correlation has only ever been parameterized. Basis set functions for each atom are used to describe the electron density of the system. While the basis set functions are how each atom's orbitals are described, basis sets that only describe filled orbitals do not result in accurate calculations, and need additional descriptions of unfilled orbitals to model the system well. However, increasing basis sets with additional orbital functions this way also increases the computational resources needed exponentially. Therefore, various strategies are used to keep the computational cost down.

The size of the molecules used here in the dispersion and cation-π chapters are large enough that, with good basis sets for all the atoms, a geometry optimization calculation of the structure would take at least a week with the computational resources available. Thus, the normal practice was used of decreasing the quality of the basis sets and then performing more calculations with higher basis set quality, increasing the quality in each one. Other ways to reduce computational costs are various ways to selectively decrease basis set quality. The first, used in various inorganic and organometallic systems, is to keep a high-quality basis set on the central atoms and use smaller basis sets on the carbons and hydrogens of the ligands. This is normally justified by the fact that the central atoms usually have much more influence on the molecule's geometry than the outlying atoms. Another way to selectively decrease the computational burden is to use 'frozen cores'. This simplification uses the fact that the inner-shell electrons of an atom are less sensitive to

their environment than are the valence electrons. The error introduced by freezing the core orbitals (i.e., constraining them to remain doubly-occupied in all configurations) is nearly constant for molecules containing the same types of atoms. ADF retains the basic core structure when frozen, but the computational program Gaussian™ uses a pseudopotential that ignores the core orbital structure. Potential problems arise when there is poor separation of the core and valence electrons, as occurs with the alkaline-earth (Ae) metals and their compounds. As explained in depth in Chapter 4, current theory on how group 2 AeX_2 molecules are able to display nonlinear geometries, in violation of simple valence electron-only models (e.g., VSEPR theory), require that more than the metals' n*s* valence shell orbitals be taken into account. Thus, the frozen core approximation may not model these molecules correctly. Therefore, the quality of the basis set will always affect computational results, as it did for the results in Chapter 4.

Another feature of computational modeling that affects all types of calculations, from Hartree-Fock to coupled cluster to DFT methods, is that geometry optimizations of ground state structures are designed to find minima on a molecule's potential energy surface (PES). Depending on the structure of the molecule under investigation, the PES may have a complicated shape, with many local minima of energy, in addition to one (or more) global minima. Optimization algorithms are designed to locate the nearest local minimum from a starting geometry, and unless a computationally intensive scan of the PES is undertaken, it is certainly possible to miss a global energy minimum. This becomes an especially severe problem with compounds of the alkaline-earth elements, as they often have "soft" energy surfaces; i.e., a few kilojoules of energy difference can easily give rise to changes in angles

of 10° or more. The use of fine integration grids can reduce the possibility of generating spurious minima, but the difficulty in locating true global energy minima remains.

Brief Description of Chapter Contents

Chapter 2 consists of a completed investigation of cation-π interactions. Cation-π interactions involve the largely noncovalent attraction of a cation with a ligand's π-electrons, which are often those of an arene or a heteroarene. These interactions incorporate electrostatic, inductive, and charge transfer effects, as well as, in some cases, dispersion forces. This is a DFT study of geometric factors that could affect the strength of cation-π interactions. The first half of the chapter is a slightly modified version of our paper published in the *Journal of Organic Chemistry* in 2011.[1] This section focuses on differences between non-conjugated olefins and aromatic rings in cation-π interactions; a chief finding was that, compared to non-conjugated olefins, the relationship between the strength of the interaction and the number of π-bonds involved is not linear.

The second half of the chapter is on asymmetric cation-π interactions, has not been published before, and was inspired by various questions and comments received when the first half was presented and published. While asymmetric cation-π interactions do not represent the theoretically strongest orientations for an isolated $M^+\cdots$arene system (i.e., η^6), in these molecules such arrangements are energetically optimum, given that they are constrained by the ligation of more strongly bound ligands. These asymmetric cation-π interactions contribute considerably to the total bonding energy in the molecules studied here. Overall, the field of investigating cation-π interactions has advanced substantially since the completion of this project, and further work should take this into account.

Chapter 3 consists of the work on σ- and π-bonding in manganese(II) allyls that was previously published in *Organometallics* in 2012.[2] Manganese(II) is interesting to study, as in its high spin configuration it does not provide ligand field stabilization, and its complexes do not exhibit orbitally directed geometries. Also, the five unpaired electrons of manganese(II) provide a source of intriguing magnetic behavior; the previous work in our group can be found in the dissertations and published works of Christin Carlson and Ryan Meier. This project itself was started by Christin Carlson, and all of her contributions to the paper were moved to the introduction of Chapter 3. This work contains the remaining characterization and an alternative synthetic method to one of the previously found compounds. Added to this were computations based on the bonding modes found in all of these Mn allyl compounds and comparisons to structurally similar Mg allyls.

Chapter 4 is an investigation of the structure and bonding of group 2 and 14 metallocenes with dispersion-corrected functionals. Despite the cations' not having valence electrons, metallocene compounds with calcium, strontium, and barium have been found to have non-linear Cp-M-Cp angles, as described in-depth in Chapter 4. Of the various theories for this phenomenon, dispersion interactions between the cyclopentadienyl rings are among the most difficult to model computationally. DFT methods, despite their generally superior treatment of electron correlation effects, are typically inadequate in describing long-range noncovalent interactions (e.g., π···π stacking, hydrogen bonding, van der Waals forces). The development of corrections to functionals that account for dispersion forces prompted the investigation described in Chapter 4.

Several of the ideas explored in this document should be immediately useful to other scientists. Very little work has been done to model 'non-ideal' cation-π interactions; i.e.,

those not involving metal cations and isolated π-systems (most commonly arenes). The description of the enthalpy dependence of the orientation of the electrons of a π-type bond is not found elsewhere. Another important investigation is that of non-centered cation-arene interactions, as there has been only one other paper published in the field. Description of such 'non-traditional' bonding types is useful to those writing molecular modeling programs for large systems, as cations often approach bond sites from an angle and are sterically hindered from a centered bonding mode. Finally, the dispersion chapter provides a warning that using dispersion-corrected functionals in systems with a low energy barrier to a change of geometry is not straightforward, and extra diligence is needed to avoid obtaining spurious results.

CHAPTER 2

A DENSITY FUNCTIONAL THEORY INVESTIGATION OF CATION-Π INTERACTIONS

Geometric Effects in Olefinic Cation-π Interactions with Alkali Metals

Introduction

Cation-π interactions involve the largely noncovalent attraction of a cation (commonly, but not necessarily, an alkali metal or NR_4^+ ion; R = H, alkyl) with a ligand's π-electrons, which are often those of an arene or heteroarene.[3,4] Such interactions, which incorporate electrostatic, inductive, and charge transfer effects, and in some cases dispersion forces,[5] appear in numerous supramolecular and biological contexts, including cyclophanes,[6,7] calixarenes,[8-12] collarenes,[13] polyaromatics,[14-17] conjugated double bonds[17] and amino acids such as tryptophan.[18-21] The interaction energies can be substantial: for example, those of the K^+ cation with benzene or water in the gas phase are indistinguishable (ca. 17.7±1.0 and 17.9 kcal mol^{-1}, respectively).[22,23] Even when weak, multiple cation-π(arene) interactions can critically influence ligand conformations and substrate binding.[24]

Although they have been less studied than those with arenes,[25-30] cation interactions with olefinic π-bonds have revealed a distinctive feature of cation-π bonding; i.e., the non-additivity of the energy contributions as a function of the number of π-bonds. For example, experimental enthalpies of binding of Na^+ to ethylene and benzene are -10.7±1.0[31] and -23.2±1.4 [32] kcal mol^{-1}, respectively, which are not in the 1:3 ratio that would be estimated on the basis of the number of π-bonds. As another instance, the binding of 1,4-cyclohexadiene to Li^+, Na^+ and K^+ has been theoretically modeled in the context of a study

of [*n*]beltenes (cyclacenes),[26] and the enthalpy of binding of benzene to the same cations was found to be only 2–6% greater than to the cyclohexadiene, not the 50% increase that might be expected. These findings appear to be general; we have examined the binding of alkali metal cations to the double bonds in (trisallyl)zincates, (M{Zn[1,3-$(SiMe_3)_2C_3H_3]_3$}),[33] and used ethylenes as simplified models of the allyl bonds. Two ethylenes arranged in a staggered manner around Li^+, Na^+ and K^+ were found to be roughly equal in binding enthalpy to a benzene ring, and three ethylene units around the metal surpassed the arene binding enthalpy by 30% or more.

Why isolated or non-conjugated olefins should display proportionally stronger binding to cations than do aromatic rings has been ascribed to general "geometrical considerations",[5,33] or more specifically in the case of 1,4-cyclohexadiene, to the flexibility in the $–CH_2–$ linkages in the ring, which can deform to increase the cation–olefin interaction.[26] We were interested in examining this particular contributor to cation-π interactions in more detail, as it might be used as a guide to improving the binding properties of ionophores with judicious design of the π-system.[5,10,13,34] We report here the results of a DFT study of geometric factors that could affect the strength of cation/π-olefin interactions.

Computational methods

The computations were performed with the Amsterdam Density Functional (ADF2009) program package.[35-37] Many computational studies of cation-π interactions that include DFT results have used the hybrid B3LYP functional[38-40] either alone or in combination with other functionals or theoretical methods,[41-57] but given that there is no one "best" DFT method for studying cation-π interactions,[58] a preliminary screening of functionals was

conducted with the $[K(C_6H_6)]^+$ cation, which has one of the better established energies of formation for a cation-π interaction (17.7±1.0 kcal mol^{-1}).[22] The interaction enthalpy ($\Delta H°_{int}$) was calculated as the difference of the total enthalpy of the complex and sum of the enthalpies of the parent π-system and the metal under consideration (eq 1).

$$\Delta H°_{int} = \Delta H°_{complex} - (\Delta H°_{parent} + \Delta H°_{M^+}) \quad (1)$$

Even though hybrid functionals incur severe performance penalties when combined with the Slater-type orbitals used in the ADF program,[59] several examples (PBE0, M06) were studied along with a range of non-hybrid functionals (BP86, BP86-D, BLYP, BLYP-D, PBE, mPBE, OPBE, TPSS, M06L). In combination with basis sets of triple-zeta quality, those functionals that reproduced the experimental binding value of $[K(C_6H_6)]^+$ within ±3 kcal mol^{-1} (PBE0, M06, BP86-D, BLYP-D, PBE, mPBE, OPBE, TPSS) were then examined with the $[Li(C_6H_6)]^+$ and $[Na(C_6H_6)]^+$ cations. The most consistent performance was found with the PBE functional[60] combined with the TZ2P basis with added diffuse functions (i.e., AUG TZ2P, taken from the ADF basis set library; the PBE/AUG TZ2P combination is denoted Protocol 1, or P1) and the meta-GGA TPSS functional[61,62] combined with the even-tempered ET TZ1diff basis (contains diffuse functions) (the TPSS/ET TZ1diff combination is denoted Protocol 2, or P2) (see Table 1). In some cases, P2 failed to give useful results, either because geometries failed to converge or frequency calculations did not complete; these cases are marked in the tables. Enthalpies were derived from the results of analytical frequency calculations; there were no imaginary frequencies for the optimized structures.

Table 1. Interaction energies ($\Delta H°$, kcal mol^{-1}) for $[M(C_6H_6)]^+$ (C_{6v})

$[M(C_6H_6)]^+$ complex	Li^+	Na^+	K^+
P1	–41.3	–23.6	–16.0
P2	–36.1	–22.7	–17.9
experimental	–39.3±3.3 [22]	–23.2±1.4 [32]	–17.7±1.0 [22]

Results and discussion

This discussion of cation-π bonding effects is divided into several parts, starting with isolated double and triple bonds, then double bonds constrained in a framework, followed by a brief examination of some substituent effects on bond strength, and finally a description of a geometric model of cation-π interactions.

Isolated double and triple bonds

The results of a series of calculations on $[M(C_2H_4)_n]^+$ and $[M(C_2H_2)_n]^+$ (n = 1,2,3) cations are provided in Tables 2 and 3 and Figure 1. These are closely equivalent to other calculations on alkali metal/ethylene/acetylene complexes in the literature, some of which are included for comparison. For the ethylene complexes, the results from the P1 and P2 protocols match each other for the Li^+ species and $[Na(C_2H_4)_{(1,2)}]^+$ to within 0.5 kcal mol^{-1}; with $[Na(C_2H_4)_3]^+$ and all the potassium ethylene complexes, the discrepancies are larger, up to 4.3 kcal mol^{-1}; neither protocol consistently produces greater binding energy. For the acetylene complexes, the results from the P1 and P2 protocols are always within 1.5 kcal mol^{-1} of each other; neither consistently suggests greater binding energy.

An examination of the trends in binding enthalpies for the ethylenes is instructive. As expected from a largely ionic interaction, the enthalpies decrease in the order $Li^+ > Na^+ >$

K^+. Averaging over both protocols, there is a roughly additive increase in the interaction energy with each additional ethylene molecule for Na^+ and K^+, of 12 and 9 kcal mol^{-1}, respectively. For Li^+, the second ethylene adds 18 kcal mol^{-1} to the binding energy, whereas the third adds only 12 kcal mol^{-1}. It is also clear that, as previously noted,[33] three ethylene molecules arranged around the metal center interact more strongly than does a single benzene molecule, and two ethylene molecules arranged on either side of the metal interact approximately as strongly as does benzene.

The results for $[M(C_2H_2)_2]^+$ complexes parallel those with ethylene (Figure 1, Table 3). The binding enthalpies of the acetylenes tend to be slightly higher, but all are within 2 kcal mol^{-1} for comparable $[M(C_2H_2)_n]^+/[M(C_2H_4)_n]^+$ systems.

An examination of the trends in binding enthalpies for the ethylenes is instructive. As expected from a largely ionic interaction, the enthalpies decrease in the order $Li^+ > Na^+ > K^+$. Averaging over both protocols, there is a roughly additive increase in the interaction energy with each additional ethylene molecule for Na^+ and K^+, of 12 and 9 kcal mol^{-1}, respectively. For Li^+, the second ethylene adds 18 kcal mol^{-1} to the binding energy, whereas the third adds only 12 kcal mol^{-1}. It is also clear that, as previously noted,[33] three ethylene molecules arranged around the metal center interact more strongly than does a single benzene molecule, and two ethylene molecules arranged on either side of the metal interact approximately as strongly as does benzene.

The results for $[M(C_2H_2)_2]^+$ complexes parallel those with ethylene (Figure 1, Table 3). The binding enthalpies of the acetylenes tend to be slightly higher, but all are within 2 kcal mol^{-1} for comparable $[M(C_2H_2)_n]^+/[M(C_2H_4)_n]^+$ systems.

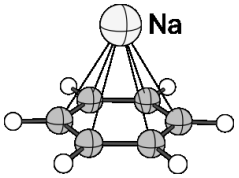

$[M(C_6H_6)]^+$ (D_{6h})
Li–*m* = 2.178; Na–*m* = 2.668; K–*m* = 3.043

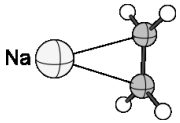

$[M(C_2H_4)]^+$ (C_{2v})
Li–*m* = 2.247; Na– *m* = 2.639; K– *m* = 3.095

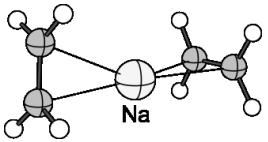

$[M(C_2H_4)_2]^+$ (D_{2d})
Li– *m* = 2.285; Na– *m* = 2.667; K– *m* = 3.153

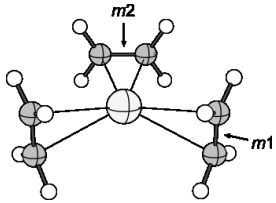

$[M(C_2H_4)_3]^+$
Li-*m* = 2.332 (D_3);[a] Na-*m*1 = 2.710; Na-*m*2 = 2.733 (C_S); K-*m*1 = 3.167; K-*m*2 = 3.169 (C_S)

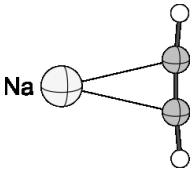

$[M(C_2H_2)]^+$ (C_{2v})
Li–*m* = 2.212; Na– *m* = 2.612; K– *m* = 3.044

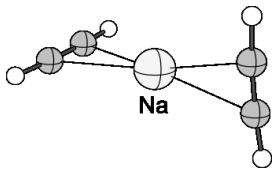

$[M(C_2H_2)_2]^+$ (D_{2d})
Li– *m* = 2.217; Na– *m* = 2.640; K– *m* = 3.101

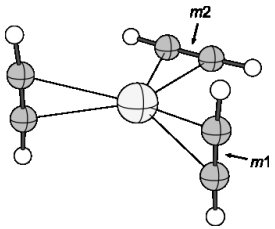

$[M(C_2H_2)_3]^+$ (C_S)
Li-*m*1 = 2.303; Li-*m*2 = 2.266; Na-*m*1 = 2.696; Na-*m*2 = 2.672; K-*m*1 = 3.134; K-*m*2 = 3.108

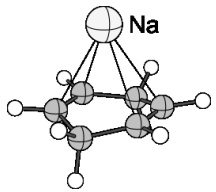

$[M(cyclohexa\text{-}1,4\text{-}diene]^+$ (C_{2v})
Li- *m* = 2.221;Na- *m* = 2.657; K- *m* = 3.053

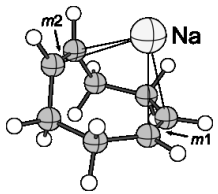

$[M(cycloocta\text{-}1,5\text{-}diene)]^+$ (C_S)
Li- *m*1 = 2.183; Li - *m*2 = 2.239; Na- *m*1 = 2.685; Na- *m*2 = 2.742; K- *m*1 = 2.598; K- *m*2 = 2.662

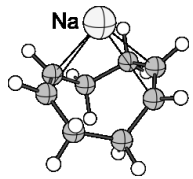

$[M(cycloocta\text{-}1,5\text{-}diene)]^+$ (C_2)
Li- *m* = 2.217; Na- *m* = 2.639; K- *m* = 3.057

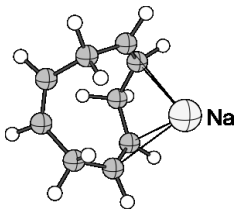

$[M(\kappa^2,\eta^4\text{-}1,4,7\text{-}cyclononatriene)]^+$ (C_S)
Li- *m* = 2.201; Na- *m* = 2.631; K- *m* = 3.042

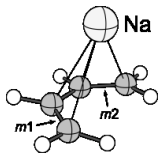

$[M(cis\text{-}1,3\text{-}butadiene)]^+$
Li-*m*1 = 2.215; Li –*m*2 = 2.200; Na-*m*1 = 2.722; Na-*m*2 = 2.649; K-*m*1 = 3.101; K-*m*2 = 3.064

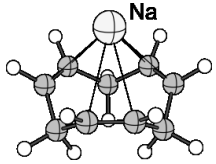

$[M(\kappa^3,\eta^6\text{-}1,4,7\text{-}cyclononatriene)]^+$ (C_{3v})
Li-*m* = 2.281; Na- *m* = 2.683; K- *m* = 3.080

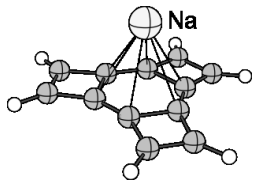

$[M(benzotricyclobutadiene)]^+$ (C_{3v})
Li-*m* = 2.194; Na-*m* = 2.640; K-*m* = 2.960

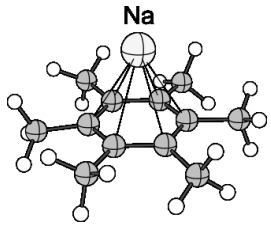

$[M(hexamethylbenzene)]^+$ (C_{3v})
Li-*m* = 2.141; Na- *m* = 2.597;K-*m* = 2.943

Figure 1. Optimized geometries of the cation-π complexes where *m* is the midpoint of a π-bond; [a]the Li^+ complex optimized to a structure (not shown) with the ethylenes in a symmetrical, canted arrangement

Table 2. Calculated energies (kcal mol^{-1}) for $[M(C_2H_4)_n]^+$

M^+	Complex	Energies	Protocol	Ref.
Li	$[Li(C_2H_4)]^+$	–18.99	MP2/6-31+G//MP2/6-31+G(d)	5
		–19.7	MP2(FULL)/6-311++G(d,p)//MP2(FULL)/6-31G(d)	17
		–22.3	PBE1PBE/aug-cc-pVTZ(C,H); cc-pCVTZ(Li)[a]	33
		–21.0	P1	this work
		–20.9	P2	
	$[Li(C_2H_4)_2]^+$	–40.6	PBE1PBE/aug-cc-pVTZ(C,H); cc-pCVTZ(Li)[a]	33
		–39.0	P1	this work
		–38.6	P2	
	$[Li(C_2H_4)_3]^+$	–51.8	PBE1PBE/aug-cc-pVTZ(C,H); cc-pCVTZ(Li)[a]	33
		–51.1	P1	this work
		–50.6	P2	
Na	$[Na(C_2H_4)]^+$	–12.36	MP2/6-31+G//MP2/6-31+G(d)	5
		–12.7	MP2/6-311+G(2d,2p)//MP2/6-31G(d)	63
		–14.9	HF/6-31G(d)	64
		–14.6±0.2	CCSD(T)/CBS (est.)//MP2(FC)/CBS	25
		–14.9	PBE1PBE/aug-cc-pVTZ(C,H); cc-pCVTZ(Na)[a]	33
		–13.9	P1	this work
		–13.5	P2	
		–10.7±1.0	experimental (CID)	31
	$[Na(C_2H_4)_2]^+$	–27.4	PBE1PBE/aug-cc-pVTZ(C,H); cc-pCVTZ(Na)[a]	33
		–26.4	P1	this work
		–26.8	P2	
	$[Na(C_2H_4)_3]^+$	*b*	BP86/TZVPP	65
		–37.5	PBE1PBE/aug-cc-pVTZ(C,H); cc-pCVTZ(Na)[a]	33
		–36.4	P1[c]	this work
K	$[K(C_2H_4)]^+$	–7.05	MP2/6-31+G//MP2/6-31+G(d)	5
		–8.02	MP2/aug-cc-pVDZ//MP2/aug-cc-pVDZ	5
		–8.29	B3LYP/6-311+G(3df,2p)//B3LYP/6-31G(d)	66
		–8.9	PBE1PBE/aug-cc-pVTZ(C,H); cc-pCVTZ(K)[a]	33
		–8.0	P1	this work
		–6.8	P2	
	$[K(C_2H_4)_2]^+$	–17.1	PBE1PBE/aug-cc-pVTZ(C,H); cc-pCVTZ(K)[a]	33
		–16.8	P1	this work
		–14.9	P2	
	$[K(C_2H_4)_3]^+$	–23.8	PBE1PBE/aug-cc-pVTZ(C,H); cc-pCVTZ(K)[a]	33
		–23.4	P1 [c]	this work

[a]The same functional/basis set combination was used for both geometry optimization and frequency calculation. [b]The binding energy was not reported; Na–C = 2.852 Å. [c]The P2 job failed to complete.

Table 3. Calculated energies (kcal mol^{-1}) for $[M(C_2H_2)_n]^+$

M^+	Complex	Energies	Protocol	Ref.[a]
Li	$[Li(C_2H_2)]^+$	–21.3	P1	
		–21.3	P2	
	$[Li(C_2H_2)_2]^+$	–41.6	P1	
		–39.9	P2	
	$[Li(C_2H_2)_3]^+$	–52.7	P1	
		–52.0	P2	
Na	$[Na(C_2H_2)]^+$	–14.5	HF/6-31G(d)	64
		–14.3	B3LYP/cc-pVTZ(C,H); AVTZ(Na)[b]	67
		–13.9	P1	
		–13.6	P2	
	$[Na(C_2H_2)_2]^+$	–26.2	P1	
		–27.1	P2	
	$[Na(C_2H_2)_3]^+$	–35.8	P1	
		–37.1	P2	
K	$[K(C_2H_2)]^+$	–8.4	P1	
		–8.2	P2	
	$[K(C_2H_2)_2]^+$	–17.0	P[c]	
	$[K(C_2H_2)_3]^+$	–24.3	P1	
		–23.5	P2	

[a] Reference is to this work, unless otherwise specified; [b]for geometry optimization, a truncated version of the AVTZ basis set was used. [c]The P2 job failed to complete.

Constrained double bonds

The results of a series of calculations on $[M(\text{cyclohexa-1,4-diene})]^+$, $[M(\textit{cis}\text{-buta-1,3-diene})]^+$, $[M(\text{cycloocta-1,5-diene})]^+$, and $[M(\text{cyclonona-1,4,7-triene})]^+$ cations are provided in Table 4 and Figure 1. The buta-1,3-diene is a conjugated system, whose cation-π complexes have been studied previously in both *cis* and *trans* forms,[17] but the *cis* form was included here for comparison, as it allows the metal cation to interact with both double bonds. Two local minima were found for the complexes with cycloocta-1,5-diene and cyclonona-1,4,7-triene; for the latter, the conformation in which only two double bonds coordinate to the metal (κ^2,η^4) is discussed in this section. In general, the results from the

use of the P1 and P2 protocols are comparable, although the discrepancy in the binding energies is larger than in the case of the isolated double bonds, and ranges up to 5 kcal mol^{-1}. For simplicity, only the results of the P1 calculations will be discussed here.

Regardless of the metal, the bonding energy of cyclohexa-1,4-diene is only ca. 2-3 kcal mol^{-1} less than two ethylene molecules, and as previously noted, is similar to that of benzene.[26] This is true even though the π-electron density of the diene and benzene is confined to one hemisphere of the metal cation, rather than being distributed around the metal. The two local minima of the cycloocta-1,5-diene complexes (with C_s and C_2 symmetry) have very similar energies (less than 0.5 kcal mol^{-1} difference for the Na^+ and K^+ systems). Their bonding energy surpasses that for the $[M(C_2H_4)_2]^+$ complexes, in the case of the C_2 conformation, by 1.5 (K^+) to 6.2 (Li^+) kcal mol^{-1}. The κ^2,η^4 conformation of the cyclononatriene (Figure 1) displays bonding energies roughtly comparable to those of the ethylenes (2.3 kcal mol^{-1} greater for Li^+, 0.8 kcal mol^{-1} less for K^+).

Noticeably different in this regard is the bonding to *cis*-buta-1,3-diene, which ranges from 4.9 to 8.3 kcal mol^{-1} weaker than to the $[M(C_2H_4)_2]^+$ complexes; in the case of Na^+, the 8 kcal mol^{-1} decrease represents a 30% drop in energy. Given the results with the ring systems above, the discrepancy is probably not principally the result of the confinement of the π-electron density to one hemisphere of the metal; this is discussed in more detail below.

[κ^3,η^6-M(cyclonona-1,4,7-triene)]$^+$

The results of calculations on the $[\kappa^3,\eta^6$-M(cyclonona-1,4,7-triene)$]^+$ cations are provided in Table 5 and Figure 1. The P1 results indicate that the bonding to the cations is weaker than in the comparable $[M(C_2H_4)_3]^+$ systems by an average of 2.4 kcal mol^{-1}, but

this is consequently considerably stronger than in the benzene systems. As the π-bonds are concentrated on one face of the metal ion, these results corroborate the minimal importance of uniform distribution of π-electron density around the metal center for optimal bonding. The results with the P2 protocol are less easily interpreted, as they indicate a progressive decrease in the binding energy from Li^+ to K^+ relative to the $[M(C_6H_6)]^+$ systems. The lithium cyclononatriene complex is 10.2 kcal mol^{-1} more stable than the $[Li(C_6H_6)]^+$ cation (cf. the 8.6 kcal mol^{-1} difference with P1), but with P2, the potassium cyclononatriene complex underbinds the comparable benzene system by 2 kcal mol^{-1}.

The molecule tetracyclo[8.2.0.02,5.06,9]dodeca-1,3,5,7,9,11-hexaene (benzotricyclo-butadiene) was examined as a planar analogue to benzene, but owing to the additional six-conjugated π electrons, the aromatic ring current essentially does not exist.[68] Although current density maps indicate that the central π-system resembles a system with three isolated double bonds, interaction between the π-bonds of the annelated rings and those of the central system generates new MOs that are spread over the entire system.[69] With the P1 protocol, there is very little change in binding energy with the lithium complex (3% increase), although the sodium and potassium analogues display increases of 28% and 23%, respectively. As with the case with the cyclononatriene complexes, the results from the P2 protocol differ somewhat from these: the lithium benzotricyclobutadiene complex shows greater enhancement compared to benzene (13%), and the increase in binding of the sodium complex (31%) is roughly the same as with P1, but the potassium complex and $[K(C_6H_6)]^+$ are equal in energy. These results leave it unclear about the net effects of the dispersed π-system, although they are clearly not parallel to those observed with hexamethylbenzene.

Table 4. Calculated energies (kcal mol^{-1}) for complexes with constrained double bonds

M^+	Complex	Energies	Protocol	Ref.[a]
Li	[Li(cyclohexa-1,4-diene)]$^+$	-35.1	MP2/6-31+G(d)//MP2/6-31+G(d)	26
		-35.1	MP2/6-311++G(d,p)//MP2/6-311++G(d,p)	26
		-37.0	P1	
		-35.0	P2	
	[Li(cycloocta-1,5-diene)]$^+$ (C_s)	-43.1	P1	
		-41.7	P2	
	[Li(cycloocta-1,5-diene)]$^+$ (C_2)	-44.8	P1[b]	
	[Li(*cis*-buta-1,3-diene)]$^+$	–26.6	MP2(FULL)/6-311++G(d,p)//MP2(FULL)/6-31G(d)	17
		-30.3	P1	
		-29.9	P2	
	[Li(κ^2,η^4-cyclonona-1,4,7-triene)]$^+$	-40.9	P1	
		-41.3	P2	
Na	[Na(cyclohexa-1,4-diene)]$^+$	-24.0	MP2/6-31+G(d)//MP2/6-31+G(d)	26
		-22.3	MP2/6-311++G(d,p)//MP2/6-311++G(d,p)	26
		-23.6	P1	
		-22.4	P2	
	[Na(cycloocta-1,5-diene)]$^+$ (C_s)	-28.6	P1	
		-27.2	P2	
	[Na(cycloocta-1,5-diene)]$^+$ (C_2)	-29.0	P1[b]	
	[Na(*cis*-buta-1,3-diene)]$^+$	-18.4	P1	
		-17.9	P2	
	[Na(κ^2,η^4-cyclonona-1,4,7-triene)]$^+$	-26.1	P1	
		-25.2	P2	
K	[K(cyclohexa-1,4-diene)]$^+$	-16.6	MP2/6-31+G(d)//MP2/6-31+G(d)	26
		-15.1	P1	
		-13.2	P2	
	[K(cycloocta-1,5-diene)]$^+$ (C_s)	-18.1	P1	
		-16.0	P2	
	[K(cycloocta-1,5-diene)]$^+$ (C_2)	-18.3	P1[b]	
	[K(*cis*-buta-1,3-diene)]$^+$	-11.9	P1	
		-10.5	P2	
	[K(κ^2, η^4-cyclonona-1,4,7-triene)]$^+$	-16.0	P1	
		-14.8	P2	

[a] Reference is to this work, unless otherwise specified; [b]The P2 job failed to complete.

Table 5. Calculated energies ($\Delta H°$, kcal mol^{-1}) for [M(κ^3,η^6-cyclonona-1,4,7-triene)]$^+$

Protocol	Li^+	Na^+	K^+
P1	-49.9	-32.8	-20.9
P2	-46.3	-30.5	-16.0

Substituted arenes

Two sets of substituted benzene complexes, [M(hexamethylbenzene)]$^+$ and [M(benzotricyclobutadiene)]$^+$, were studied in a preliminary examination of some approaches to modifying cation-π binding energetics (see Figure 1 and Table 6). Previous studies comparing the bonding of ethylene and 2,3-dimethylbut-2-ene (i.e., tetramethylethylene) have indicated that the enhanced π-electron density provided by the methyl groups increased the binding energies by 40-50% for the Li^+ complex and by ca. 30% for the Na^+ complex.[26] Enhancements of the binding energy are also observed on permethylation of the benzene ring; with both the P1 and P2 protocols, the increase is in the order $Li^+ > Na^+ > K^+$, with an enhancement of 12–16 kcal mol^{-1} for the Li^+ complexes, and 4–7 kcal mol^{-1} for the K^+ counterparts.

Table 6. Calculated energies ($\Delta H°$, kcal mol^{-1}) for substituted systems

M^+	Complex	Energies	Protocol
Li	[Li(hexamethylbenzene)]$^+$	-52.9	P1
		-51.8	P2
	[Li(benzotricyclobutadiene)]$^+$	-42.7	P1
		-40.8	P2
Na	[Na(hexamethylbenzene)]$^+$	-31.8	P1
		-32.1	P2
	[Na(benzotricyclobutadiene)]$^+$	-30.1	P1
		-29.8	P2
K	[K(hexamethylbenzene)]$^+$	-23.1	P1
		-22.1	P2
	[K(benzotricyclobutadiene)]$^+$	-19.6	P1
		-17.9	P2

Evaluation of angular dependence

It is clear that on a per π-bond basis, olefinic bonds display greater interaction energy with alkali metal cations than does benzene.[26,33] Regularly spaced distribution of the electron density around the metal (as in the $[M(C_2H_4)_{(2,3)}]^+$ systems) is not an adequate explanation for the difference, however, as the constrained olefinic systems bind just as well to the cations despite having their π-electron densities confined to a single hemisphere of the metal. A more likely source for the greater binding interaction lies in the greater ligand flexibility offered by olefins, which can optimize the orientation of the π-bonds toward the cations.[26] We developed a simple geometric model to examine this possibility.

An angle θ can be defined by the normal to the π-bond and a line drawn from the mid-point of the π-bond to the cation; it serves as a measure of the orientation of the π-electron density (Figure 2). With this definition, the perpendicular orientation of ethylene toward a cation is set at θ = 0°, and larger values of θ reflect greater rotation of the bonds. The angle θ also varies with the distance of the cation to the π-bond, becoming smaller with longer separations. In the case of benzene, θ (using P1) varies from 34.0° in $[Li(C_6H_6)]^+$ (Li–π-bond midpoint = 2.178 Å) to 25.5° in the K^+ analogue (K–π-bond midpoint = 3.043 Å).

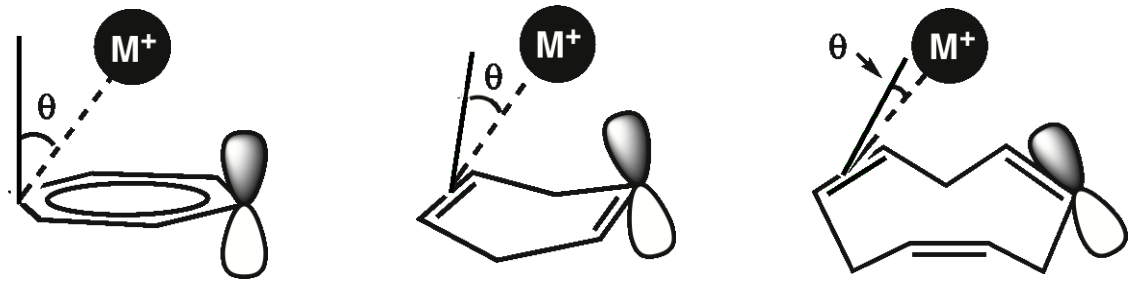

Figure 2. Definition of the angular displacement of the π-bonds toward a metal. The solid line is the normal to the π-bond, taken as perpendicular to the ring plane in arenes (at left), or assumed to lie above the plane defined by the two carbons generating the π-bond and the carbons bonded to them, as in cyclohexa-1,4-diene (middle) or cyclonona-1,4,7-triene (right). For ethylene (isolated olefin), the orientation angle = 0°.

Plots of the P1 interaction energies versus the orientation angle θ for the three different metals are given in Figure 3. The enthalpies were divided by the number of π-bonds in each system so that all the complexes could be considered on a single plot. The binding energies naturally group themselves into three areas, in the order $Li^+ > Na^+ > K^+$. For the lithium complexes, the relationship between θ and the binding energy proves to be quite strongly linear (slope = 0.23, $r^2 = 0.84$); there is a variation in energy of 8.6 kcal mol^{-1} over a Δθ range of 36.6°.[70] Besides ethylene itself, the strongest interaction energies are found for cyclooctadiene and cyclononatriene (no. 2–4 in Figure 3); i.e., in large and flexible rings in which the double bonds are able to orient themselves more directly toward the cations than in the arenes. Noticeable here is the comparatively weak binding of *cis*-buta-1,3-diene (no. 9); the rigidity of its conjugated π-system places it in the same region of the plot as the arenes, with a less-than-optimum orientation of the π-bonds toward the cations.

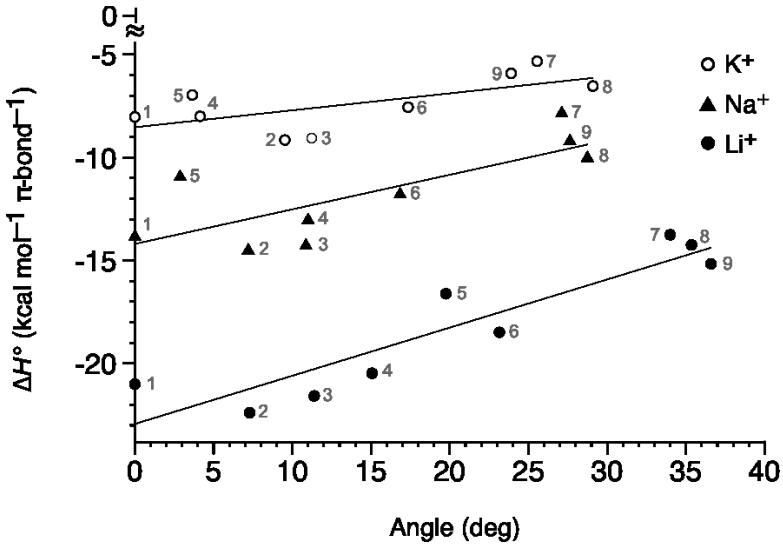

Figure 3. Plot depicting the decrease in the binding energy as a function of the displacement angle of the lone pairs; the best-fit lines for each metal center are also given. The ligands are: 1, ethylene; 2, cycloocta-1,5-diene (C_2); 3, cycloocta-1,5-diene (C_s); 4, κ^2,η^4-cyclonona-1,4,7-triene; 5, κ^3,η^6-cyclonona-1,4,7-triene; 6, cyclohexa-1,4-diene; 7, benzene; 8, benzotricyclobutadiene; 9, buta-1,3-diene.

The complexes with sodium display less angular dependence than do those of lithium; the slope of the line (0.17) has decreased, and the scatter is now greater (r^2 = 0.60). The potassium complexes continue the trend, with an even more nearly horizontal slope (0.08) and less correlation (r^2 = 0.43). The drop in correlation with Na^+ and K^+ compared to Li^+ partially reflects the greater distance from the cations to the π-bonds with the former two, so that the exact positioning of the metals relative to the ligands is not as critical as for the smaller Li^+; the more limited range of θ values in potassium complexes compared to those for lithium (Δθ = 29.1° and 36.6°, respectively) is an indication of this.

Since the stronger binding of isolated and non-conjugated olefins relative to arenes is just as evident in the Na^+ and K^+ complexes as with the Li^+ counterparts, other factors in addition to geometric orientation must be contributing to the strength of the cation-π interactions. One of these is likely the inherent polarizabilities of the ligands involved. Among the energetic components of cation-π interactions, ion-quadrupole interactions, $E_{ion\text{-}q}$, and ion-induced dipoles, E_{ind}, are prominent.[71,72] Both energies are directly proportional to the polarizability of the π-bond, defined more specifically by Q_{zz}^M and α_{zz}^M, which are the components of the quadrupole and the dipole polarizability tensors, respectively, along a line connecting the ion and the center of gravity of the molecule. Experimental values of polarizability are lacking for most of the molecules studied here, but α_{zz}^M for benzene and ethylene, for example, are 7.37 and 3.78 (10^{-40} Cm^2V^{-1}), respectively,[73] i.e., in a 1.95 to 1 ratio. Polarization energy terms in molecules are not strictly additive,[74] but it appears that two ethylene molecules can be competitive with benzene in their contributions to the net binding energy.

Conclusions

The strength of cation-π interactions is a subject of considerable interest, particularly in regard to the way they might be strengthened with suitable modifications to the π-electron sources. In the course of this study, we have confirmed that the number of π electrons in a ligand, *per se*, is not an adequate predictor of the strength of cation-π interactions to alkali metal cations. Equidistant distribution of electron density around a cation is not a critical element in the binding energy, either; e.g., three double bonds confined to one hemisphere of the metal are essentially as effective as three equally disposed π-bonds.

The orientation of the π-bonds toward the cation plays clearly plays a role in the net cation-π interaction energy. The relative weakness of the cation-benzene interaction compared to cation-ethylene is partially a result of the aromatic ring's rigid structure, and the non-optimum orientation of its π-electrons toward the metal center. The latter effect can account for up to a variation of almost 9 kcal mol^{-1}/π-bond in lithium complexes, but less in complexes of sodium and potassium, with their longer metal-ligand distances. The inherent polarizability of the π-bond source needs more attention as a means for improving the bonding interaction with olefins. To the extent that ligand substituents can enhance such polarization,[75-77] this provides a potentially fruitful avenue for further exploration.

Asymmetric Cation-π Interactions

Introduction

The previous section focused on differences in cation-π interactions between non-conjugated olefins and aromatic rings; a chief finding was that the relationship between the strength of the interaction and the number of π-bonds involved is not linear. Despite this evidence for relatively lower interaction strength per bond, aromatic rings are the π-systems

most often studied, as they make up a large percentage of the known cation-π interactions. Part of the reason for this is the widespread occurrence of aromatic rings in biological systems (e.g. tryptophan, tyrosine, phenylalanine); the sheer abundance of appropriate substrates therefore suggests that they will be often encountered. Aromatic rings are not always found to have perfectly centered cations, however, as was the case in the systems modeled above. This prompted an investigation into the positional dependence of the cation to a directionally fixed π-system. These asymmetric interactions have various structural causes that will be detailed later in this section.

Previously, the similarity of the binding enthalpy of two ethylenes or a benzene to a cation was found to be related to the inability of the π-system in benzene to orient its bonds in an optimal fashion towards a cation.[1] Less-symmetrical configurations are observed in 40% of the structures displaying cation-π binding to aromatic ring systems in the Cambridge Crystallographic Data Center November 2010 (CCDC) database. The importance and lack of study of these types of interactions were also noticed by Sherrill *et al*. who found the potential energy surfaces of several off-axis configurations including perpendicular, side-on interactions.[78] An initial goal of these studies, therefore, was to determine the relative stabilities of K^+-benzene interactions in a large range of arrangements other than the standard C_6 symmetric arrangement and those few investigated by Sherrill *et al*. Even if a cation has been forced off the C_6 axis, there are a variety of different geometries it could assume relative to the aromatic ring system; some of these are seen in Figure 4. These vary from η^5 to η^1 interactions, with accompanying binding energies of -15 kcal mol^{-1} to -6 kcal mol^{-1}, respectively.

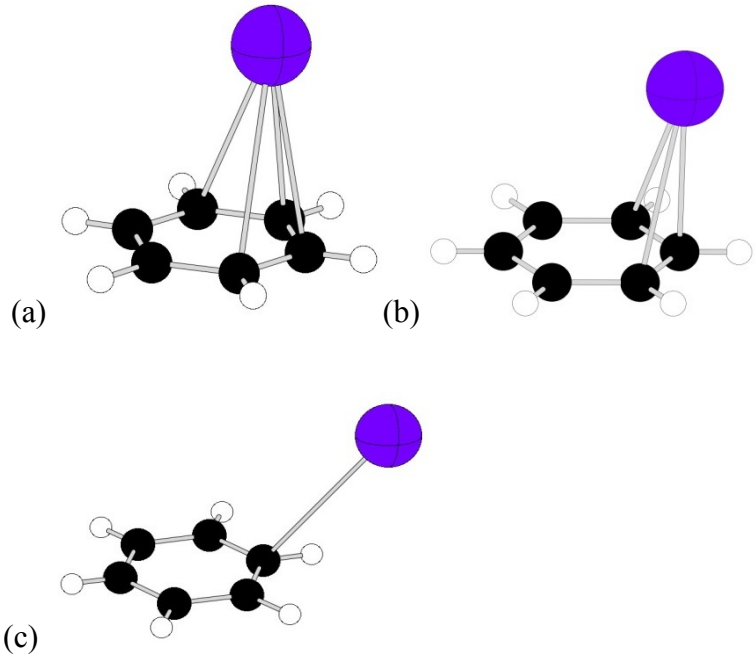

Figure 4. Examples of the possible geometries of asymmetric interactions of a cation and benzene: a) η^4; b) η^3; c) η^1

These off-centered interactions can be found in several different types. The first type occurs when the metal ion is in a "pocket" that constrains the interaction, as seen in Figure 5. The second type of off-centered interaction occurs when the cation is bridging between the arene residues of two molecules that do not align due to other geometric considerations, as seen in Figure 6. The final interaction results from the cation itself preferentially binding to other ligands, such that the electronics inhibit more coordination to the π-system, as seen in $[K(18\text{-crown-6})(\eta^2\text{-}C_6H_6)_2]^+$ (Figure 7, see below) and expanded upon in a later section.

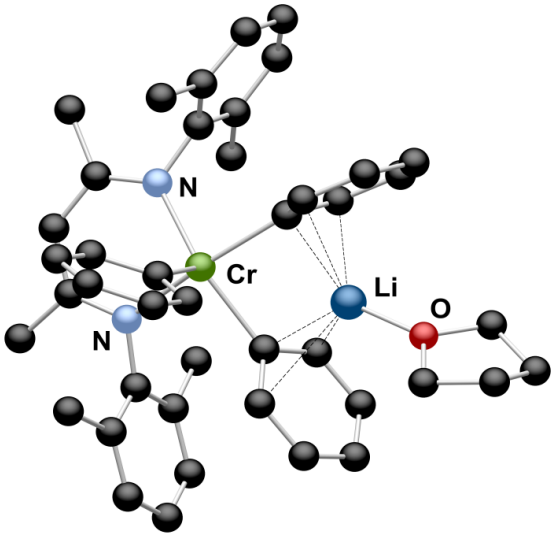

Figure 5. Example of intra-fragment interaction and a pocket interaction where the Li^+ cation preferentially binds in an η^3 manner to two arenes than an η^6 manner to one arene. [79]

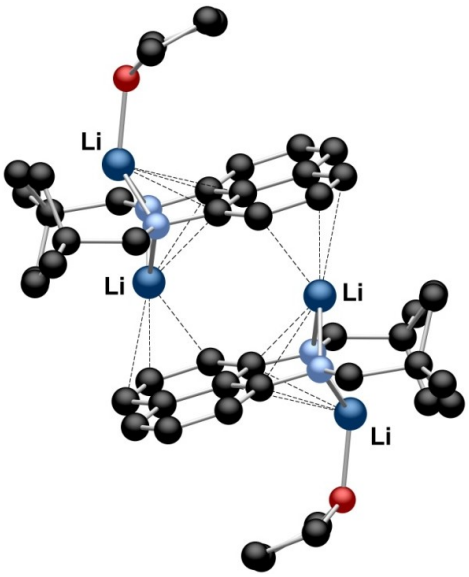

Figure 6. Example of asymmetric interlayer interaction $[\{Li(\mu\text{-}B')(thf)\}(\mu\text{-}Li)]_2$ (B′ = 1,8-$\{N(CH_2Bu^t)\}_2C_{10}H_6$). [80]

Cation-π bonds affect the structures of many molecules but can sometimes go unnoticed or unmentioned. The examples collected from CCDC are used to illustrate the different instances of cation-π bonding and the corresponding acknowledgement, or lack thereof, in the literature.

Illustrating the general lack of notice given to these asymmetric interactions: some of the articles initially describing the examples used in this investigation do not mention the cation-π bonding present in the molecule; for others the cation-π interactions provide fortuitous stability to the compounds under study; in other cases, ligands with the possibility of cation-π interactions were deliberately chosen for the compounds;[81] in still other instances, the inclusion of cations into the structures was the goal of the experiment.[82]

In publications describing these compounds, the cation-π interactions were often credited with stabilizing reactive species, but the degree and nature of the stabilization were not investigated in the original papers, and after a brief mention in the discussion were subsequently ignored. Therefore, a DFT study of such critical cation-π interactions, their relative strength, and a quantification of the stability they add to their associated molecules seemed worthwhile.

Since this investigation was completed several others have noticed the presence and importance of these asymmetric interactions. One example is from those working to improve the description of cation-π interactions in molecular mechanics for specific amino acids[83] or more generally for proteins.[84]

Results and discussion

Three different strategies were used to investigate the energetic dependence of the relative placement of a cation to a fixed π-system. The first was to constrain all but one

direction of freedom of the cation relative to the arene for distance dependence. The second strategy was to allow more degrees of freedom for the cation relative to the arene. Finally, molecules were selected from the literature and analyzed as molecular fragments, so that only the cation-π interactions were taken into consideration. Only one of the studied molecules retained an off-centered arene after geometry optimization and also completed frequency calculations without error messages.

The [K(18-crown-6)(η^2-C_6H_6)$_2$]$^+$ system

Attempts were made to directly study several of the smaller full crystal structures from the CCDC that display cation-π interactions. All but one of these structures were hindered by their size such that some did not finish a geometry optimization calculation while others were not modeled correctly. These difficulties led to the computational approach described in the final section where cation-π fragments were taken from crystal structures to include a larger sample set of cation-π type bonds.

Coordinates for the cation [K(18-crown-6)(η^2-C_6H_6)$_2$]$^+$ were taken from the complex [K(18-crown-6)(η^2-C_6H_6)$_2$][(La(η^5-$C_5H_3Bu^t_2$-1,3)$_2$)$_2$(μ-η^6:η^6-C_6H_6)].[85] This cation converged to an η^2 geometry for both benzene molecules. The [K(18-crown-6)(η^2-C_6H_6)$_2$]$^+$ system was found to have a ΔE = -9.64 kcal mol^{-1} binding interaction between the cation and both benzenes. The cation [K(18-crown-6)(η^2-C_6H_6)$_2$]$^+$ is an illustrative example of the nature of asymmetric cation-π bonds, as the potassium ion binds preferentially to the 18-crown-6 ether, leaving the benzene molecules to bind in an asymmetric manner.

The geometry optimization of the [K(18-crown-6)(η^2-C_6H_6)$_2$]$^+$ fragment demonstrated that the η^2 bonding mode in the crystal structure[85] of [K(18-crown-6)(η^2-C_6H_6)$_2$][(La(η^5-$C_5H_3Bu^t_2$-1,3)$_2$)$_2$(μ-η^6:η^6-C_6H_6)] was a departure from the normal η^6 bonding mode, and

not an artifact of crystal packing, and such distortions may be inherent in other structures as well.

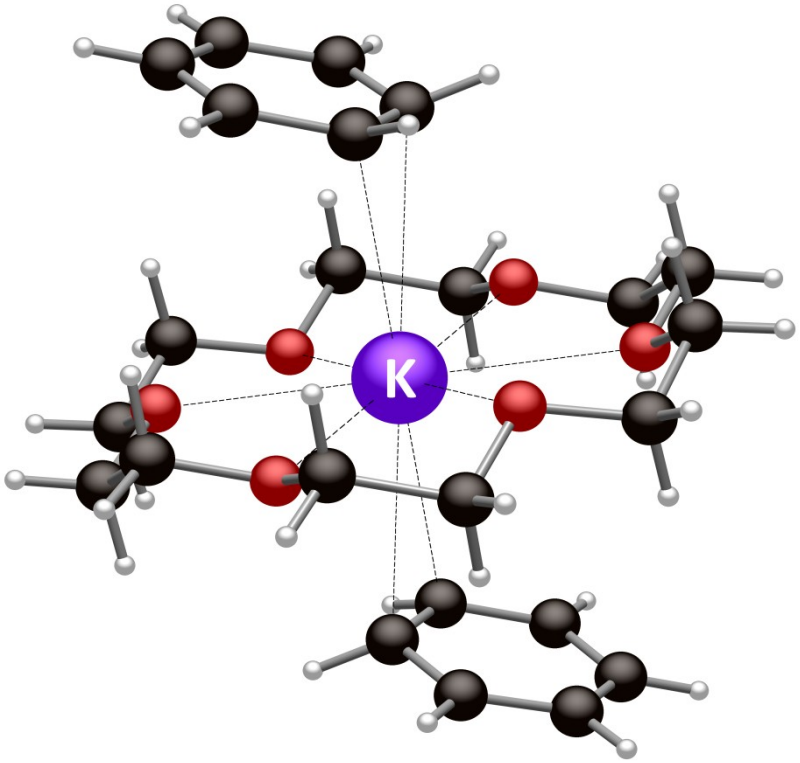

Figure 7. The geometry optimized $[K(18\text{-crown-}6)(\eta^2\text{-}C_6H_6)_2]^+$ cation showing its two η^2 bound benzenes.

Insight into this molecule and the nature of its cation-π bond can be found from the trends in similar complexes in the literature,[86-92] as discussed below, where arenes bind to a potassium cation encapsulated in an 18-crown-6 molecule. When bound with a single arene, this fragment usually binds in an off-centered η^6 fashion whereas it has a lower coordination number when bound with two arenes. The neutral potassium-encapsulated crown ether complex that binds with one additional ligand usually coordinates the lone

arene in a non-centered η^6 fashion, and this complex always binds in an η^6 fashion when the single arene has an anionic charge. This suggests some electronic dependence.

Structurally, when bound in an η^6 fashion to an arene, the potassium ion is no longer centered with respect to the crown ether, but moves to be equally close to the crown ether and the arene. This differs from the molecule with two arenes, where the cation is centered with respect to the crown ether. This movement indicates the presence of steric hindrance in molecules with two arenes, and that η^6 coordination with an arene is more favorable than being centered with respect to the crown ether. Therefore sterics play a part in the off-centered binding of the benzene in $[K(18\text{-crown-6})(\eta^2\text{-}C_6H_6)_2]^+$ as well.

For example, there are other potassium-encapsulated crown ether compounds that exhibit off-centered binding. Two compounds that mimic the off-centered interaction with two arenes are $[K([18]\text{crown-6})]_3[\eta^6,\eta^6\text{-}C_{60}](\eta^3\text{-}C_6H_5CH_3)_2$[86] and [(K(18-crown-6)) (μ^2-hydroxyl(diphenyl) borate (η^1-phenyl))(K(18-crown-6))(μ^2-(η^1-phenyl)(diphenyl) borate hydroxyl).[87] The latter is a coordination polymer that alternates the monomer between a head to head orientation and a foot to foot orientation, coordinated to K(18-crown-6) units. The bridging molecule is hydroxyl(triphenyl)borate, which coordinates through the hydroxyl on one side and coordinates with a phenyl in an η^1 manner on the other side.

These off-centered compounds also occur when one arene ring is replaced with a different coordinated base. Specifically, thf coordinates opposite the arene in the compound $[Y(N(SiMe_3)_2)_3]$[K(18-crown-6)(THF)(η^2-toluene)],[88] while the toluene is bound in an η^2 fashion. When the coordinated base is a bridging carbonyl as in $[(Pz^{tBu}\ Me_2Si)_3SiW(CO)_4]$-($\mu^2$-CO)K(18-crown-6)($\eta^3$- toluene)],[89] the arene also remains off-centered.

These can be contrasted to potassium encapsulated crown ether fragments that only bind to one additional ligand. As mentioned earlier, when the arene is neutral it is usually bound in an η^6 fashion but imperfectly centered. However in some instances steric interactions appear to interfere as in [K(18-crown-6)(η^2-toluene)][U(OSi(OtBu)$_3$)$_4$],[90]which has a toluene molecule bound in an η^2 fashion to the potassium cation. A methyl of the anion complex is close to the potassium cation, at 3.7Å, on the opposite side of the cation from the toluene and likely affected the toluene's coordination. Also, the [(η^3-$CH_3C_6H_5$)K-[18]-crown-6] counter ion is another of these fragments that have an off-centered structure[91]. In [(η^3-$CH_3C_6H_5$) K-[18]-crown-6] [K{μ-η^1:κ^1:η^1:κ^2-2,6- (2,6-i$Pr_2C_6H_3$-N)$_2$ -4-CH_3-C_5H_2N}$_2$Cr],[91] the anion fragment sits in a pocket made by the iPr groups which by sterics and perhaps crystal packing influenced the off centered interaction, or the relatively close K^+ - iPr interaction (avg K-C = 3.92Å) could have influenced it as well.

When the lone coordinated arene is anionic, it is more commonly bound in an η^6 fashion to the potassium crown ether fragment. Despite being bound in an η^6 fashion, some can be considered asymmetric based on the Δ K-C bond distance. In the case of the compound (18-crown-6)(η^6-toluene) potassium,[92] the range of K-C bond distances is large at 3.04–3.31 Å.

From these various molecules found in the literature, evidence suggests that the interaction of an arene with the $[K(18\text{-crown-6})]^+$ fragment is influenced by the classic subtle blend of electronics and sterics. When there is a second arene, or a σ-donor coordinated on the opposite side of the encapsulated potassium cation to the initial arene, the arenes will coordinate in an η^1 to η^3 range, with the majority in an η^2 fashion. Since the

cation preferentially binds to the crown ether, the ability of similar crown ether complexes with just one arene to bind in an η^6 fashion points to an energetic limit to such binding.

Constrained Systems

In computational modeling of the $(\eta^x\text{-}C_6H_6)\cdots K^+$ interaction, three different geometries were explored with an energy decomposition study. A potassium ion centered on the C_6 axis of benzene was used as a control. Two other configurations were examined with the K^+ ion in the plane of the benzene. In one case, the K^+ ion was collinear with the C-H bond, and in the other the K^+ ion was located between two hydrogens. The distance between the ring and the potassium cation was steadily increased, with energy decomposition and charge transfer calculations performed at every distance. Below is the graph of the distance dependence of the enthalpies (Figure 8).

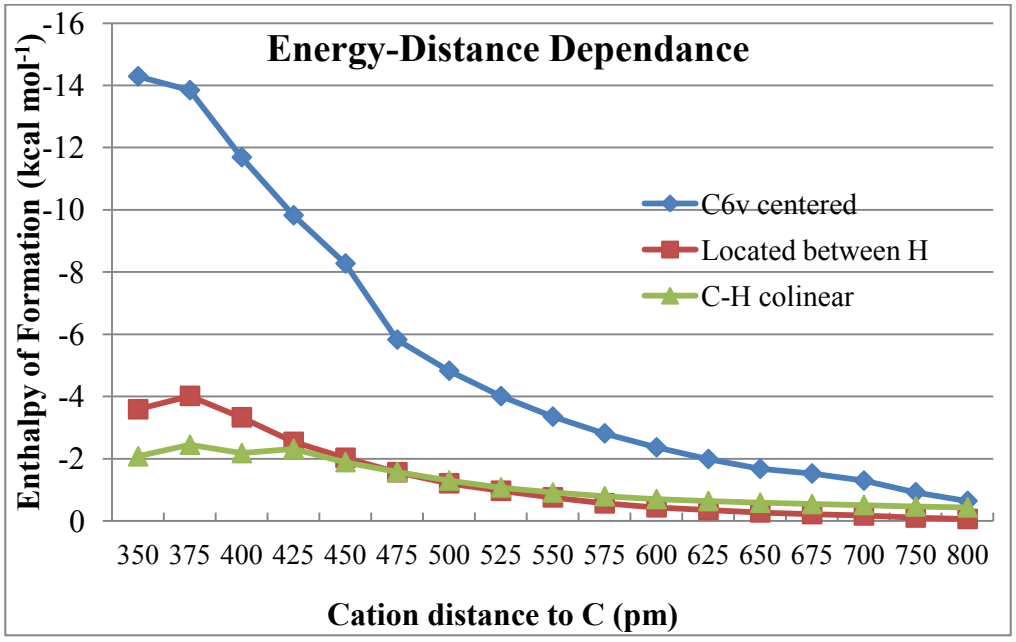

Figure 8. Graph of the interaction enthalpy vs. distance between K^+ cation and benzene

This graph shows the distance dependence of the enthalpy of formation that would be expected in this system. Also shown is the predictable preference of centered cations over the other calculated directions. Close to the benzene the enthalpy is greater by 3-7 times, and even the centered cation does not drop in enthalpy to 4 kcal mol^{-1}, the maximum value found with the other directions, until ~525 pm.

This directional dependence would be unusual for a purely electrostatic interaction. However, Cubero *et al*. make the case that polarization and induction effects along with electrostatics comprise the cation-π interaction.[93] The directionality of π-density in general and the shape of the π-density in benzene specifically is what enables asymmetric binding to be feasible in these systems. Specifically, a slip of the binding mode from centered to η^5, η^4, η^3 or η^2 will still have the cation overlapping with a large amount of the benzene's π-orbitals. As stated earlier, this makes sense in light of the findings of the previous section in this chapter, where there was enthalpy dependence on the angular displacement of the π-bonds toward the cation. Therefore, the next part of this investigation studied fragments of real structures with various binding hapticities to find the enthalpy of formation of these alternative binding modes, to determine the enthalpy loss with decreasing hapticity, and to see if the systems with lower ligand hapticities have a reasonable or even competitive amount of enthalpy.

Non-centered cation-π binding modes

Due to the difficulty of constraining a potassium cation and benzene into binding in a specific η^2, η^3, or η^4 fashion, the coordinates of K^+-arene fragments were extracted from published crystal structures and simplified to a basic cation-benzene system. Single point calculations were used with these systems to preserve the off-centered interaction. The

enthalpy of formation was found by subtraction of the system's arene fragment from the parent configuration. Geometry optimization was not used so that the asymmetric binding mode would be maintained. Normally geometry optimization is needed to remove artifacts inherent to crystal structures of which consistently short carbon-hydrogen bond distances and the underestimation of other polar bond lengths always occur. However, the enthalpy of formation was always determined from the individual fragments each time, and all the enthalpy determinations were performed identically. Any systematic errors from this should be small, as the non-centered η^6 interactions are within 1 kcal mol^{-1} of the geometry-optimized and centered structure. These single point structures ranged from non-centered η^6 interactions to η^1 interactions. Most of the non-centered interactions are η^2 or η^3, which have average interaction enthalpies of -9.35 kcal mol^{-1} and -11.66 kcal mol^{-1}, respectively. The η^2 interactions have a large range of enthalpies (-12 kcal mol^{-1} to -6 kcal mol^{-1}) due to the flexibility of positions, as can be seen in Figure 9.

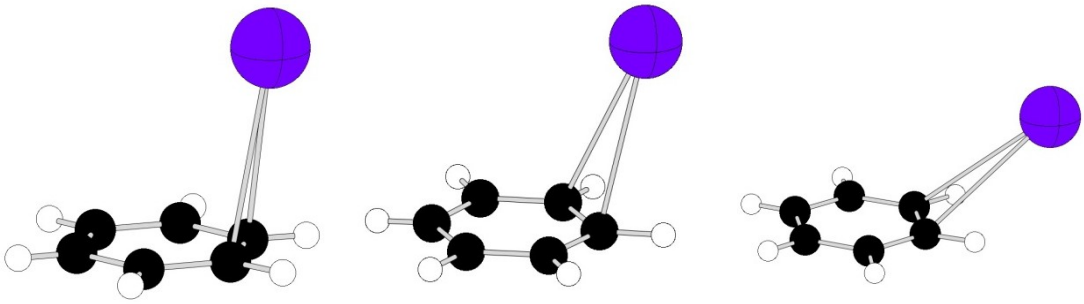

Figure 9. Examples of the range of η^2 geometries found in the K+/benzene interaction.

These non-centered binding interactions are competitive with η^6-centered interactions, as can be seen in the example of pocket interactions (Figure 5). In this case, the Li^+ cation prefers to bind to two rings in an η^3 fashion instead of a single ring in a centered η^6 fashion. Figure 10 is a plot of the bonding hapticity vs. the enthalpy of formation.

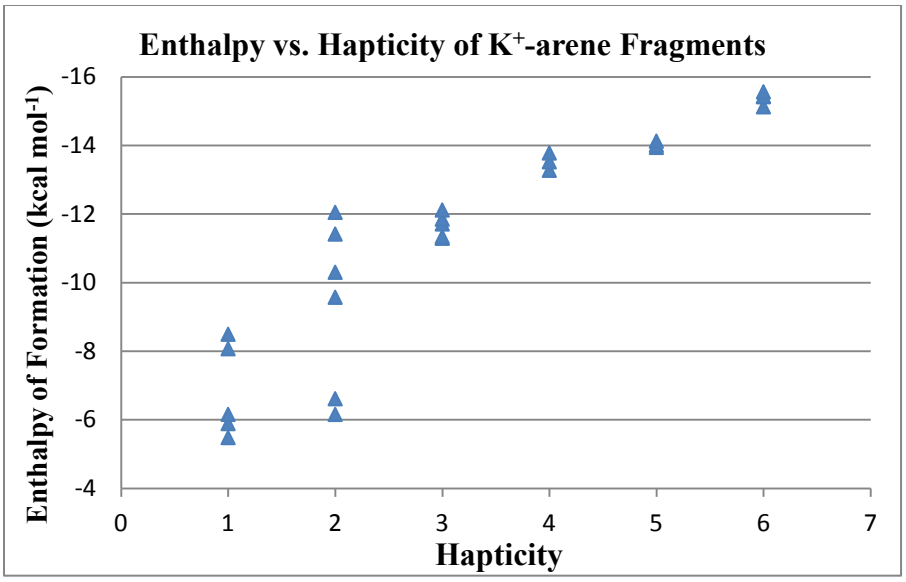

Figure 10. Graph of enthalpy vs. hapticity in K^+-benzene fragments found in published crystal structures.

In contrast to Figure 8, Figure 10 shows that there is still a considerable amount of energy involved in these off-centered interactions, as the enthalpy falls to half the η^6 value only at a bonding hapticity of 2 or less. Also evident from in Figure 10 is that the enthalpy does not correspond in a linear fashion to mono- and di-hapto geometries. The enthalpy values for η^1, η^2, and η^3 bonding hapticities overlap. Because of this previously mentioned flexibility of the η^2 interactions, another metric of these models was considered. The enthalpy of formation in these systems does correlate better to the distance between a cation and its π-system. Shown below is the enthalpy of formation compared to three distances: cation-centroid, the average of cation to ring carbon distance, and the average cation to 'bonded' carbon distance (Figure 11).

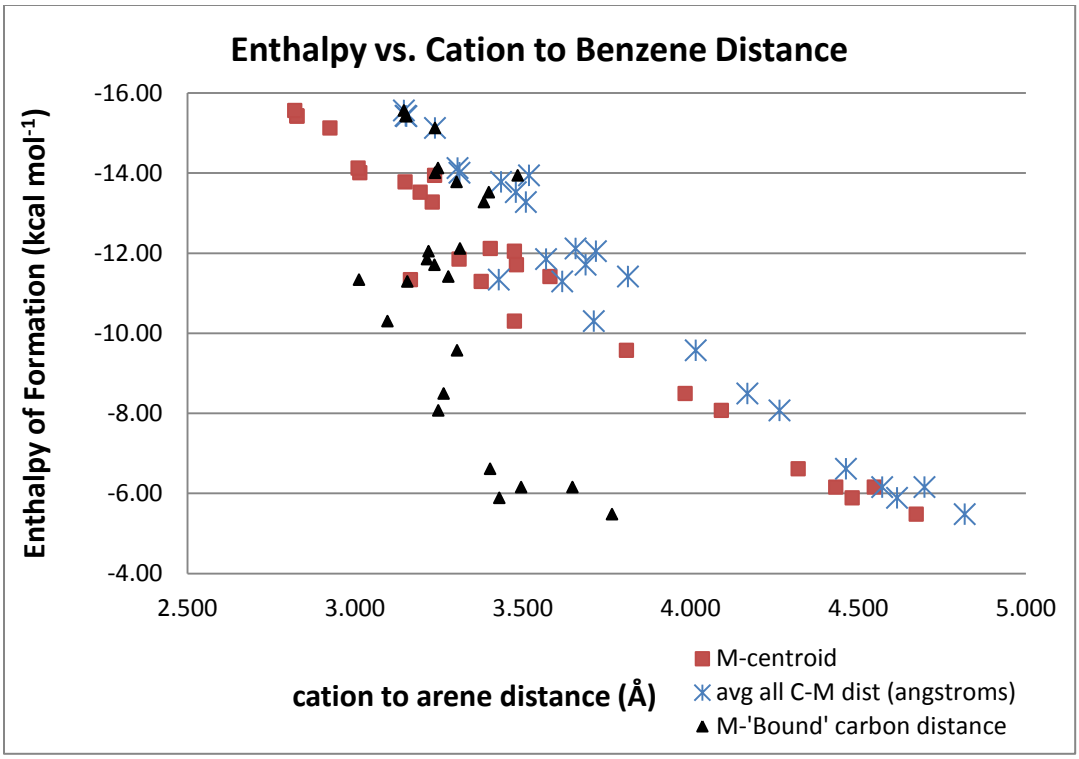

Figure 11 Enthalpy dependence on distance between the cation (K^+) and benzene ring. Three methods of measurement are described here: a) the cation distance to the benzene centroid b) the average of all six cation-benzene carbon distances; c) the average of the distance from the cation to the 'bonded' carbons on the benzene ring.

Once again, in Figure 11 as in Figure 10, taking into consideration the degree of bonding proves to be a poor model for these systems. Part of the reason for this is that there are no completely reliable criteria for setting cut-off distances between bonded and non-bonded ring carbons, and therefore specifying hapticities is somewhat subjective. In some of the η^5 structures, carbon-cation distances of more than 3.6 Å are not considered bonded when it is an outlier from the other distances. Also the deformation and spatial orientation of the involved substructures are taken into consideration. However, in some of the η^1 and η^2 structures, the cation-carbon distances of 3.65 to 3.75 Å are considered bound in this study, as there is both visual evidence of interaction based on spatial orientation and not-

insignificant amounts of enthalpy of formation. In these cases, there is often a large gap in the distances between bound and not-bound carbons that supports the assigned hapticities.

Conclusion

In conclusion, while the asymmetric interactions do not represent the theoretically strongest orientations for an isolated $M^{+}\cdots$arene system (i.e., η^6), in these molecules such arrangements are energetically optimum, given that they are constrained by the ligation of more strongly bound ligands. These asymmetric cation-π interactions contribute considerably to the total bonding energy in the molecules studied here; additional computational investigations may help to quantify their importance over a broader range of systems.

CHAPTER 3

σ- VS. π-BONDING IN MANGANESE(II) ALLYL COMPLEXES

Introduction

Transition metal complexes with high-spin d^5 configurations are without ligand field stabilization energy, and characteristically display high kinetic lability and a broad variety of stereochemistries.[94] Of the several ions that possess such an arrangement, only high-spin Mn(II) is common enough that its occurrence can be regarded as one of the defining features of the organometallic chemistry of the element; the discontinuity of the properties of Mn(II) complexes relative to other first row counterparts is such that they have been styled the 'black sheep' of the organometallic world.[95]

Comparisons have been made between complexes containing high-spin Mn(II) and those of magnesium, in that the bonding in their respective compounds is highly polar, a trait that accounts for some similarities in the structures and reactivities of their compounds. Thus Cp_2Mn and Cp_2Mg are both monomeric sandwich complexes in the gas phase, although their respective M–C bond lengths of 2.38 [96] and 2.34 Å [97] differ by less than the ca. 0.1 Å separation in ionic radii (e.g., 0.83 and 0.72 Å for 6-coordinate Mn(II) and Mg^{2+}, respectively),[98] and in the solid state, Cp_2Mn is a coordination polymer, whereas Cp_2Mg remains a monomer. The indenyl complexes $Ind_2Mn(thf)_2$[99] and $Ind_2Mg(thf)_2$[100] also display some of the 'same, but not the same' characteristics. In the manganese complex, the metal is η^1-bonded to one indenyl ligand and η^3-bonded to another, whereas in the magnesium species, the indenyl ligands are identically bonded

in an unusual η^1/η^3-bonding mode involving a weak interaction with the bridgehead carbon. Both Cp_2Mn[101,102] and Cp_2Mg[103,104] have been used in CVD processes to dope semiconductors.

It is also instructive to consider comparisons between Mn(II) and Mg allyl complexes, as the allyl anion is an inherently flexible ligand that can display either $\eta^1(\sigma)$-bonding, $\eta^3(\pi)$-bonding, or various combinations of the two. Until recently, it was a common perception that σ-bonding is the universally preferred mode for Mg–allyl bonding.[105] Under the proper conditions, however, magnesium allyls can engage in π-type bonding, and although it has not been isolated as a stand-alone compound, the parent $(\pi\text{-}C_3H_5)_2Mg$ complex has been shown in several computational studies to be the most stable conformation of the compound.[30,106] In contrast, allyl ligands on manganese that display σ-bonding are rare. Among the first to be described was the yellow allyl β-diketiminate **1** (Ar = 2,6-(*i*-Pr)$_2$C$_6$H$_3$).[107] This σ-bound allyl (Mn–C = 2.132 Å) displays strongly localized bonding (Δ_{CC} = 0.14 Å).

When three equivalents of Li[1,3-(SiMe$_3$)$_2$C$_3$H$_3$] are allowed to react with $MnCl_2$ in thf, the red-brown tris(allyl) manganate Li(thf)$_4$[{1,3-(SiMe$_3$)$_2$C$_3$H$_3$}$_3$Mn] (**2**) is isolated.[108] The anion contains both an η^3-bonded and two η^1-bonded allyl ligands. The two σ-bonded allyls display nearly identical Mn–C lengths averaging 2.186 Å, whereas the distance to the π-bonded allyl is considerably longer, at 2.348–2.470 Å. Despite the spread in the latter values, the difference between the C–C bonds is only 0.01 Å, indicating complete π-electron delocalization. Magnetic measurements on the complex indicate a $S = 3/2$ spin state for the Mn(II) center in the solid state from 100–300 K,[109] similar to the behavior of some tris(cyclopentadienyl) manganates.[110,111]

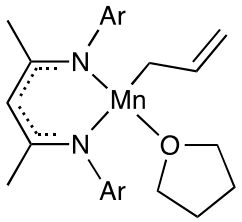

1

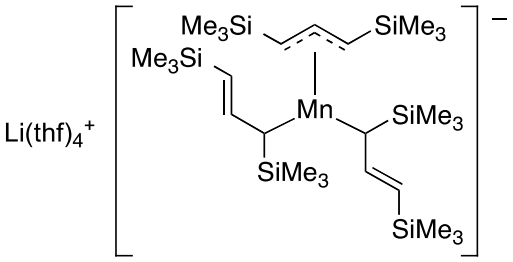

2

Considering the limited number of known allyl complexes containing Mn(II) centers, and the inconsistent structural correlations between organo-manganese and -magnesium complexes, it was of interest to develop such comparisons more fully. Of particular concern was the determination of the role coordinated solvent or other ligands might play in the bonding preferences (σ vs. π) of manganese allyl ligands. This work was started prior to that presented in the Results section of this text.[2] The compounds $A'_2Mn(thf)_2$ (**3**) and $A''_2Mn(tmeda)$ (**4**). ([1,3-$(SiMe_3)_2C_3H_3$] = A′; [1,1′,3-$(SiMe_3)_3C_3H_2$] = A′′) were previously synthesized and characterized completely. While $K_2MnA'_4$ (**5**) was also synthesized previously, it was not fully characterized; the compound was resynthesized so that acceptable microanalysis and magnetic measurements could be obtained. As compounds **3** and **4** are referenced in the text, the remainder of this introduction is a brief summary for reference.

$A'_2Mn(thf)_2$ (3)

A drawing of $A'_2Mn(thf)_2$ is provided in Figure 1, displaying the numbering scheme referred to in the text, and selected bond lengths and angles are given in Table 1. The manganese atom lies on a two-fold symmetry axis, so that only half of the molecule is unique. The allyl ligands display localized bonding, with the single and double carbon-carbon bond lengths at 1.470(3)

and 1.336(3) Å, respectively. The Mn–C bonds are also a near match for the sigma-bonded allyls in **2** (ave. 2.186 Å).

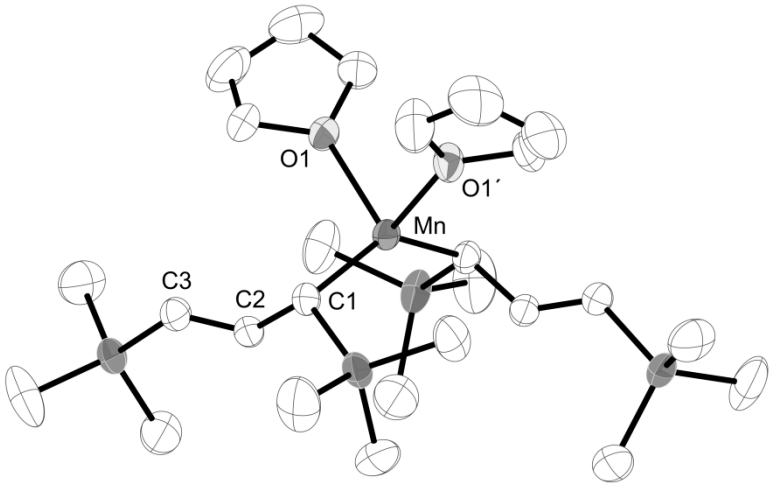

Figure 1. Thermal ellipsoid plot of the non-hydrogen atoms of **3**, illustrating the numbering scheme used in the text. Thermal ellipsoids are shown at the 50% level.

Complex **3** is isostructural with the magnesium analogue, A´$_2$Mg(thf)$_2$.[30] Interestingly, the average M–C distance in the magnesium complex (2.196 Å) is 0.022 Å longer than in the Mn analogue, despite the ca. 0.1 Å larger radius of Mn(II).[98]

A´´$_2$Mn(tmeda) (**4**)

As with **3**, **4** crystallizes as a C_2-symmetric monomer, with the metal coordinated by two η^1-allyl ligands; the carbon atom with only one $SiMe_3$ group is bound to the metal. Two nitrogen atoms of the tmeda ligand complete the distorted tetrahedral environment. A drawing of the molecule is provided in Figure 1, displaying the numbering scheme referred to in the text; selected bond lengths and angles are given in Table 2.

The Mn–C distance is 2.189(3) Å, close to that in **3**, and as with **3**, the allyl ligands in **4** display localized bonding, with the single and double carbon-carbon bond lengths at 1.469(4) and 1.372(4) Å, respectively.

A drawing of A´´$_2$Mn(tmeda) is provided in Figure 2, displaying the numbering scheme referred to in the text.

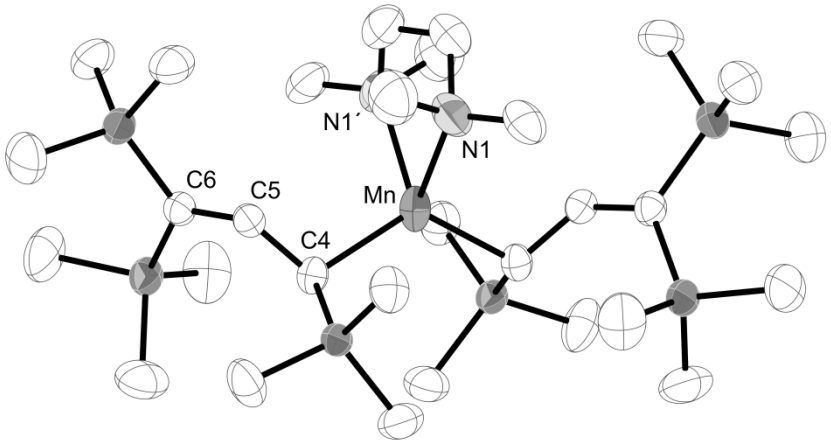

Figure 2. Thermal ellipsoid plot of the non-hydrogen atoms of **4**, illustrating the numbering scheme used in the text. Only the major conformation of the disordered tmeda ligand is shown. Thermal ellipsoids are shown at the 50% level.

Results

Formation of allyl manganese complexes

In an attempt to prepare a thf-free bis(allyl) complex analogous to the magnesium derivative,[30] diethyl ether was used as the solvent in place of THF; the goal was to produce an ether adduct that could then be desolvated. Instead, a potassium manganate was isolated (**5**),

whose formula indicates that the reaction between the allyl anion and manganese chloride occurred in a 4:1 ratio (eq 1).

$$4\ K[A'] + MnCl_2 \xrightarrow{Et_2O} K_2MnA'_4\ (\mathbf{5}) + 2\ KCl\downarrow \qquad (1)$$

The allyl complexes vary in shade from colorless (for **3**) to yellow-orange (for **5**), and all are highly air- and moisture-sensitive.

Solution magnetic susceptibility measurements.

For the η^1-complexes, **3** and **4**, a high spin state (5 unpaired electrons) would be expected from their pseudo-tetrahedral environments (Figure 1 and Figure 2 respectively). It is not as obvious from its structure that **5** should possess a high-spin center, but a magnetic moment (μ_{eff}) of 5.5 BM was found for it, also consistent with a high-spin Mn(II) system (spin-only value = 5.92 BM).

Solid state structure

$K_2MnA'_4$ (5). A drawing of the molecule is provided in Figure 3, displaying the numbering scheme referred to in the text; selected bond lengths and angles are given in Table 3. To a first approximation, the compound forms a one-dimensional coordination polymer, in which it is possible to visualize an equivalent of K[A′] co-crystallizing with the tris(allyl) manganate $[A'_3Mn]^-$, the total charge balanced with another K^+ cation. Thus a repeat unit could be considered to be $\{[MnA'_3]K[A'][K]\}_n$. Two of the allyl ligands on the Mn cation are σ-bonded and the third is π-bonded. Both σ-allyls are π-coordinated to potassium cations, promoting the polymer in two directions; the π-allyl ligand is terminal. Each of the potassium atoms is

coordinated to an additional K[A´] before the chain reverts to a Mn core. There are two independent polymer systems in the asymmetric unit. Potassium coordination spheres are completed by methyl groups of the correct orientation from symmetry-equivalent polymers K···CH_3 = 3.29 Å), such that a weak two-dimensional lattice is observed (in the *ab* plane) where every other layer repeats along the *c*-axis (see Figure 4). The interleaving layers are formed by the same weak two-dimensional interactions, but with the other independent polymer of the asymmetric unit.

Although there are two crystallographically independent manganese centers, they are similar, and only one of them will be discussed here. The coordination environment around the manganese centers is much like that in the manganate anion **2**. The two Mn–C bonds to the sigma-bonded allyls are 2.197(6) and 2.232(7) Å; the slightly longer average distance than found in **3** and **4** reflects the higher coordination number of the metal in **5**. The π-bonded allyl is somewhat slipped from symmetrical coordination, with terminal bonds of 2.385(7) and 2.477(7) Å, not dissimilar to those in **2** (2.398(4) and 2.470(4) Å).[108] The C-C bonds in the allyl unit differ by only 0.033 Å, indicating virtually complete electron delocalization in the anion.

The bonding of the allyl ligands to the potassium atoms is irregular; K1 is η^2-bonded to the (C13-C15) allyl at an average distance to C14/C15 of 3.10 Å (the K1–C13 contact is at 3.34 Å). It also displays a contact at 3.09 Å to the methyl group C12 on Si3 (the calculated K···H(C) distance is 2.53 Å, and is probably energetically significant). The allyl bridging between K1 and K2 (C4-C6) is delocalized ($\Delta_{C\text{-}C}$ = 0.041 Å), and displays η^3-bonding to the potassiums, with average K–C distances of 2.999 Å (to K2) and 3.058 Å (to K1). K2 also displays a single contact at 3.009 Å to C33. The range of distances is similar to that observed in the coordination

polymers $\{K[A']\}_\infty$ and $\{K[A'](thf)_{3/2}\}_\infty$.[112] A related manganese species, $K[3\text{-}CH_3\text{-}1,5\text{-}(Me_3Si)_2C_5H_4]_3Mn$, has been reported by Ernst and coworkers. In that complex, Mn–C distances range from 2.17–2.18 Å and K–C distances are 2.9–3.3 Å, similar to those found for the present complex.[113]

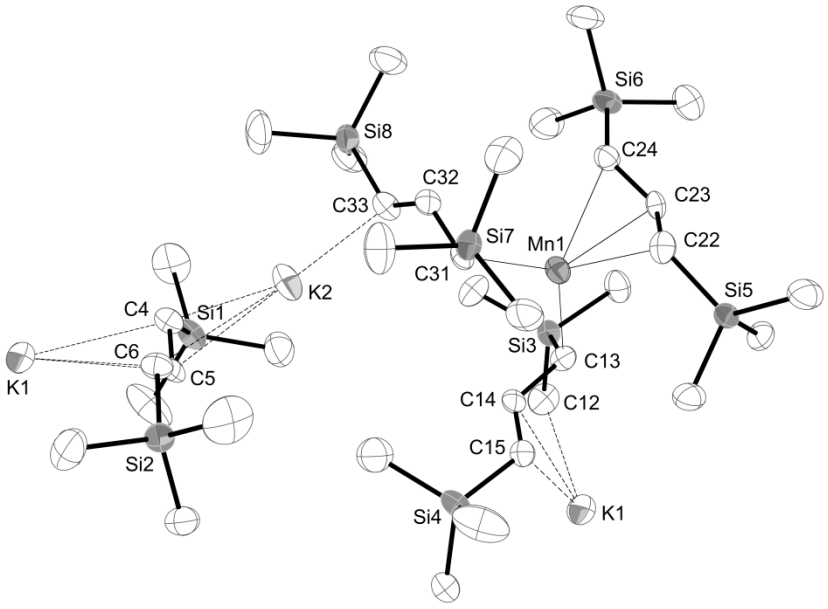

Figure 3. Thermal ellipsoid plot of a portion of the non-hydrogen atoms of the coordination polymer of **5**, illustrating the numbering scheme used in the text. Thermal ellipsoids are shown at the 50% level.

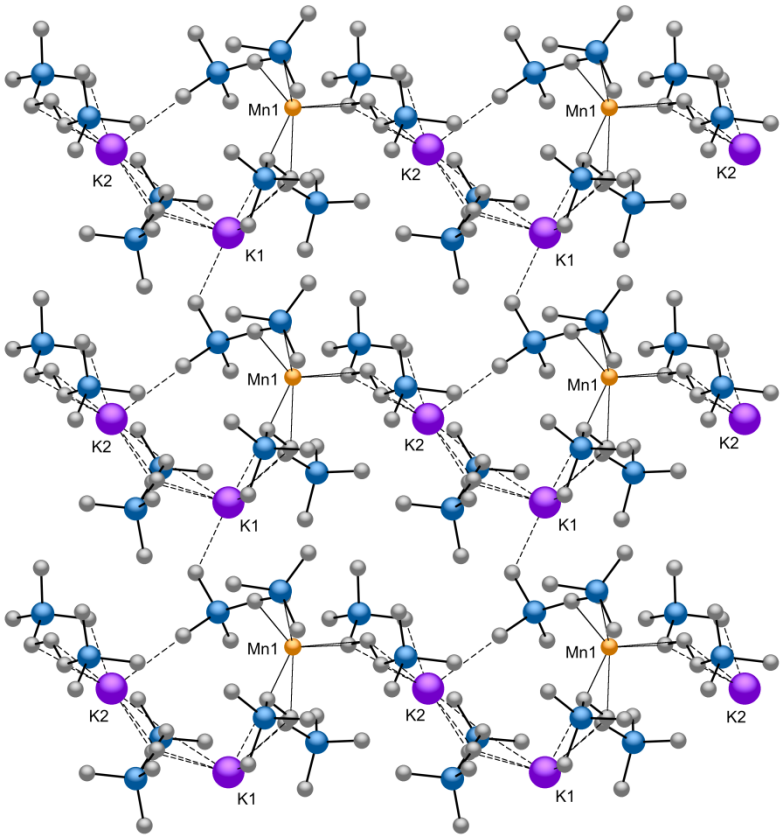

Figure 4. Partial packing diagram of **5** (the *c* axis is vertical). Hydrogen atoms are omitted for clarity.

Computational Results

To investigate the mixed η^1/η^3 allyl binding found in **2** and **5**, and the η^1-only binding found in **3** and **4**, a computational study was performed on various conformations of high-spin Mn(II) allyl complexes; these complement previous calculations on $[A'_3Mn]^-$ and the $[(C_3H_5)_3Mn]^-$ anion.[108] To evaluate the energetic effect that donor ligands could have on the structures, bis(allyl)manganese(II) was examined first. With the use of symmetry constraints, several stationary points can be found for conformations with purely σ-bonded geometries ((η^1-

$C_3H_5)_2Mn$), but all of them are high-energy saddle points on the potential energy surface with four or more imaginary vibrational frequencies. The most energetically stable, with $N_{imag} = 4$ (from 14*i* to 206*i* cm^{-1}) and C_s symmetry (Figure 5a), has Mn–C1 = 2.076 Å and Mn–C4 = 2.063 Å, and a C–Mn–C angle of 154.2°. The π-electrons in the allyl ligand are strongly localized, with a C1-C2/C2-C3 bond length difference of 0.16 Å (the comparable C4-C5/C5-C6 difference is 0.18 Å).

Removal of the C_s symmetry constraint causes $(\eta^1\text{-}C_3H_5)_2Mn$ to converge to a C_2-symmetric conformation and two slipped η^3-bound ligands (Figure 5b). The C1–C2 and C2–C3 distances differ by only 0.039 Å, indicating that substantial delocalization of the π-electrons has occurred. The Mn–C lengths span the range of 2.152 (to C1) to 2.448 Å (to C3), however; the latter is at the upper end of known Mn–C(π) distances. The angle between the two C_3 planes is 25.6°. The $(\eta^3\text{-}C_3H_5)_2Mn$ configuration is a potential energy minimum and is much more stable than the structure in Fig. 5a (by 24.1 kcal mol^{-1} ($\Delta H°$), 26.3 kcal mol^{-1} ($\Delta G°$)). Adding SiH_3 groups to the allyl ligands has no effect on the amount of slippage (Figure 5c), with a Mn–C range of 2.159–2.458 Å; the corresponding C1-C2/C2-C3 bond length difference shrinks only to 0.035 Å. The C_3 planes have become somewhat more parallel, with an interplanar angle of 12.0°. In calculations on main group allyls complexes (M = Be, Mg), SiH_3 substitution on allyl ligands has been found to "regularize" the bonding, reducing slippage and increasing delocalization of the π electrons. The slight effect of silyl substitution in $(\eta^3\text{-}C_3H_5)_2Mn$ parallels that found in previous calculations on manganese allyl complexes.[108]

Addition of a single THF molecule to the $(\eta^3\text{-}C_3H_5)_2Mn$ complex results in a mixed hapticity species $(\eta^3\text{-}C_3H_3)(\eta^1\text{-}C_3H_3)Mn(thf)$ (Fig. 5d). The π-bound allyl is more symmetrically bound

than in $(\eta^3\text{-}C_3H_5)_2Mn$ (2.254–2.339 Å), with the difference in C-C bond distances now only 0.007 Å. The σ-bound allyl has localized C-C distances of 1.464 and 1.358 Å and a bonding Mn–C1 distance of 2.084 Å, but the Mn···C2 separation of 2.70 Å is too long for a bonding interaction.

Adding a second THF molecule causes the molecule to converge with two σ-bonded allyls in a structure similar to that of **3** (Fig. 5e). The Mn–C1/C1′ distance of 2.126 Å is similar to the value of 2.174(2) Å in **3**. The Mn···C2 separation at 2.79 Å is clearly out of bonding range. The allyl ligands display localized π-bonding, with C1-C2 and C2-C3 distances differing by 0.11 Å.

Several other molecules were examined of the type $[(C_3H_5)_2MnE]^{n-}$ (E = MeCN, n = 0; E = H, Cl; n = 1) (Figure 6). In all cases, geometry optimization led to molecules of mixed allyl hapticity, $(\eta^3\text{-}C_3H_3)(\eta^1\text{-}C_3H_3)MnE$, with a delocalized π-bonded ligand ($\Delta_{C\text{-}C} < 0.035$ Å) and strongly localized σ-bonded ligands ($\Delta_{C\text{-}C} > 0.085$ Å) (see Appendix).

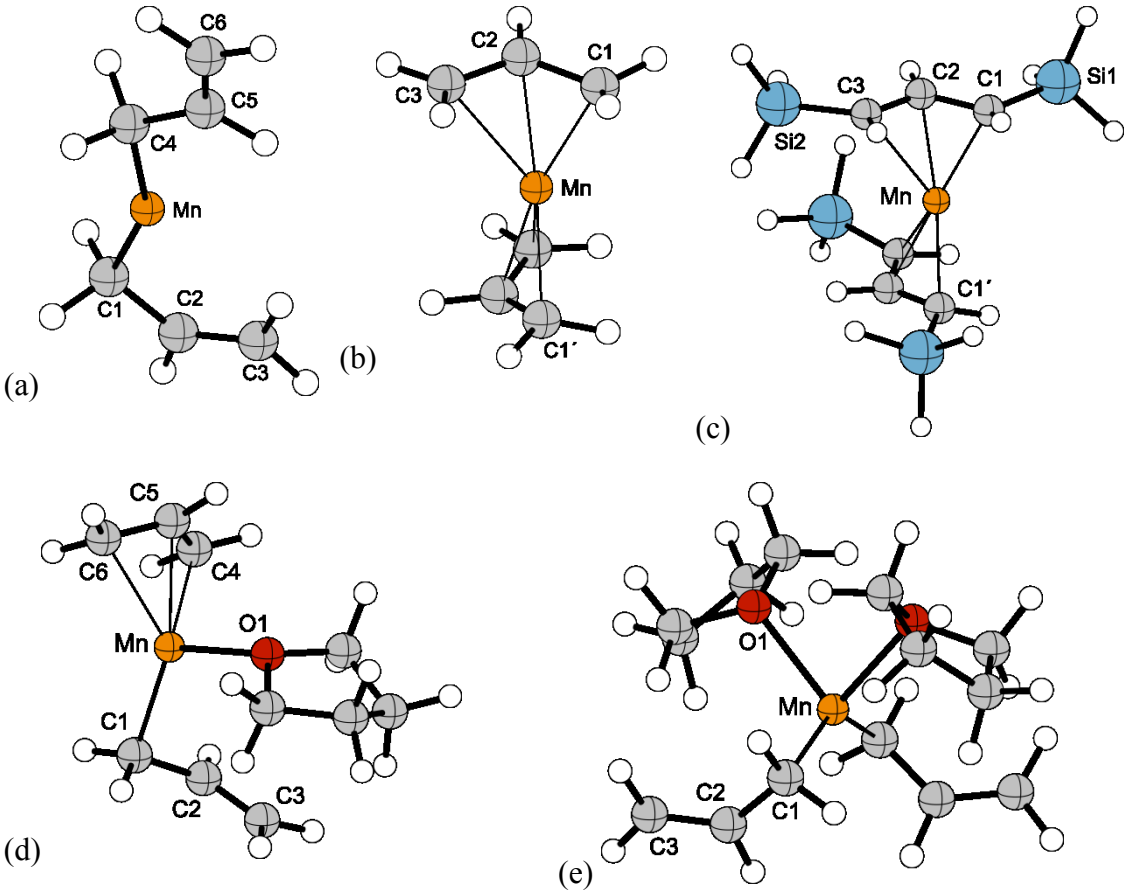

Figure 5. Calculated structures of bis(allyl)manganese complexes: (a) $(\eta^1\text{-}C_3H_5)_2Mn$, C_s symmetry; (b) $(\eta^3\text{-}C_3H_5)_2Mn$, C_2 symmetry; (c) $(\eta^3\text{-}1,3\text{-}(SiH_3)_2C_3H_3)_2Mn$, C_2 symmetry; (d) $(\eta^1\text{-}C_3H_5)(\eta^3\text{-}C_3H_5)Mn(thf)$; (e) $(\eta^1\text{-}C_3H_5)_2Mn(thf)_2$, C_2 symmetry.

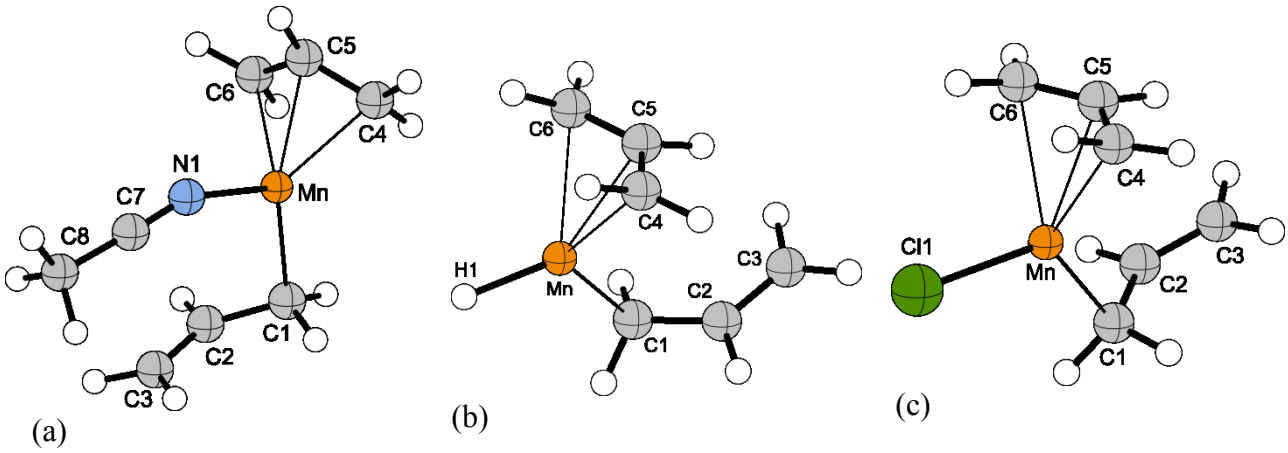

Figure 6. Calculated structures of $[(C_3H_5)_2MnE]^{n-}$ complexes: (a) E = MeCN; Mn–N1 = 2.082 Å; Mn–C1 = 2.092 Å; Mn–(C4/C6) = 2.206/2.429 Å; (b) E = H; Mn–Hl = 1.709 Å; Mn–C1 = 2.185 Å; Mn–(C4/C6) = 2.474/2.366 Å; (c) E = Cl; Mn–Cl1 = 2.322 Å; Mn–C1 = 2.149 Å; Mn–(C4/C6) = 2.273/2.551 Å.

An examination of the inherent symmetry of the (allyl)–Mn interaction was conducted with several mono(allyl) complexes: $[(C_3H_5)Mn]^+$, $(C_3H_5)MnH$, and $(C_3H_5)MnCl$ (Figure 7). The allyl ligand in the cationic complex (Fig. 7a) has a localized π-bond ($\Delta_{C\text{-}C}$ = 0.11 Å) but is oriented in what could be considered as a highly slipped η^2-conformation (Mn–C1 = 1.994 Å, Mn···C2 = 2.482 Å; Mn–C1–C2 = 90.2°). Addition of a hydrogen to make the neutral $(C_3H_5)MnH$ species (Fig. 7b) results in complete delocalization of the π-electrons; the structure minimizes to one with C_s symmetry, with a necessarily centered allyl ligand (Mn–C1/C3 = 2.293 Å; Mn–C1 = 2.267 Å). Replacing the terminal hydrogen with a chlorine atom (Fig 7c) results in some relocalization of the π-bond ($\Delta_{C\text{-}C}$ = 0.078 Å), and the allyl ligand again displays a slipped η^2-conformation (Mn–C1 = 2.089 Å, Mn–C2 = 2.318 Å). It is clear that the bonding of the allyl ligand to high-spin Mn(II) is a highly sensitive function of the identity of other ligands on the metal center.

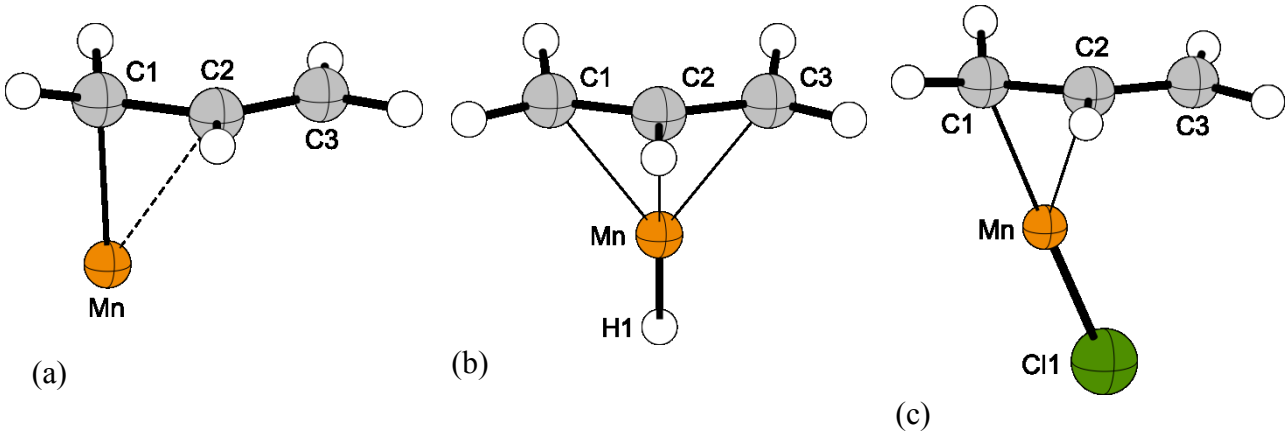

Figure 7. Calculated structures of mono(allyl) Mn(II) complexes: (a) $[(C_3H_5)Mn]^+$; (b) $(C_3H_5)MnH$; (c) $(C_3H_5)MnCl$.

Discussion

Unlike the case with other first row transition metals Cr, Fe, Co, and Ni, a monomeric bis(π-allyl)complex of manganese does not appear to be easily synthesized with either the parent $C_3H_5^-$ ligand or with bulky trimethylsilylated versions. Without the ligand field strength from the allyl ligands to force spin-pairing in the metal, the d^5 configuration of Mn(II) causes the metal to behave as a more electropositive element, maximizing its coordination number while avoiding steric oversaturation. An illustration of this is found in the fact that the $K_2MnA'_4$ manganate, with its four associated allyl ligands per manganese center, is formed from a reaction mixture with only a 2:1 allyl:Mn stoichiometry.

Several features of the complexes are worth special mention. One is the notable asymmetry in η^3-bonded allyl ligands on high-spin Mn(II) centers. This was first observed in the crystal structure of **2**,[108] and similar slippage occurs in **5**. The slipped bonding was reproduced in calculations on **2** and the simplified $[(C_3H_5)_3Mn]^-$ anion, thereby demonstrating that neither

crystal packing effects nor silyl substitution was responsible.[109] It was suggested that an intramolecular interaction between the π- and σ-bonded allyls was the source of the ligand slippage. Although this might be true, slippage is also observed in $(\eta^3\text{-}C_3H_5)_2Mn$ (Figure 5b), and thus it does not require the presence of σ-bonded allyls.

The fundamental geometric features of the allyl–Mn(II) bond were investigated through calculations on a series of mono(allyl) species, including $[(C_3H_5)Mn]^+$, $(C_3H_5)MnH$, and $(C_3H_5)MnCl$. The allyl ligand in the $[(C_3H_5)Mn]^+$ cation was found to be σ-bonded, with localized C–C and C=C bonds (1.472 and 1.359 Å, respectively), and partial sp^3 hybridization is evident in the bond angles around C1 (sum of angles = 347.3°) compared to the geometry around C3 (sum of angles = 360.0°), as expected for essentially exact sp^2 hybridization. However, the orientation of the ligand is more like one that is π-bonded, but highly slipped; the Mn–C1–C2 angle of 90.2° is much more acute than the nearly tetrahedral angle of 108.3° found for Mn–C1–C2 in **3**, for example. The origin of the asymmetry can be traced to the particular ordering of the manganese and allyl orbitals; the HOMO of $[(C_3H_5)Mn]^+$ involves the interaction of the 4s orbital of Mn with a (partially hybridized) p orbital on carbon. The Mn–C interaction is antibonding with respect to the π-bond of the allyl (Fig. 8a). It should be noted that optimization of a version of $[(C_3H_5)Mn]^+$ with enforced C_s-symmetry results in a transition state geometry (N_{imag} = 1; 340*i* cm^{-1}) that is nevertheless only 4.7 kcal mol^{-1} higher in energy ($\Delta H°$, 6.1 kcal mol^{-1} ($\Delta G°$)) than the asymmetric ground state. The low energy cost of changing between the symmetric and asymmetric forms suggests that the metal-allyl bonding is easily perturbable.

Addition of a hydrogen to make the neutral $(C_3H_5)MnH$ complex (Fig. 8b) shifts the relative ordering of the orbitals; as noted above, the bonding in the allyl ligand is now completely

symmetrical, and the sum of angles around the terminal carbons is 355.8°. The HOMO is now largely composed of the ψ_2 orbital of the allyl anion,[114] with a smaller admixture of the Mn d_{yz} orbital. With the $(C_3H_5)MnCl$ complex (Fig. 8c), relocalization of the C–C bonds occurs; the sum of bond angles around C1 (346.8°) and C3 (359.8°) is similar to that found in the ground-state $[(C_3H_5)Mn]^+$ cation. As with the latter, the HOMO largely reflects interaction of the 4s orbital of Mn with a carbon (C1) 2p orbital of the allyl anion. Given the ease with which it is possible to shift from η^1 to η^3 bonding, it seems inappropriate to speak about a 'normal' bonding mode of the allyl ligand to high-spin manganese(II).

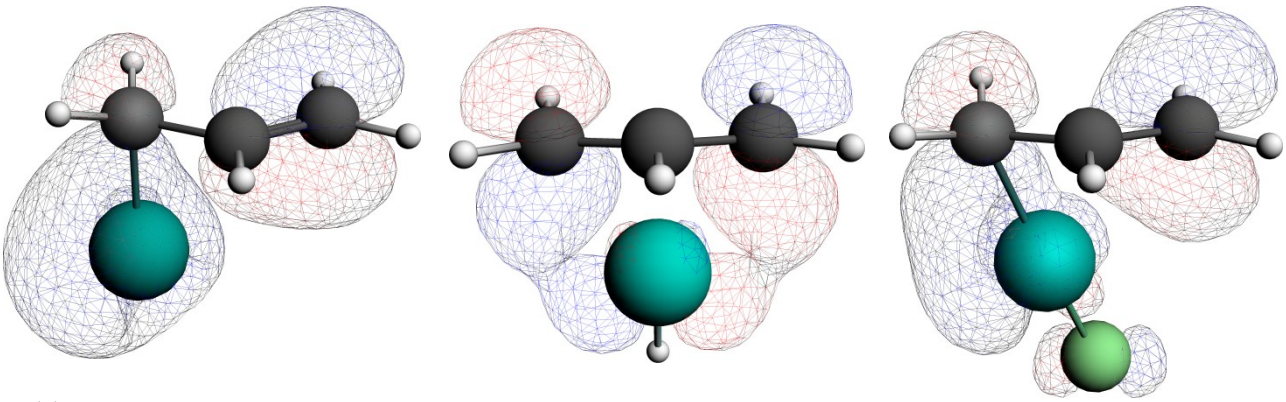

Figure 8. HOMOs of high-spin mono(allyl) Mn(II) complexes: (a) $[(C_3H_5)Mn]^+$; (b) $(C_3H_5)MnH$; (c) $(C_3H_5)MnCl$.

A second point to be made about the bonding of allyl ligands to Mn(II) involves the attempt to find a stable configuration with multiple η^3-bound ligands to the metal. Starting from $(\eta^3\text{-}C_3H_5)_2Mn$, any attempt to add an additional neutral (THF, MeCN) or charged (H^-, Cl^-, $C_3H_5^-$ [109])

ligand results in slippage of one of the allyls, so that a complex of the form $[(\eta^3\text{-}C_3H_5)_2MnL]^{n-}$ does not appear to be likely with high-spin Mn(II). The reasons for this do not appear to be steric, as slippage of an allyl is predicted to occur with a ligand as small as H^-. Electronic influences are undoubtedly involved here; Layfield found that putting manganese in an intermediate spin state (S = 3/2) led to the prediction that a complex with the structure $[(\eta^3\text{-}C_3H_5)_2(\eta^1\text{-}C_3H_5)Mn]^-$ could indeed be stable.

Conclusions

Both experimental and theoretical methods have been used to help probe the complex behavior of manganese(II) allyl systems. In some respects, high-spin Mn(II) and Mg^{2+} display similar structural chemistry, as evidenced by the existence of isostructural $(\eta^1\text{-}A')_2M(thf)_2$ complexes for both metals. In addition, computations suggest that although $(\pi\text{-}C_3H_5)_2M$ complexes represent stable minima on the potential energy surface, addition of an additional ligand such as THF will result in slippage to form the mixed hapticity species $(\eta^3\text{-}C_3H_5)(\eta^1\text{-}C_3H_5)M(thf)$. Actual examples of monomeric complexes with such mixed hapticity ligands are not yet known for magnesium, but one has been identified with the heavier Group 2 congener calcium,[115] and of course mixed-mode allyl ligands are a prominent feature of the manganese species **2** and **5**.

Despite such parallels, manganese is a less electropositive metal than is magnesium, and has available d orbitals that may permit the existence of a larger variety of bonding modes than is now known. Such compounds may expand the usefulness of manganese allyl complexes in synthetic and catalytic applications.[116]

Experimental Section

General considerations

All manipulations were performed with the rigorous exclusion of air and moisture using high vacuum, Schlenk, or glovebox techniques. Infrared data were obtained on a Thermo-Mattson Satellite FT-IR spectrometer as KBr pellets prepared as previously described.[117] Elemental analyses were performed by Desert Analytics (Tucson, AZ).

Materials

Hexane and Et_2O were distilled under nitrogen from potassium benzophenone ketyl,[118] and anhydrous tetrahydrofuran (THF) was purchased from Aldrich and used as received. Anhydrous manganese(II) chloride was used as received from Aldrich or Acros. Toluene-d_8 and benzene-d_6 were vacuum distilled from Na/K (22/78) alloy and stored over type 4A molecular sieves prior to use.[118] K[A´] was prepared as previously described.[119,120]

Magnetic measurements

Solution magnetic susceptibility measurements were performed on a Bruker DRX-400 spectrometer using the Evans' NMR method. The material (5–10 mg) was dissolved in toluene-d_8 or benzene-d_6 in a 1.0 mL volumetric flask. The solution was thoroughly mixed, and approximately 0.5 mL was placed in a NMR tube containing a toluene-d_8 or benzene-d_6 capillary. The calculations required to determine the number of unpaired electrons based on the data collected have been described elsewhere.[121-125] The values are considered to be accurate to $\pm 0.2\ \mu_B$.

Synthesis of $K_2MnA'_4$ (5)

Under nitrogen, $MnCl_2$ (0.124 g, 1.00 mmol) in diethyl ether (20 mL) was added to a flask equipped with a stirring bar. An addition funnel containing K[A´] (0.453 g, 2.00 mmol) in diethyl ether (20 mL) was attached to the flask. At room temperature, the K[A´] solution was added to the $MnCl_2$ while stirring. After stirring overnight, the diethyl ether was removed under vacuum, and hexane was added to the remaining residue. This solution was filtered and evaporated to yield 0.2772 g (0.31 mmol, 15.6% yield) of **5**. Anal. Calcd. for $C_{36}H_{84}K_2MnSi_8$: C, 49.42; H, 9.68; K, 8.94; Mn, 6.28. Found: C, 48.26; H, 9.54; K, 7.21; Mn, 5.94. Solution magnetic susceptibility ($\mu_{eff}^{T(K)}$): 5.5[298].

General procedures for X-ray crystallography

A suitable crystal was located, attached to a glass fiber, and mounted on a Siemens SMART system for data collection at 173(2) K. Data collection and structure solution was conducted at the X-ray Crystallography Laboratory at the University of Minnesota by W. W. Brennessel and/or V. G. Young, Jr. All calculations were performed with the current SHELXTL suite of programs. Final cell constants were calculated from a set of strong reflections measured during the actual data collection. Relevant crystal and data collection parameters for the compound are given in Table 1.

The structure was solved using SIR97[126] and refined using SHELXTL-97.[127] The space group was determined based on systematic absences and intensity statistics. A direct-method was calculated that provided most of the non-hydrogen atoms from the E-map. Several full-matrix least squares/difference Fourier cycles were performed that located the remainder of the non-hydrogen atoms. All non-hydrogen atoms were refined with anisotropic displacement

parameters. All hydrogens except the allylic hydrogens atoms were placed in ideal positions and refined as riding atoms with relative isotropic displacement parameters; the allyl hydrogens were treated as described in the Supporting Information.

Computational details

The computations were performed with the Amsterdam Density Functional (ADF) program package.[128] Several different functionals were tested for use, including BP86-D3, PBE-D3, BLYP-D3, BP86-D3(BJ), PBE-D3(BJ), BLYP-D3(BJ), M06L, TPSS, TPSS-D3, TPSS-D3(BJ), and OLYP. The -D3 functionals incorporate dispersion corrections according to Grimme's DFT-D3 method.[129] The -D3(BJ) methods incorporate the Becke-Johnson damping function as well.[130] Full geometry optimizations were carried out with all-electron valence triple-ζ Slater-type basis sets with double-polarization functions for all atoms (TZ2P) from the ADF basis set library (integration level of 6). The BP86-D3(BJ) functional was selected for subsequent work; the geometries of all molecules converged with it, and it gave realistic structures as tested against experimentally known examples. As a point of calibration, the geometry of 1,1′-$(MeCp)_2Mn$ was calculated; the average Mn−C distances were found to be 2.414 and 2.126 Å for the high- and low-spin structures, respectively, in good agreement with the experimentally determined values from electron diffraction of 2.433(8) and 2.144(12) Å.[131,132]

Table 1. Selected Distances (Å) and Angles (deg) for **3**

atoms	distance	atoms	angle
Mn–C(1)	2.174(2)	C(1)–Mn(1)–C(1A)	137.16(14)
Mn–O	2.172(2)	O(1A)–Mn(1)–O(1)	86.87(10)
C(1)–C(2)	1.470(3)	O(1)–Mn(1)–C(1)	104.17(8)
C(2)–C(3)	1.336(3)		
	Displacement of Si(1) from C_3 plane: 1.31 Å (45.8°)		
	Displacement of Si(2) from C_3 plane: 0.12 Å (3.6°)		

Table 2. Selected Distances (Å) and Angles (deg) for **4**

atoms	distances	atoms	angle
Mn–N(1)	2.337(6)	C(4A)–Mn–C(4)	122.81(17)
Mn–C(4)	2.189(3)	C(4)–C(5)–C(6)	131.3(3)
C(4)–C(5)	1.469(4)		
		Displacement of Si(1) 4.35° (= 0.141 Å)	
		Displacement of Si(2) 6.85° (= 0.223 Å)	
		Displacement of Si(3) 49.9° (= 1.44 Å)	

Table 3. Selected Distances (Å) and Angles (deg) for **5**

atoms	distance	atoms	distance
K(1)–C(5)	2.995(8)	Mn(1)–C(31)	2.197(6)
K(1)–C(6)	3.027(8)	Mn(1)–C(13)	2.232(7)
K(1)–C(15)	3.060(8)	Mn(1)–C(23)	2.342(7)
K(1)–C(14)	3.146(7)	Mn(1)–C(22)	2.385(7)
K(1)–C(4)	3.153(7)	Mn(1)–C(24)	2.477(7)
		C(13)–C(14)–C(15)	128.8(7)
		C(22)–C(23)–C(24)	129.1(6)
		C(31)–C(32)–C(33)	130.6(6)

CHAPTER 4

INVESTIGATION OF CLASSIC UNUSUAL STRUCTURES WITH NEW DFT FUNCTIONALS CONTAINING DESCRIPTIONS OF DISPERSION FORCES

Introduction

The bent alkaline earth metallocenes (MCp^*_2; $Cp^* = C_5Me_5$, M = Ca, Sr, Ba) have posed an intriguing puzzle since their gas-phase structures were first determined 3 decades ago. The homoleptic decamethylmetallocenes of group 2 do not have a geometry with cyclopentadienyl rings that are oriented parallel to each other in the gas phase, as would be expected for highly polar, if not strictly ionic, compounds, but instead display a ring-centroid –M– ring-centroid angle of less than 180°. (The terms "bent" and "linear" will be used to refer to these ligand-M-ligand angles in the remainder of this work.) The bent nature of these metallocenes has long been supported by both crystal structures and gas-phase measurements. In 1986, $CaCp^*_2$ was determined to have a ligand-M-ligand angle of 154(3)° while $MgCp^*_2$ was linear,[133] and $SrCp^*_2$ and $BaCp^*_2$ were determined to have 149(3)° and 148(6)° angles, respectively, in 1987.[134] These ligand-M-ligand bent structures surprised the inorganic community and still prompt controversy over the source of the bending. A simple hard sphere model would predict linear molecules, as these are centered on 2+ charged metal ions and do not have any valence electrons to affect their shape, let alone the valence d-electrons that affect the transition metals. The authors of the two gas-phase papers cited above stressed that the structures were thermal averages, and that the equilibrium structures might still be linear; the energy barrier for the $CaCp^*_2$ bending angle of

20° would be a low 4 kJ/mol and the energy needed with $SrCp^*_2$ and $BaCp^*_2$ even lower at 2 kJ mol^{-1}. Both of these initial works point out the parallels between these structures and the bent alkaline earth dihalides.

In the gas-phase, the alkaline earth dihalides were found to have permanent dipoles and thus be bent in Klemperer's molecular beam experiment in 1963.[135] This geometry is counter to what the VSEPR model predicts for these molecules, and has made them the focus of much study and debate. Several theories have been put forward trying to explain and/or unify this with the VSEPR model. Hayes initially proposed that the 3d orbitals played an important part in the bending of CaF_2. He pointed out that the *n*d energy level is below that of the (*n*+1)p for calcium, strontium, and barium, and demonstrated through calculations that adding d-orbitals models the molecules well, but declined to comment on the exact nature of the d-orbitals' involvement.[136,137]

Another theory put forward to rationalize the non-linear alkaline-earth halides is the polarized ion model. This model assumes purely ionic (electrostatic) interactions between the metal and ligands, with a polarizable metal core (soft) and hard ligands. Initially proposed by Rittner, this theory described the mutual polarization of the ions in a molecule by the electrostatic fields of the others.[138]

The polarized ion model was extended by Guido and Gigli,[139] who contend that with proper application of electrostatics, it is possible to achieve bent structures with this model despite its limitations. They took into account the fact that the angular dependence of various forces is more important than their magnitude, and emphasized that the polarizability of doubly charged group 2 ions was non-trivial, a fact that had previously been ignored. The charge-charge and the induced dipole terms favor a linear structure, whereas the charge-dipole and dipole-dipole terms favor a

bent structure. Using BaF_2 as an example, they graphed these various terms with respect to angle and showed that the negative ion-positive dipole increases faster than the repulsive terms as the angle goes from linear to bent, and thereby energetically stabilizes the molecule in a bent geometry.

Bader *et al*.'s calculation of the Laplacian for the bent group 2 dihalides supported the polarized ion model. It showed how the outer shell of the core of these molecules were perturbed and distorted by interaction with the halide ligands. The eight outer core electrons 'condensed' into four regions of electron density in roughly a tetrahedral formation, and the halide ligands were positioned so that they were not in any of these regions, but each was opposite of one of these regions. They explain why MgF_2 is linear while the remainder of the group 2 difluorides are bent: "The polarization of the Mg core, a closed shell, requires the mixing of the 3s and 3p orbitals of the next quantum shell whereas the outer shell of the Ca, Sr, or Ba core is incomplete and more easily polarized, as it requires only the mixing in of the d orbitals from the same quantum shell." [140]

As can be seen in the preceding quotation, both d-orbital participation and core polarization were considered to be equally critical in the determination of these molecule's structures; equivalently, the sub-valent shell and the valence shell are equally important in bending. Kaupp *et al*. state in their 1991 computational paper that "the d-orbital participation in bonding is more important for the heavy alkaline earth metals than for the group 12 elements."[141] They warn, however, that the bending angles and frequencies they calculated should not be taken too seriously as there was ambiguity in some of the group 2 dihalides like CaF_2, which is sometimes considered *quasilinear*.

The classification of molecules such as CaF_2 and $SrCl_2$ as *quasilinear* is due to the low energy barrier between bent and linear structures. Many calculations have been performed on these two, but the best descriptions of these quasilinear molecules were calculated with the high level coupled-cluster method on CaF_2 in 2004[142] and $SrCl_2$ in 2006.[143] CaF_2 was calculated to have a energetic barrier to linearity of only 54 cm^{-1} (0.15 kcal mol^{-1}). The calculated angle falls within the range of experimental data, which Koput *et al*. mentions is large, owing to its being gathered from isolated molecules in various low temperature rare-gas matrixes or from high temperature gas-phase molecules.[142] In the 2006 article on $SrCl_2$,[143] in addition to calculations to the gas-phase strontium dichloride, calculations were also performed that modeled $SrCl_2$ in an argon matrix similar to the previously performed IR experiments. The authors found it likely that the $SrCl_2$ interacted with the argon matrix, which would cause the discrepancy between the IR data and high temperature electron diffraction data. Most important to the present study is the bending potential energy curve. The curve is shallow until just past 150°, with a maximum at 180° only 0.1 kcal mol^{-1} above the minimum.[143]

Whereas the halides are hard enough to polarize the softer alkaline earth ions, the cyclopentadienyl ligand does not have the electronegativity to do the same. Other explanations for the bending of the group 2 metallocenes have been suggested instead. An early computational paper by Bosnich investigated with molecular mechanics calculations the effects of van der Waals attractive forces on the bending of alkaline earth decamethylmetallocenes.[144] In this 1993 paper, they found the differences in energy between bent and linear to be less than 2.1 kcal mol^{-1}. Electrostatic forces did not alter the minimized geometries of their work, and they concluded that the difference in total energy is essentially the same as the difference in van der Waal

energy, and that van der Waals attractive forces were the dominant force in causing the molecules to be bent. The Bosnich paper[144] mentioned and then a 1995 paper by Timofeeva[145] expanded the comparison between the group 2 metallocenes and the group 14 metallocenes. The 1995 paper focused on the metal-ligand distance dependence of main group metallocenes, and contrasted the group 14 metallocenes with the group 2 metallocenes; the former, with their lone pair of electrons on the metal centers, offer an easier explanation for bending.

However, the importance of the lone pair of electrons to group 14 bending was put in doubt with the molecular mechanics study by Timofeeva *et al*.[145] The molecular mechanics model did not include any terms describing the effects of a lone pair electrons, but was still able to describe the bent structures in group 14 metallocenes. They carefully explain that their results do not rule out a stereochemically active lone pair as their model does not need it, but they suggest that the lone pair orbitals have predominantly *n*s character. Overall their conclusion was that dispersion was the dominant force in the bending of the group 2 and 14 metallocenes they studied, and crystal packing forces were not the cause or dominant force controlling the angles.[145]

This suggests that the similarities between group 2 and group 14 metallocenes are much greater than expected and the bending of both is influenced by dispersion forces. With the similarities between the bonding in group 2 and 14 metallocenes, further questions are raised about possible similarities between the group 2 dihalides and metallocenes. Is CaF_2 bent for similar reasons as $CaCp^*_2$? Or is CaF_2 bent for a different reason, given that dispersion plays no role in the group 2 dihalides and the Cp ligand is not as electronegative as those halides? In addition, given that on the basis of molecular mechanics calculations dispersion effects have

been credited as the source of bending in the metallocenes, could the use of dispersion-corrected density functional theory calculations help to corroborate this?

Dispersion forces were first described in Johannes van der Waals' 1873 doctoral dissertation and then expanded upon by London.[146] They are mathematically described by the series expansion $-C_6R^{-6} - C_8R^{-8} - C_{10}R^{-10}$ - …[146] It has become important to computationally model dispersion forces correctly, as they are critical in rare gas dimers, π-π stacking, molecular crystals, adsorption on solid surfaces,[147] and molecular recognition processes, and are critical in describing the interactions of graphene sheets and the functioning of biomolecules. One paper calculating interactions of linear hydrocarbons with carbon nanotubes found that the Hartree-Fock method only models repulsion.[148] Many papers have been written on the insufficient description of dispersion forces in various methods of calculation.[147,149-152]

The correct description of dispersion forces is not inherent to all types of calculations, but can be added in a post hoc manner to some of them. As mentioned above, dispersion is easily added to molecular mechanics through appropriate parameterization of the force fields used. Also, coupled cluster theory can satisfactorily describe dispersion forces if the single and double electron excitations are calculated iteratively, the triple electron excitations are calculated perturbatively, and the complete basis set limit extrapolation is used.[151] The Hartree-Fock method cannot model dispersion as it includes electron exchange, but not dynamical correlation, and dispersion forces are a purely correlation effect.[149,152] Møller-Plesset (MP2) corrections to Hartree-Fock theory overbinds at dispersion distances, but switching to MP3 models them well.[19] DFT methods can in theory describe dispersion interactions, however current DFT should actually be considered DFA ('Density Functional Approximation'), as the exact functional is not

known, and all available functionals are approximations. Most of the common DFT functionals calculate exchange and correlation based on local properties, but dispersion forces need to be described by non-local DFT properties.[151] One review paper goes so far as to say that "the 'hereditary sin' of DFT [is] a failure to describe the dispersion energy".[151] DFT methods are still popularly used despite their deficiencies, as these approximations are relatively accurate for their computational cost. Wave function theories, like coupled cluster theory, scale $N^5 - N^7$ (N = number of electrons) while DFT only scales N^3.[153]

The excellent cost to accuracy ratio of DFT prompted the interest and effort that produced the recent appearance of dispersion-included functionals and dispersion corrections that can be added to existing functionals. Truhlar's approach was to use extensive empirical parameterization from training sets that included compounds that relied on dispersion forces.[154,155] (The Minnesota class of functionals, such as M05 and M06, are among these.) The other method that has been developed was to make a patch with the first term of the series expansion (C_6R^{-6}); the latter approach requires that additional terms (e.g., damping functions) be added to smooth the transition from short- to long-range interactions, and to minimize the occurrence of local minima defects.[156,157] There is now a renewed appreciation of dispersion forces with this ability to model them.

Group 2 atoms are also difficult to describe computationally as there is poor separation between the core and valence electrons. When the electrons are described in the basis set, normal methods of describing the core and valence separately cannot be used as there is correlation between the subvalent electrons and valence electrons as well as involvement from the (n-1) unoccupied d-orbitals.[158]

In addition to the bent group 2 metallocenes, there are other molecules constructed around alkaline earth metal centers that display 'non-VSEPR' geometries, and are usefully included in this study. Among these is the homoleptic alkyl calcium $Ca(C(TMS)_3)_2$, which has a bent ligand-Ca-ligand angle (149.7(6)°).[159] Three features make this calcium compound an ideal molecule for this study. The first is that the ligand is large and there exists enough overlap between the two ligands for dispersion interaction between the two. Second is that not only is there a crystal structure, but also it crystallizes as a monomer, unlike the heavier $BaCp^*_2$, which is a coordination polymer, and thus is characterized more readily with computational means. Finally, it is a calcium compound. Calcium is the first element of the group 2 elements to produce bent structures and not only does it not have any filled d-orbitals, but it also does not need any of the relativistic corrections that are required by the heavier elements to achieve satisfactory correspondence with experimental data. Since there are not any filled d-orbitals, computations can be performed without d-orbitals in their basis sets, so that only one possible cause of bending, dispersion forces, is present.

This study is an initial exploratory investigation into the functionality/usefulness of dispersion-corrected functionals in modeling stereochemically non-rigid systems. The initial questions this study sought to answer were: are there any similarities between the reasons for bent and linear group 2 and 14 metallocenes? Can any of the alkaline earth dihalide bending theories be applied to groups 2 and 14 metallocenes? To what extent can the dispersion-corrected functionals be used in modeling the factors that contribute to bent and linear geometries in these main group compounds?

Use of dispersion-corrected functionals in the computational investigation of group 2 and 14 organometallic compounds

As mentioned previously, there are structural similarities between the group 14 and group 2 metallocenes, so the initial phase of this investigation was to use select molecules from these corresponding group 14 structures as a control. Before the crystal structure of decaphenylstannocene was reported in 1984, all of the known structures of group 14 metallocenes had bent geometries. When Wilkinson confirmed the bent structures of (dicyclopentadienyl)tin and -lead in 1959, he also proposed a simple model that had a sp^2 -type lone pair filling the empty space between the rings in the bent metallocene[160] (to this day, many textbooks still use this as an explanation). Early analysis of Mössbauer[161,162] and photoelectron spectra[163] appeared to support this model, with one example being the report of lone pair donation in dicyclopentadienyltin(II) boron trifluoride (II).[162] When new bent group 14 metallocenes were synthesized and published, molecular orbital calculations and bonding type investigations were often included and used to support this model. These calculations led to a disagreement on whether the lone pair was the HOMO or the fifth occupied.[164-167] Therefore the linear metallocenes of group 14, the first of which was decaphenylstannocene (1984),[168] were a surprise when discovered. The lone pair of electrons on the metals meant that the structures of these molecules could not be easily rationalized with simple models (e.g., VSEPR). The conclusion in the paper was that the lone pair for the linear metallocene was stereochemically inert.[168] (As there were no short intermolecular contacts, crystal packing forces were deemed less likely.) Stereochemically inert lone pairs have been observed in halides of the heavy p-block metalloids, such as TeF_6^{2-}. These compounds have AX_6E electron configurations, but some of

them are strictly octahedral, indicating that the lone pairs are not exerting any stereochemical influence. In these cases, calculations indicate that the lone pairs occupy orbitals of high n*s* character, and are therefore nondirectional.

The stereochemical activity of a metallocene-based lone pair became a difficult topic to discuss when the crystal structure of decamethylsilicocene was discovered, considering that this molecule crystallizes in both linear and bent configurations in the same unit cell.[169] The cocrystallization of two forms indicated that the difference in energy between them is less than crystal packing forces, but the absolute structural preference could not be determined at the time of publication in 1989; NMR measurements were interpreted in terms of a linear structure, but gas electron diffraction measurements indicated a bent structure.[169] The small difference in energy still prevents a reliable determination of geometric preference.

Some of these compounds have more evident reasons for being linear. Another parallel tin complex, one found by Sitzmann, is decaisopropylstannocene, which has sterically bulk ligands and a closest interring Me···Me′ contact of 3.84 Å.[170] The previously mentioned decaphenylstannocene, along with decaisopropylstannocene, also have similarly close contacts, so van der Waals repulsion likely inhibits any bending, but the reasons for the lack of bending in the others discussed below are not so evident.

A sterically based explanation for linear metallocene geometries cannot be used with the $[Pb\{C_5Me_4(SiMe_2Bu^t)\}_2]$,[171] $[Sn\{C_5Me_4(SiMe_2Bu^t)\}_2]$,[172] and $[Pb\{C_5(iPr)_3H_2\}_2]$ ($PbCp^{3\text{-}iPr}_2$)[173] compounds. The two of these that crystallized with the same ligand, $[Pb\{C_5Me_4(SiMe_2Bu^t)\}_2]$[171] and $[Sn\{C_5Me_4(SiMe_2Bu^t)\}_2]$,[172] do not have the steric bulk that the previous tin complexes had, and the lead and tin molecules have larger intramolecular ligand contacts (4.30 and 4.26 Å

respectively), which indicates that another reason for their linearity other than intramolecular steric crowding is involved.

This, then, is the initial premise of our DFT investigations; i.e., that some of the reasons mentioned as the cause of bending in group 2 metallocenes, such as dispersion forces or polarization of the metal ions, may also be found as the cause of bending in analogous group 14 complexes. The group 14 part of this investigation started with three questions: Are some of these stereochemically non-rigid systems intrinsically linear? Are these structures inherently bent, but crystal-packing forces restrict them to linear structures? Are we unable to decide between these alternatives, given the limitations of current theory? A compound chosen for this in-depth study as a counterpart to the alkaline earth metallocenes was $[Pb\{C_5(iPr)_3H_2\}_2]$ ($PbCp^{3-iPr}_2$), a group 14 metallocene that is both linear and has no intramolecular Me···Me′ contacts closer than 4.1 Å, outside normal van der Waals contact distance.[173]

Computational method and details

The computations were performed with the Amsterdam Density Functional (ADF2014) program package.[35-37] Initial structures were based on crystallographically determined structures when they were monomeric or when no monomeric crystal structures exist, were modified from similar structures in the same period (e.g., $CaCp^*_2$ used for $SrCp^*_2$ computations). In some cases final structures of previous computations were used to provide comparison, and those are marked in the relevant data table. Final geometry optimization calculations were performed without imposed symmetry. Relativistic effects were modeled with ZORA (Zeroth-Order Regular Approximation) and included only scalar effects.

In combination with basis sets of triple-zeta quality with doubly polarized Slater functions (TZ2P), the BP86[174,175], PBE[60], and BLYP[39,174] functions were used along with the versions patched with Grimme's D3[156] dispersion correction (BP86-D3, PBE-D3 and BLYP-D3), as well as the parameterized M06L functionals. The integration grids were at the teVelde 5 level or better. This is the standard set of parameters used for these calculations. Changes to these parameters were either for experimental purposes or as increases in quality to ensure geometry optimization convergence. All parameters are mentioned in the data tables (Tables 1–8). Frequency calculations were performed at the same level of theory as used in the geometry optimization; where imaginary frequencies were generated, they are noted in the data tables.

Results of DFT Calculations

Computations and structure of $PbCp^{3\text{-}iPr}_2$ and $PbCp^{4\text{-}Me}_2$

As stated above, the molecule $PbCp^{3\text{-}iPr}_2$ that was chosen as a foil for the alkaline earth metallocenes was investigated first. The geometry optimization of the crystal structure geometry of $PbCp^{3\text{-}iPr}_2$ with the functionals BP86 and PBE converged to a linear geometry similar to the crystal structure (#4 and #10 in Table1). The initial calculation of the crystal structure geometry with the dispersion-corrected functionals, BP86-D3 and PBE-D3, converged, against expectations, to a bent shape with centroid-lead-centroid angle range of 154.6-159.1° (#1 and 7 in table 7). When this bent geometry was reoptimized with the dispersion-uncorrected BP86 functional, the calculation returned the structure to a linear geometry similar to the crystal structure (#3).

Table 1. The properties of referenced calculations of the $PbCp^{3\text{-}iPr}_2$ molecule (Int = Integration grid; Start geom = how was the starting geometry was obtained)

#	Functional	Basis Set	Int	Dispersion correction	Symmetry imposed? Relativity correction applied?	Start geom	End angle	Me-Me closest contact (Å)	Bond energy (Hartree)
1	BP86-D3	TZ2P	5	Yes	No; Yes	Crystal structure (parallel)	155.646	3.803	-15.52443821
2	BP86-D3	TZ2P	5	Yes	Yes; Yes	**1**	Forced parallel	4.45	-15.52195125
3	BP86	TZ2P	5	No	Yes: C(2H) Relativity corrected	**1**	180.000	4.571	-15.41757089
4	BP86	TZ2P	5	No	No; Yes	**3**	178.130	4.520	-15.41753557
5	BP86-D3	Pb: DZ; C, H: DZP	7	Yes	No; Yes	**1**	154.594	3.909	-15.42671106
6	BP86-D3	TZ2P	5	Yes	No; Yes	Crystal structure preopt with 5 cycles of BP86 int grid 3	155.202	3.895	-15.52505971
7	PBE-D3	TZ2P	5	Yes	No; Yes	Crystal structure (parallel)	159.249	3.998	-15.68901379
8	PBE	TZ2P	5	No	No; Yes	**7**	165.221	4.1946	-15.63113397
9	PBE-D3	Pb:QZ4P C, H: DZP	6	Yes	No; Yes	**3**	159.043	4.028	-15.59302346
10	PBE	Pb:QZ4 C, H: DZP	6	No	No; Yes	**3**	180.000	4.472	-15.53430265
11	M06L	PbTZ2P; C TZP; H DZP	6	Yes	No; Yes	Crystal structure (parallel)	164.899	4.016	-16.47908044

Further efforts were aimed at determining if the unexpectedly bent structures of $PbCp^{3\text{-}iPr}_2$ were computational artifacts. One approach, intended to remove possible artifacts introduced initially, was to pre-optimize the crystal structure. This pre-optimization was completed with the

functional BP86 with an integration grid at 3 for five geometry optimization cycles to correct C-H bond lengths (#6). When computations of the optimized crystal structure were performed with the dispersion corrected functionals, BP86-D3 or PBE-D3, the final geometry again had a non-linear centroid-lead-centroid angle.

Also, based on the alkaline earth metallocene theory that core polarization contributes to bending and thus a minimal metal basis set cannot be used if there is to be any chance of matching experimental structures, a DZ quality basis set was used on the lead atom. For the lead atom, DZ is the smallest possible basis set in ADF; it does not have added polarization functions and few d-functions. However, this too optimized to a bent geometry (#5).

Similarly the M06L functional, where dispersion forces are incorporated by empirical parameterization, converged to a non-linear geometry (#11). Thus all the functionals that had corrections for dispersion forces produced bent geometries. Therefore the bent geometry of $PbCp^{3\text{-}iPr}{}_2$ is not likely to be an artifact from the set-up and execution of these calculations. These results raise questions about both the calculated and experimentally determined geometries of $PbCp^{3\text{-}iPr}{}_2$; e.g., is the computed bent structure an artifact of the density functional and/or basis set combination used in this study? Would the (currently unavailable) gas phase structure of the metallocene demonstrate that it is actually bent, but intermolecular interactions in the solid state force the relatively "floppy" molecule to adopt a linear geometry for the benefit of more efficient crystal packing?

There is support for the possibility that some of these functionals produce artifacts. In 2012 Austin, Petersson, and Frisch presented their APF functional.[176] They designed it to have a reduced amount of the attractive and repulsive long-range spurious interactions seen in most

common functionals. These spurious interactions were known previous to their investigation, however they created a way to determine what and where they were on the potential energy surface and used it to linearly combine two functionals that had opposite spurious interactions. The various DFT functions were compared to high-end wavefunction calculations using HF as a baseline as it has no electron correlation and therefore no description of dispersion interactions. All of the conventional functionals they surveyed had spurious attractive and repulsive interactions in the dispersion bonding range.

Once a truly dispersion-less functional was created, a correction term that decayed with the appropriate R^{-6} term was then added. Therefore spurious interactions need to be considered as a possible cause of contradictory results, and that conventional DFT functionals may not be able to describe adequately the effects of dispersion on structure. This means that the true geometry may not be determined with available DFT functionals.

After determining optimized geometries for the molecules, the energies and orbitals provided in the output were studied. As mentioned in a previous section, an early and still widely used model of group 14 metallocenes proposed that a metal-centered sp^2 lone pair is the explanation for the bending in these molecules. The calculated energies and shapes of the HOMOs (highest occupied molecular orbitals) and LUMOs (lowest unoccupied molecule orbitals) of the metallocenes were considered as a part of the present investigation. The percentages of atomic orbitals that contribute to certain molecular orbitals were used to help indicate whether any could be considered to constitute an 'sp^2' type orbital, and thus whether the sp^2 lone pair model needed revision.

The plots of the HOMO-2 and HOMO-4 of the bent $PbCp^{3\text{-}iPr}_2$ structure (BP86-D3, #1) are pictured in Figure 1. The plot of the HOMO-2 shows the π-type inter-ligand interaction, and the plot of the HOMO-4 shows the electron density on the lead cation. The HOMO-4 illustrates the electron density of the non-bonding lone pair. It was calculated to have 14.53% contributed from the lead 6s orbital, but does not have any contributions from the lead p-orbitals.

a. 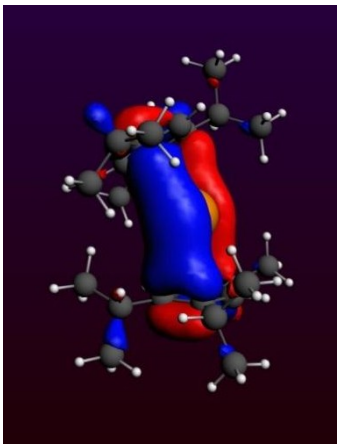 b. 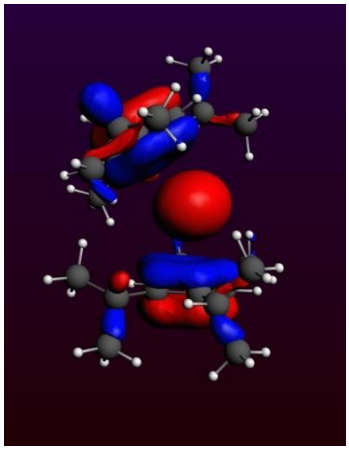

Figure 1. a. HOMO-2 of $PbCp^{3\text{-}iPr}_2$ (BP86-D3, #1); b. HOMO-4 of $PbCp^{3\text{-}iPr}_2$ (BP86-D3, #1).

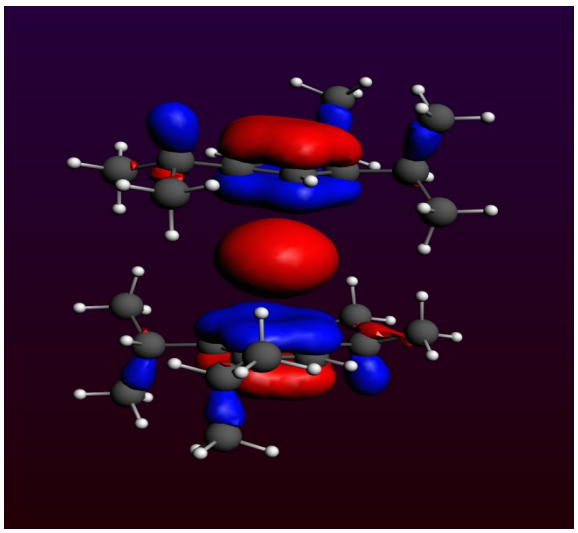

Figure 2. HOMO-4 of the linear $PbCp^{3\text{-}iPr}_2$ conformation calculated with BP86 (#3). The shape of the orbital on the metal cations is similar to that in the bent configuration with 17.32% of the electron density contributed from the lead 6s orbital.

Figure 2 pictures the HOMO-4 of the linear $PbCp^{3\text{-}iPr}_2$ structure that was calculated with the BP86 functional (#3). The calculated contributions from the lead are again from s-orbitals with 17.32% of the electron density contributed from the lead 6s orbital. The electron density on the lead atom is similar in both bent and linear structures, with only s-orbital contributions from the lead atom. The computed HOMO-4 of the $PbCp^{3\text{-}iPr}_2$ molecule with the BP86 and the BP86-D3 functionals are different from those expected for a lead molecule with a non-bonded electron pair in a sp^2-hybridized molecular orbital, and is not consistent with a lone pair explanation for the bending.

Energy differences between molecules can only meaningfully be compared if the same functionals, basis sets, and integration levels are used. Therefore for comparison, a calculation of the $PbCp^{3\text{-}iPr}_2$ structure with BP86-D3 with no restrictions (#1) and one with imposed linear geometry (#2) was performed. The difference in energy between bent and linear structures was slight, with the bent structure favored by 1.6 kcal mol^{-1}. This difference in energy may be too small to represent significant data. For calculations in general, energy differences between computed and experimental values of $\leq$ 1 kcal mol^{-1} are considered to have reached 'chemical accuracy'. However, as this is an organometallic compound with a heavy metal center, it is likely that the error of the calculation is (ca. 2 kcal mol^{-1})[177] is comparable to the energy difference between the confirmations.

While $PbCp^{3\text{-}iPr}_2$ is calculated to have a bent structure with the D3 dispersion correction added to the functional, there is uncertainty in the conclusion about the 'true' structure that stems from the fact that the energetic differences between the two conformations are so small. This is

compounded by the generally inadequate treatment of dispersion effects in functionals (discussed above) [176], which also weakens confidence in the significance of the results.

A group 14 metallocene that has been established to be bent in the solid state, $PbCp^{4\text{-}Me}_2$, was chosen for comparison with the crystallographically linear $PbCp^{3\text{-}iPr}_2$. The bent $PbCp^{4\text{-}Me}_2$ molecule is typical of substituted $PbCp_2$ molecules with a 139.7° Cp – Pb – Cp angle. Unlike the $PbCp^{3\text{-}iPr}_2$ molecule, $PbCp^{4\text{-}Me}_2$ optimized to bent structures with both the dispersion-corrected and uncorrected forms of BP86 functional. (#12 and 14, Table 2) There was a significant difference in angle between the two types of functional. The average bending angle of this molecule with the dispersion uncorrected BP86 functional was 165°, which is 25° from the crystal structure angle. When the dispersion patched BP86-D3 functional was used, the average angle in $PbCp^{4\text{-}Me}_2$ was 144°, and within 5° of the crystal structure value. Therefore, in this case, the dispersion-correction was not needed to ensure the bending in this molecule, but it did model the $PbCp^{4\text{-}Me}_2$ molecule better than without.

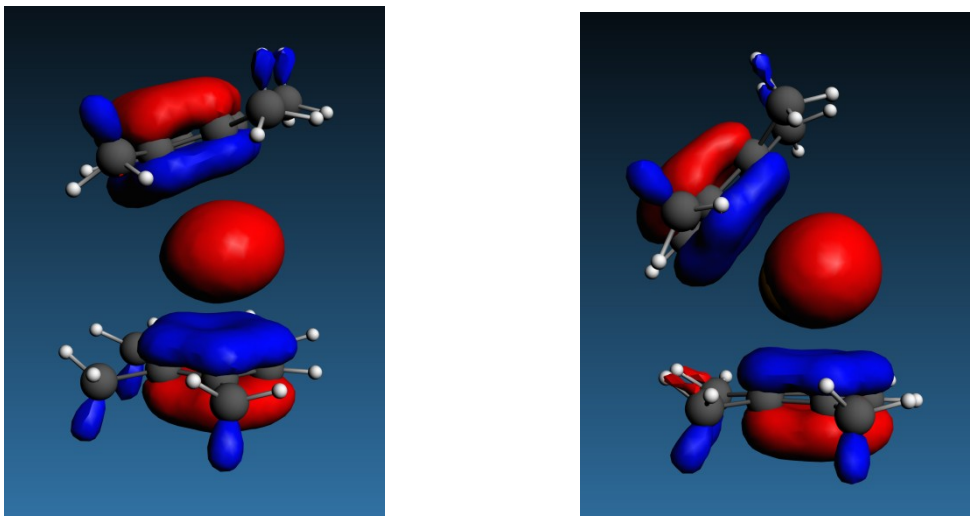

Figure 3 The bent $PbCp^{4\text{-}Me}_2$ molecule. Left is the HOMO-4 calculated with the dispersion-uncorrected BP86 functional, and the HOMO-4 on the right is calculated with the dispersion corrected BP86-D3 functional.

Table 2. The properties of referenced calculations of the $PbCp^{4\text{-}Me}{}_2$ molecule (Int = Integration grid; Start geom = how was the starting geometry was obtained)

#	Functional	Basis Set	Int	Dispersion correction?	Symmetry imposed? Relativity correction applied?	Start geom	End angle	Me-Me closest contact (Å)	Bond energy (Hartree)
12	BP86-D3	TZ2P	5	Yes	No; Yes	Crystal structure (bent)	142.782	4.012	-9.50518581
13	BP86-D3	Pb: DZ, C, H: DZP	5	Yes	No; Yes	Crystal structure (bent)	142.729	4.010	-9.43347906
14	BP86	Pb: QZ4P C,H TZ2P	7	No	No; Yes	**12**	165.627	5.074	-9.45390618
15	BP86	Pb:DZ5p frozen core C,H TZ2P	6	No	No; Yes	**12**	163.948	5.009	-9.44934407
16	BP86-D3	Pb:DZ5p frozen core C,H TZ2P	6	Yes	No; Yes	**12**	145.972	3.865	-9.50027808
17	BP86	Pb:DZ5d frozen core C,H TZ2P	6	No	No; Yes	**15**	165.735	5.241	-9.43363893
18	BP86-D3	Pb:DZ5d frozen core C,H TZ2P	6	Yes	No; Yes	**16**	144.008	3.957	-9.48511068

As seen in Figure 3, the HOMO-4 of the $PbCp^{4\text{-}Me}{}_2$ molecule appears to have a substantial amount of s-character. The calculated molecular orbital of the structure in Figure 3 has 18.88% contribution from the lead 6s orbital, while the dispersion corrected structure has some p-character with 18.35% contribution from the lead 6s orbital and 3.61% contribution from the lead $5p_y$ orbital. This conclusion is similar to that made about nature of the HOMO-4 in the molecule $PbCp^{3\text{-}iPr}{}_2$; i.e., that even the known bent group 14 metallocenes do not have a metal-centered sp^2 lone pair.

The dispersion-corrected BP86-D3 functional was able to reproduce the bending angle of $PbCp^{4\text{-}Me}{}_2$ more closely than did the corresponding non-corrected BP86 version. These

calculations show that the geometry is extremely sensitive to the functional used, and that there are enough inconsistencies in the results to cast doubt on whether the added dispersion interaction corrections themselves are the source of the bending. However, expectations for this section changed on analysis of the lead structures. The lead compounds chosen for comparison and control instead produced bent and linear structures within the DFT computational error. The ambiguity of the preferred geometry for lead molecules with their incredibly shallow potential energy surfaces will likely remain until not only the exchange, but also the electron correlation of the exact density functional can be calculated directly.[150]

The modeling of the similarly 'floppy' alkaline earth metallocenes may well encounter related limitations, as the energy difference between bent and linear geometries is expected to be small, and the accurate computation of dispersion interactions between the ligands is likely to be difficult.

Computations and structures of group 2 complexes

The structures of the group 2 metallocenes have been baffling and challenging scientists for many years and have been investigated before, with calculations ranging in sophistication from molecular mechanics[144] to DFT to *ab initio* approaches. The prevailing opinion is that a combination of van der Waals forces and polarization from d-orbital overlap is involved in the bending of these structures. Now that dispersion forces can be modeled in DFT calculations, they can be investigated along with the previously investigated polarization and orbital overlap in these stereochemically non-rigid systems.

Given that the dispersion-corrected functionals did not function as expected with the lead-containing molecules, and knowing that the conformation of the alkaline-earth systems is also likely to be a very sensitive function of the level of theory employed, this investigation cannot be expected to provide definitive answers about the origin of bent or linear geometries. They do, however, highlight some of the ambiguities involved in these types of investigations.

Decamethylcalcocene

The calculations with the decamethylcalcocene, $CaCp^*_2$, molecule were typical of the results obtained with the group 2 systems. This molecule has been structurally authenticated both in the solid state[178] and in the gas-phase[133], and has been found to be bent in both environments (ring centroid–Ca–ring centroid angles of 147° and 154(3)°, respectively). As expected, the geometry optimization of the $CaCp^*_2$ molecule converged to a bent structure with angle of 155.7° when the typical parameters — the functional BP86 with added dispersion corrections (BP86-D3, #20, Table 3) and a large basis set with extra polarization functions, TZ2P — were used. In addition to the BP86-D3 functional, the M06L functional also converged as expected to a bent structure with an angle of 159° (#24), similar to the angle of 156° obtained with the BP86-D3 functional.

When the functional used was not dispersion-corrected (BP86, #19), the final structure was linear. This could indicate that the dispersion forces are necessary for this bending to happen. Since the ambiguity of the results in the lead section causes some uncertainty for results based on dispersion forces, more computations were conducted in attempt to establish this conclusion more thoroughly.

An initially encountered oddity arose from the just described set of calculations based on the initial geometry. When another geometry optimization of the $CaCp^*_2$ molecule was performed

Table 3. The properties of referenced calculations of the $CaCp^*_2$ molecule (Int = Integration grid; Start geom = how was the starting geometry was obtained)

#	Function	Basis Set	Int	Dispersion	Symmetry imposed? Basis set modification	Start geom	End angle	Me-Me closest contact (Å)	Bond energy (Hartree) imaginary frequencies
19	BP86	TZ2P	5	No	No	UI builder	178.654	5.168	-10.69421964
20	BP86-D3	TZ2P	5	Yes	No	UI builder	155.719	3.986	-10.75793193 -10 cm^{-1}
21	BP86-D3	TZ2P	5	Yes	No; Relativity correction	linear	180.000	5.073	-10.74715168 from ADF update check series
22	BP86	TZ2P	5	No	No	**19**	178.686	5.176	-10.69416234
23	BP86	Ca: QZ4P; C,H: TZP	6	No	C2sym	**20**	175.046	4.963	-10.66716557
24	M06L	Ca: QZ4P; C,H: TZ2P	8	Yes	No	**20**	158.933	3.972	-11.42854862
25	BP86-D3	Ca:3pSZ C:TZP1s H:TZP	7	Yes	No; Large frozen core used	**20**	179.033	5.397	-10.69421830
26	BP86-D3	Ca: 3pTZ2P C:TZP1s H:TZP	6	Yes	No; Large frozen core used	**20**	155.861	4.013	-10.71673428
27	BP86-D3	Ca: 3pDZ C:TZP1s H:TZP	5	Yes	No; Large frozen core used	**26**	157.458	4.071	-10.69607734
28	BP86	Ca:QZ4P C:TZP1s H:DZP	5	No	No; Frozen cores on carbons	**43**	172.595	4.871	-10.65341178

with the same functional and basis set, BP86-D3 and TZ2P, but with a linear instead of a bent initial structure, the optimized structure remained linear (#21). When the bond energy is compared, the bent optimized geometry (#20) is about 2 kcal mol^{-1} more stable than the linear optimized geometry (#21). As noted in the previous section, this amount is very close to the error limits currently achievable with DFT methods on compounds containing heavy metals, and therefore the results were ambiguous.

As the d-electrons and polarizability of the metal cation are believed to be critical to the ability of these compounds to bend, the geometries of a series of molecules with varying amounts of d-electron functions in the basis set and without the standard added polarization functions were calculated. Unlike with the basis sets used for the lead compounds, a SZ (single-zeta quality) basis set, which did not have any d-electron functions, was available for this computation. As expected, when the SZ basis set was used on the central cation with the BP86-D3 functional, the resulting structure was not bent. When the basis set was increased to the next level, DZ (double-zeta), which does have d-electron functions, it converged to a bent structure. The angle of the bent structure converged with the DZ basis set was in agreement to the computation with the larger, high quality basis set (TZ2P).

This calculation was completed with a frozen core basis set, keeping the dispersion-patched functional, BP86-D3. As the core electrons in group 2 are not well separated from the valence orbitals, and the latter could potentially influence the bending in these structures, the '3p' basis set with a frozen core up to an including the 3p electrons was used to prevent the 'outer core' (3s and 3p) electrons from adjusting during the geometry optimization. Again both the TZ2P (#26) and SZ (#25) quality basis sets were used in this pair of computations. The geometry optimization with the frozen core and TZ2P quality basis set converged to a bent structure with an angle of 156°, but the optimization with the frozen core and SZ quality basis set converged to a linear structure from a bent structure. This suggests that the bending of these molecules is impossible without the polarization or d-electron functions in the basis set. However, as noted above, this molecule also needs the added dispersion functions for the molecule to converge to a bent geometry. When the SZ basis set was increased to DZ quality (#27), having d-electron

functions but no explicitly added extra polarization functions, the geometry optimized to a bent structure with an angle of 157°. In contrast, when the quality of the metal cation was increased to the best the program had to offer, QZ4P, with the BP86 functional there was not any significant bending due to the basis set alone (#28).

Decamethylstrontocene

The computational results of decamethylstrontocene ($SrCp^*_2$) are largely similar to the $CaCp^*_2$ results. Decamethylstrontocene is found to be bent in the gas-phase (149(3)°),[134] but has yet to be structurally authenticated in the solid state. Geometry optimization was performed with the dispersion-patched functionals PBE-D3 (#40, Table 4), BP86-D3 (#31), and BLYP-D3 (#37), all of which converged to bent structures with angles in the range of 150.5–151.4°. That these computations optimized to bent structures with angles close to the known value was expected based on the results of $CaCp^*_2$. Also calculated was the geometry optimization with the functional M06L (#35), which is parameterized to provide an accounting for dispersion forces; the molecule converged as expected to a bent structure with an angle of 141.4°. This angle is ~10° more acute than the previous group of functionals, and unlike the previous group is outside the range of error of the $SrCp^*_2$ gas-phase angle measurement. Unexpectedly, a geometry optimization calculation with the functional PBE (#38) converged to a bent structure with an angle of 159.7° even though PBE does not have any added or built-in dispersion. A plausible explanation for this result could be that the potential energy surface of these molecules is very shallow and as the starting geometry of this calculation was taken from a previously optimized bent structure, it converged to a local minimum on the potential energy surface.

Table 4. The properties of referenced calculations of the $SrCp^*_2$ molecule (Start geom = how was the starting geometry was obtained)

#	Functional	Basis Set	Integration Dispersion correction?	Symmetry imposed? Relativity correction applied?	Start geom	End angle	Me-Me closest contact (Å)	Bond energy (Hartree) imaginary frequencies
29	BP86	TZ2P	7; No	No; Yes	**21**	180	5.597	-10.66904559
30	BP86-D3	TZ2P	7; Yes	No; Yes	**21**	178.255	5.430	-10.72982437 -21,-19 cm^{-1}
31	BP86-D3	TZ2P	7; Yes	No; Yes	No bias	150.550	3.957	-10.73344102 -5 cm^{-1}
32	BP86	TZ2P	5; No	No; Yes	**31**	179.063	5.553	-10.66920715
33	BP86	Sr: QZ4P TZ2P other	5; No	No sym; No correction	**31**	172.273	5.228	-10.67000471
34	BP86	Sr:DZ C,H: DZP	6; No	No; Yes	**44**	176.824	5.409	-10.58286115
35	M06L	Sr: TZ2P C,H: DZP	7; Yes	No; Yes		141.369	3.726	-11.36417845
36	BLYP	TZ2P	6; No	No; Yes	**35**	~180		-10.26793068
37	BLYP-D3	TZ2P	6; Yes	No; Yes	**31**	151.376	4.049	-10.33470875
38	PBE	TZ2P	6; No	No; Yes		159.686	4.547	-10.81549436
39	PBE-D3	TZ2P	5;Yes	D(5D); Yes	**29**	180.000	5.539	-10.84717344
40	PBE-D3	TZ2P	5; Yes	No; Yes	**31**	150.689	4.030	-10.85043334
41	BP86	Sr: QZ4P C: 1s TZP H:DZP	5; No	No-sym	**43**	172.489	5.200	-10.63579807

Also calculated were a few geometry optimizations that produced expected results. The first calculation with the original non-corrected functional, BP86 (#29), used a D_{5d} symmetrized structure of $CaCp^*_2$, with Sr replacing Ca. As expected based on the $CaCp^*_2$ results, this computation of $SrCp^*_2$ converged to a linear symmetrized structure even when the symmetry constraints for calculations were turned off. This calculation was repeated with a bent initial geometry (#32) and again optimized to an essentially linear structure. The functional BLYP was

also used (#36), and on optimization of an initially bent metallocene, it optimized to a linear geometry as expected.

Repeating the results observed with $CaCp^*_2$, the geometry optimization of $SrCp^*_2$ with symmetrically perfect linear structures using the functionals BP86-D3 (#30) and PBE-D3 (#39) resulted in linear structures. With both a bent and linear structure computed with the same functional, energy comparisons can be made. The bent structures, with both the BP86-D3 and the PBE-D3 functionals, converged to a potential energy minima at 151°, and were more stable than the perfectly linear structures by 2.3 kcal mol^{-1} and 2 kcal mol^{-1}, respectively.

Another $CaCp^*_2$ calculation that was repeated for $SrCp^*_2$ was the geometry optimization of the dispersion non-corrected BP86 functional, with a basis set that included the highest number of polarization functions and added d and f orbital functions that the ADF program provides. Similarly to the $CaCp^*_2$ calculation, the $SrCp^*_2$ geometry optimization (#33) did not optimize to a bent structure.

As seen in previous calculations, the initial geometry can affect the final geometry in these systems as they have shallow potential energy surfaces. Therefore this previous geometry optimization was repeated with a more acute initial angle and the same highest-quality basis set that was used in the previous calculation (#41). Once again, the $SrCp^*_2$ geometry optimization optimized to a linear structure.

Decamethylbariocene

Unlike the decamethylcalcocene and decamethylstrontocene calculations mentioned above, decamethylbariocene, $BaCp^*_2$, converged to a bent structure with both dispersion-corrected and

dispersion non-corrected functionals. Only when the initial geometry was linear with D_{5d} symmetry and symmetry constraints were imposed during geometry optimization (#44, Table 5)

Table 5. The properties of referenced calculations of the $BaCp^*_2$ molecule (Start geom = how was the starting geometry was obtained)

#	Functional	Basis Set	Integration Dispersion correction?	Symmetry imposed? Relativity correction? Basis set modification	Start geom	End angle	Me-Me closest contact (Å)	Bond energy (Hartree) imaginary frequencies
42	BP86	TZ2P	5; No	No; Yes	**29**	148.413	4.310	-10.68632877
43	BP86-D3	TZ2P	5; Yes	No; Yes	**32**	140.345	3.877	-10.75061777
44	BP86-D3	TZ2P	7; Yes	Yes; Yes	**30**	180.000	5.795	-10.74429552 -21, -19 cm^{-1}
45	BP86-D3	TZ2P	5; Yes	No; Yes	**32**	140.347	3.878	-10.75024135 ADF update consistency check
46	BP86	TZ2P	5; Yes	No; Yes	**32**	159.363	4.828	-10.68502657
47	BP86	Ba: QZ4P C,H: T2ZP	6; No	Yes: C_2 sym; Yes; Yes: large frozen core used initially, but not in final	**43**	160.436	4.920	-10.68580490
48	BP86-D3	Ba: DZ.d4 C,H: T2ZP	6; Yes	No; No	**43**	141.051	3.943	-10.74544565
49	BP86-D3	TZ2P	6; Yes	No; Yes	**44** with X-M bond length doubled	140.389	3.920	-10.75040062
50	PBE	TZ2P	5; No	No; Yes		144.763	4.230	-10.83315154
51	PBE-D3	TZ2P	5; Yes	No; Yes		140.426	3.973	-10.86744659

did the geometry of $BaCp^*_2$ converge to a linear structure, but with imaginary frequencies at -19 and -21 cm^{-1} that indicate that the geometry did not reflect a minimum, local or otherwise. All of

the non-constrained geometry optimizations of decamethylbariocene converged to a bent structure as expected from its structural authentications as being bent in the solid state, with a 131° centroid-mtal-centroid angle,[178] and in the gas-phase, at 148(6)°.[134] The geometry optimization with the BP86 functional without added dispersion functions converged to a bent structure with an angle of 148° (#42). This is unexpected, both as the initial geometry was linear, and as decamethylcalcocene and decamethylstrontocene required functionals with the added D3 description of dispersion interactions to converge to a bent structure. All calculations with dispersion-corrected functionals converged to bent geometries of $BaCp^*_2$ with angles in the range 140-141°. The first calculation with the dispersion corrected BP86-D3 was initiated with a linear geometry (#43), but unlike with $SrCp^*_2$ and $CaCp^*_2$, which were presumably trapped in a local minimum at a linear structure, converged to a bent structure. This calculation was repeated once more after the yearly ADF program update (#45), but the structure of $BaCp^*_2$ did not optimize to a linear geometry without the previously described symmetry constraints. When the functional was changed to the dispersion-corrected PBE-D3 (#51), the geometry optimization converged similarly to those just mentioned above, with an angle of 140°.

Similarly to $CaCp^*_2$, $BaCp^*_2$ was optimized with the dispersion corrected BP86-D3 functional and the lowest quality basis set available for barium, DZ (#48). The unoccupied d-electron functions were unable to be excluded completely as SZ, the only basis set that excludes them, is not provided for heavier elements like barium. This geometry optimization converged to a bent structure despite the lack of polarization functions and unoccupied orbital functions.

As mentioned above, the computation with the functional BP86, a functional without dispersion-corrections, converged to a bent geometry, counter to expectations. This calculation

was repeated with a perfectly symmetrized initial structure (#46), but again $BaCp^*_2$ optimized to a bent structure. Also calculated was the geometry optimization with the PBE uncorrected functional (#50), where $BaCp^*_2$ optimized to a bent structure with an angle of 145°. The dispersion-uncorrected BP86 (#42) and PBE (#50) functionals were the only two with angles (148.4° and 144.8°, respectively) within the error of the 148(6)° gas-phase structure. The dispersion-corrected functionals produced angles that were more acute than this by 8-11°. The geometry optimization of $BaCp^*_2$ with the functional BP86-D3 converged to a centroid-metal-centroid angle of 140° (#43); compared to the molecule restrained at 180° (#44), the bent molecule was 4 kcal mol^{-1} lower in energy.

Decamethylmagnesocene

Decamethylmagnesocene, $MgCp^*_2$, was only briefly studied, as it is found it to be linear when structurally authenticated.[133] As mentioned in previously published work, due to short metal-ligand distances in $MgCp^*_2$, the steric hindrance of the pentamethylcyclopentadienyl ligands inhibit any bending.[12] A linear structure for $MgCp^*_2$ is to be expected when the shortest Cp*-Cp* distances are compared between various compounds. The shortest Cp*-Cp* distances in the bent $CaCp^*_2$ and $YbCp^*_2$ are about 410 pm, for example, while distance between rings in the parallel $MgCp^*_2$ structure is also 410 pm.[133] Therefore, $MgCp^*_2$ was calculated once each with both the dispersion non-corrected BP86 (#52, Table 6) and the dispersion-patched BP86-D3 (#53) functional for thoroughness and to check for functional induced artifacts. These computations converged as expected to the linear geometry.

Table 6. The properties of referenced calculations of the $MgCp^*_2$ molecule (Start geom = how was the starting geometry was obtained)

#	Functional	Basis Set	Integration Dispersion correction?	Symmetry imposed? Basis set modification	Start geom	End angle	Me-Me closest contact (Å)	Bond energy (Hartree)
52	BP86	TZ2P	5; No	No	**31**	180.000	4.564	-10.62819737
53	BP86-D3	TZ2P	5; Yes	No	**31**	173.762	4.030	-10.69613112
54	BP86-D3	Mg: Zora QZ4P; C,H: TZ2P	6; Yes	ADF calculated symmetry imposed	**20**	177.811	4.212	-10.69692566
55	BP86	TZ2P large frozen core on all	6; No	No; Relativity correction; large frozen core used	**43**	180.000	4.642	-10.60879118
56	BP86-D3	Mg: QZ4P; C,H: TZ2P	6; Yes	No; Relativity correction; large frozen core used	**43**	176.153	4.122	-10.69219323

Previous calculations of decamethylstrontocene

The $SrCp^*_2$ molecule has recently been investigated and published by Nief *et al*. in 2013. Their work was a computational investigation into $SmCp^*_2$ that used the isovalent strontium compound as a more ionic counterpart to the samarium compound.[179] Two of their geometry optimization calculations were performed with the same computational suite as used in this work, ADF, with the functionals B3LYP-D and B3LYP-D3, while the remainder were calculated with the Gaussian program. Given the knowledge of this prior work, after completing the calculations of the $SrCp^*_2$ molecule for the present work, Nief's B3LYP and AIM calculations were repeated with additions based on the findings of the present work.

The B3LYP-D and B3LYP-D3 functionals used by Nief *et al*. with the ADF program were not used for the current work despite the fact that the uncorrected functional, B3LYP, is one of

the most widely used density functionals. It is known that while B3LYP works well for small organics, it does poorly for heavier elements, highly charged compounds, and molecules that have internal charge separation.[180,181] This is likely due to its method of creation, namely parameterization from a training set based on the noble gases instead of being derived from first principle theory. Most relevant to this work is the fact that there were not any compounds that had dispersion type interactions included in the training set.[152] It has become apparent with improvements in computing power and basis sets that the accuracy of B3LYP, which historically was often combined with Pople's relatively small 6-31G basis set for computational efficiency, is often the result of a fortuitous canceling of errors,[150] which introduces great uncertainty when this functional is used to extrapolate past its well-studied domain with small organic molecules. In their paper introducing the dispersionless APF functional, Petersson, Austin, and Frisch used the classic test model for dispersion interaction, the Ar_2 dimer, to find spurious interactions that the various functionals may have in the dispersion region. This showed that the B3LYP functional predicts a *repulsive* interaction instead of an attractive one, with attractive forces from 2–3 Å and with spurious repulsive forces past 3 Å, where the range of dispersion interactions begins.[150] With a perfectly dispersionless functional, a computation with the added dispersion interactions term would be less likely to optimize to a false local minima. Petersson, Austin, and Frisch were able to create a description of dispersion forces that included not only the R^{-6} decay of the first term, but also the R^{-8} and R^{-10} terms. This is important as higher order terms in dispersion perturbation contribute 20–30% of dispersion energy.[151] In other attempts to model dispersion interactions, often the only correction employed is an upscaling of the C_6 term, which by itself is an inadequate treatment, as it introduces long-range attraction errors.[151] Therefore,

functionals like B3LYP that made no attempt to model the R^{-6} decay are more likely not to describe these long-range interactions correctly.[176]

Along with the choice of functional in ADF, the Nief group's goal of using the $SrCp^*_2$ molecule as an ionic isovalent comparison to $SmCp^*_2$ led to a different approach and conclusion from the one used and reached in the present work. They concluded that only dispersion-corrected functionals produced bent final structures while the uncorrected functionals produced linear structures, and that therefore the unusual bending in decamethylstrontocene was only due to dispersion forces.

The work of the Nief group, however, is subject to the same impediments as were found when investigating the lead and group 2 structures in the present work, that difference in energies between bent and linear are too close to the error of the calculations to produce meaningful results and that the results in this work point to a combination of dispersion forces and polarization through d-orbital interaction with the core electrons.

A few other items reported by Nief *et al*. were counter to expectations, which prompted a repeat of their calculations with the functionals used in the present work. Part of their analysis was the atoms in molecules (AIM) bonding analysis[182], which they used to support their thesis that decamethylsamarocene is more covalent than decamethylstrontocene. The AIM analysis finds the location of the minima in electron density between two atoms and the path energy at that point. This density also gives information on the type of bond between the two atoms. With their dispersion-corrected functional, B3LYP-D, there were only three of the ten expected bond-points between the pentamethylcyclopentadienyl ligands and the strontium cation. Their single-point computations with the B3LYP and B3LYP-D functionals, used for AIM analysis, were

repeated for this work with a larger basis set, along with the BLYP-D3 and PBE-D3 dispersion-corrected functionals and the BP86 and BLYP functionals. Images of AIM calculated results with the B3LYP-D, the PBE-D3, and the BP86 functionals are found in Figures 4 to 6, respectively. Of these repeated and new computations, only the repeat of the single point AIM calculation with the B3LYP-D functional did not produce the ten expected C–Sr bond critical points (BCP). This data is summarized in Table 7. The linear structures all contained the expected 10 BCP, and the other bent structures contained 13 BCP, which includes three bond critical points between the two cyclopentadienyl ligands that could indicate dispersion interactions.

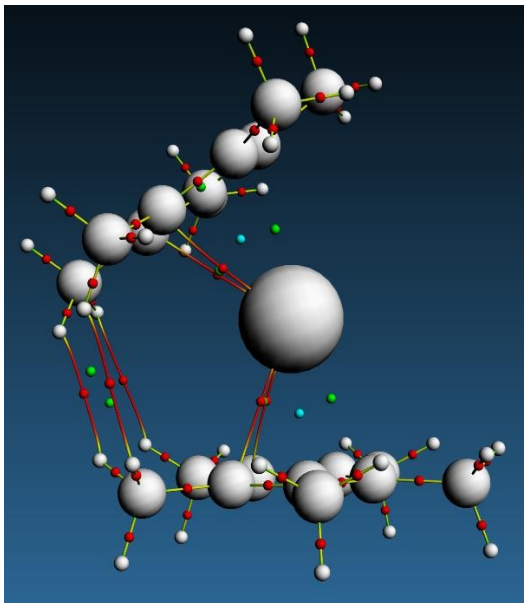

Figure 4. AIM plot of $SrCp^*_2$ calculated with the B3LYP-D functional and the TZ2P basis set. There are AIM bond paths from only two ring carbons of each cyclopentadienyl to the strontium cation, and bond critical paths between the two ligands. This structure was calculated as described by Nief *et al*. and the result is very close to the one found in their 2013 paper.[179]

Table 7. A summary of AIM (atoms in molecules) analysis of decamethylstrontocene. For each functional used, the sum of the path energies from each ligand is given along with their total and average for comparison between the functionals. Also included is the total number of bond critical points calculated and the total between strontium and its ligands.

Functional	Cp^*_1 - M path energy (au)	Cp^*_2- M path energy (au)	Sum of M-X bond path energy (au)	avg energy per M-C bond critical path (au)	$N_{\text{all bond critical paths}}$ ($N_{\text{M-X paths}}$)
B3LYP	0.13185	0.13194	0.26379	0.026379	13(10)
B3LYP-D	0.0512	0.0512	0.1024	0.0256	7(4)
PBE-D3	0.13391	0.13382	0.26773	0.026773	13(10)
BP86	0.126	0.126	0.252	0.0252	10(10)
BLYP	0.1145	0.1146	0.2291	0.02291	10(10)

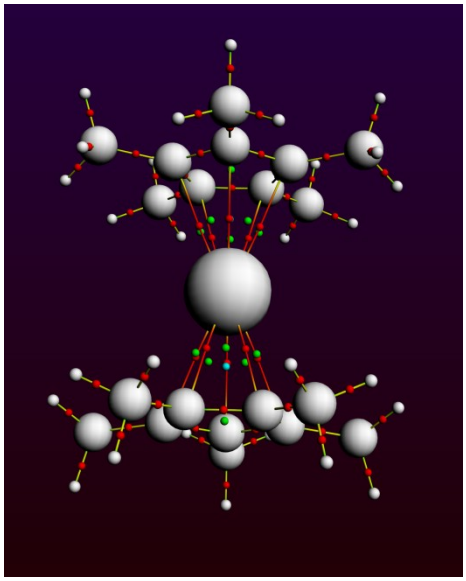

Figure 5. AIM plot of $SrCp^*_2$ calculated with the BP86 functional but without the D3 correction. The red lines with red dots between the cyclopentadienyl rings and the central cation indicate calculated bond critical paths. This figure shows that there are bond critical paths from all ten cyclopentadienyl ring carbons to the strontium cation.

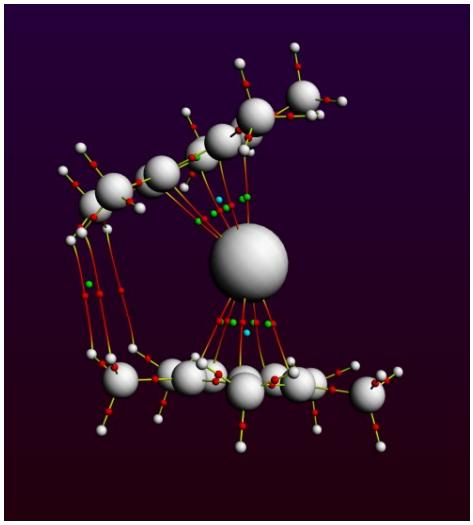

Figure 6. AIM plot of $SrCp^*_2$ calculated with the PBE functional, the D3 correction and the TZ2P basis set. There are AIM bond critical paths from all ten of the cyclopentadienyl ring carbons to the strontium cation. Also in this bent structure are bond critical paths between the two ligands that indicate dispersion interaction adding to the bonding energy.

The numbers of the repeated AIM single point calculation with the B3LYP-D functional are in agreement with Nief *et al.*'s numbers, but are low compared to the numbers of other functionals used here. A well-cited paper written by Tassell and Kaltsoyannis, which included the AIM analysis of metallocenes and other ligands on actinides, found overall that the AIM Cp–M densities were all less than halide–M bonds in isostructural molecules, and as expected neither type of bond densities was as large as the covalent C–C bond densities of the ligands.[183] The criteria used by Tassell and Kaltsoyannis for AIM analysis was that bond density over 0.2 would be considered covalent and under 0.1 would be ionic for the bond critical point (BCP). Units are not regularly referenced with these values, but when cited are in au. An important discussion by Tassell and Kaltsoyannis was of the density of the C–M bond paths in the cyclopentadienyl ligand. When taken individually, their density is much lower than any other in similar molecules.

They then suggested that for Cp the energy of the 5 C–M paths should be added together as one path density, which produced densities in the correct range. The functionals used to calculate AIM bond critical points other than B3LYP-D in this work had densities in the range of the reference paper; namely 0.2 > density > 0.1 per Cp. For example, the single point AIM calculation with the PBE-D3 functional found a BCP of 0.13 hartrees per Cp ligand for a bent decamethylstrontocene molecule. In Nief's paper, the 'more covalent' Sm as well as the Sr compounds all had BCP densities that indicated ionic bonds. Even when adding the five Cp C–M bonds together, the BCP for a Cp ligand was significantly below the cut-off stipulated by Tassell and Kaltsoyannis for ionic bonding, namely 0.081 and 0.052 for their samarium compounds and 0.020 for $SmCp^*_2$ with the B3LYP functional.

When using different functionals with higher quality basis sets, the computations designed to reproduce the previous work generate AIM plots with bond paths indicating that, within the limitations of AIM calculations, the strontium cation fully bonds to the two cyclopentadienyl anions.

Computational artifacts from DFT theory

During the course of this investigation, when unexpected results were examined, it was found several times that various artifacts that were introduced in the set-up of the calculations did not get corrected during geometry optimization. This serves as a caution against automatically following common computational practices when working with conformationally floppy systems.

In the case of this study, the calcium and strontium metallocenes converged to a linear geometry when dispersion-corrected functionals were not used (#19 and #29, respectively). The process of optimization of these linear geometries was the source of artifacts of local minima on the potential energy surface in the computation of the dispersion-corrected functionals, BP86-D3 (#21, #30) and PBE-D3 (#39), later on. Essential to the procedure used for the convergence of these molecules was to gradually increase in quality of basis sets and integration values up to TZ2P and teVelde 5 minimum, respectively, instead of starting with these values. Prior computational studies[184,185] optimized these metallocenes to bent structures without dispersion-corrected functionals, unlike this work. The inability to replicate the bent structures could be due to this process of reoptimizing at successively higher levels of theory to minimize the use of computational resources, or that those previous studies were performed in different computational suites, ones that allowed customization of the basis sets for higher quality.

Another common practice, as structures converge to symmetrical geometries, is to use imposed symmetry in subsequent iterations to offset the increase in time and processor cost that the gradual increase in quality of basis sets and integration values requires. This caused the strontium and calcium metallocenes to converge to symmetrical (D_{5d}) geometries, instead of converging to near linear geometries ($170 < \theta < 180°$) (e.g., #29 vs. #32). Subsequently, when these perfectly symmetrical geometries were used as the source of the starting coordinates for computations using the dispersion-corrected functionals, BP86-D3 and PBE-D3, it was found that the linear structure is a local minimum on the potential energy surface for the bent geometries (e.g., #21 used for #30). When bent geometries were used as starting structures, or the ligand-cation distances were initially set at twice the normal values, the geometry

optimization converged to bent geometries that were more energetically stable than the linear ones.

Computations and structural analysis of $Ca(C(SiMe_3)_3)_2$

As stated in the introduction, $Ca(C(SiMe_3)_3)_2$ also displays a non-linear C-Ca-C angle of 149.7(6)° in its crystal structure, with ligands large enough that dispersion forces should exist in the molecule and affect its structure. As with the heavier $AeCp^*_2$ molecules, $Ca(C(SiMe_3)_3)_2$ is bent despite lacking valence electrons or d-electrons. The calculations of this molecule demonstrate that dispersion forces cannot be the only cause of bending and that the availability of polarized basis sets is critical for allowing molecules to bend during geometry optimization.

In a similar manner to computations with decamethylcalcocene, the geometry optimization of $Ca(C(SiMe_3)_3)_2$ with the dispersion-corrected BP86-D3 functional and TZ2P basis set converged to a bent structure with an angle of 146.6°, which is within 3° of the crystal structure angle (#58, Table 8). The other dispersion corrected functionals used, PBE-D3 (#67) and BLYP-D3 (#70), also converged within this same 3° range. These computations with $Ca(C(SiMe_3)_3)_2$ are in better agreement with its experimental data than the computations of decamethylcalcocene, which had angles that optimized to more than 10° away from the crystal structure angle. Computations on $Ca(C(SiMe_3)_3)_2$ with the M06L functional (#71), which incorporates corrections for dispersion by construction, did not optimize to a geometry close to the crystal structure. Instead, the $Ca(C(SiMe_3)_3)_2$ molecule converged to a structure that had a C-Ca-C angle of 115.6°. As was the case with $SrCp^*_2$ (#35), the parameterized M06L functional generated the most acute angle for this molecule by 30°.

Table 8. The properties of referenced calculations of the $Ca(C(SiMe_3)_3)_2$ molecule (Start geom = how was the starting geometry was obtained)

#	Functional	Basis Set	Integration; Dispersion correction	Symmetry imposed? Basis set modification	End angle	Me-Me and Ca-C avg (Å)	Bond energy (Hartree)
57	BP86	TZ2P	5; No	No	148.9	4.132 2.474avg	-15.14901564
58	BP86-D3	TZ2P	5; Yes	No	146.6	4.000 2.428avg	-15.28160676
59	BP86-D3	Ca:SZ TZP other	7; Yes	No	177.5	4.142 2.502avg	-15.27647431
60	BP86-D3	Ca:DZ TZP other	6; Yes	No	151.6	4.034 2.437avg	-15.22173755
61	BP86-D3	Ca:DZP TZP other	5; Yes	No	147.4	3.981 2.418avg	-15.23270188
62	BP86	Ca:SZ, TZP other	7; No	No	180.0	4.251 2.549avg	-15.14565551
63	BP86	Ca:DZ, TZP other	6; No	No	180.0	4.316 2.479avg	-15.08855659
64	BP86	Ca:DZP, TZP other	6; No	No	147.8	4.151 2.464avg	-15.10067942
65	BP86-D3	Ca3p TZ2P; C:1sTZP; Si:2pTZP H:TZP	5; Yes	No; large core	149.9	4.015 2.445avg	-15.20466889
66	BP86-D3	Ca:3pSZ; C:1sTZP; Si:2pTZP H:TZP	6; Yes	No; large core	178.8	4.298 2.518avg	-15.20847729
67	PBE-D3	TZ2P	5; Yes	No	146.1	4.125 2.442avg	-15.43388813
68	PBE	TZ2P	5; No	No	147.1	4.149 2.466avg	-15.36148010
69	BLYP	TZ2P	5; No	No	150.0	4.221 2.503avg	-14.61180410
70	BLYP-D3	TZ2P	5; Yes	No	149.8	4.079 2.452avg	-14.74961634
71	M06L	TZ2P	6; Yes	No	115.6	3.614 2.404avg	-16.36314193

Contrary to expectations based on the group 2 metallocenes, the dispersion non-corrected functionals used, BP86 (#57), PBE (#68), and BLYP (#69), also converged to bent structures with the $Ca(C(SiMe_3)_3)_2$ molecule. Not only did they converge to bent structures, but the C-Ca-C angles calculated were just as accurate as those with the dispersion-corrected functionals

(excluding M06L) used for this molecule. This similarity in angles, despite the difference in dispersion forces between the two functionals, lends credence to the theory that dispersion forces are not the only cause of these bent molecules. Therefore, just as with the group 2 metallocenes, a series of calculations was conducted where basis sets were used that varied in amounts of polarization and d-orbital functions.

These previous computations with the $Ca(C(SiMe_3)_3)_2$ molecule produce consistent bent angles regardless of the presence of dispersion corrections in the functional. The next group of computations explored the effect of limiting d-orbital or polarization functions in the basis sets, as was done with the metallocenes, to ascertain if their absence would have an effect on the bending angle. As mentioned earlier about the basis sets used in this set of calculations, the SZ basis set does not have any d-orbital or polarization functions, the DZ basis set has no polarization and a limited number of d-orbital functions, and the DZP basis set has both d-orbital and polarization functions; all three basis sets are of lower quality in contrast to the high quality of the TZ2P basis set used for the previous $Ca(C(SiMe_3)_3)_2$ geometry optimizations. These lower quality basis sets were only used on the calcium cation, as it is the polarizability and presence of d-orbital functions in calcium that is proposed to affect the bent nature of the molecule.

The use of the SZ basis set on calcium produced linear structures with both regular (#62) and dispersion-corrected (#59) functionals. This result with the dispersion-corrected functional was observed previously in decamethylcalcocene (#25) where linear structures were computed when a basis set that did not include d-orbital and polarization functions was used. This supports the theory that polarizability and the availability of the 3d orbitals is important in these calcium-containing molecules.

When the DZ basis set was used, the results with regular (#60) and dispersion-corrected (#63) functionals differed from each other. Similar to decamethylcalcocene (#27), the dispersion-corrected functional (#63) converged to a bent molecule with the DZ basis set. However, when the DZ basis set was used on the calcium cation with a non-dispersion-corrected functional (#60), the structure of $Ca(C(SiMe_3)_3)_2$ optimized to a linear geometry. The dispersion-corrected functional was able to bend this molecule with the basis set DZ where the uncorrected functional was not able to do so.

Finally, the geometry optimization with the DZP basis set, when either dispersion-corrected (#61) or dispersion–uncorrected (#64) functionals were used, converged to bent structures with angles in the range of 147-148°.

As mentioned in the introduction to this chapter, the alkaline-earth elements do not have as much separation between core electrons and valence electrons as the rest of the periodic table. The alkaline-earth elements are thought to have an 'outer core' of electrons that interacts with ligands (e.g., the (*n*-1)p level; 3p for Ca, 4p for Sr, 5p for Ba). This outer core is posited to interact with low energy unfilled d-orbitals to polarize the outer core electrons, which causes the bending in various alkaline-earth molecules. Since the outer core is thought to play a part, a feature that freezes various amounts of core electrons was tested to find if it would inhibit bending in the $Ca(C(SiMe_3)_3)_2$ molecule. For the calcium cation, in an attempt to freeze the interacting outer core electrons, the chosen basis set out of those offered by ADF was the one that included the electrons frozen through 3p. When this computation was completed with the dispersion-corrected BP86-D3 and the 3p-frozen TZ2P basis set (#65), the molecule converged to a bent geometry with an angle of 149.9° while when the basis set of the calcium cation was

then changed a SZ frozen core (#66) the optimized geometry was linear. This suggests that a basis set without d functions or polarization functions can inhibit bending when a dispersion-corrected functional is used. Also, for this molecule, the results suggest that the d-orbital and polarization functions in the basis set are needed for a bent geometry.

Conclusions

These calculations do not completely resolve the long-standing questions around the unusual structures of the heavy group 2 decamethylmetallocenes, but they do contribute some points to the ongoing discussion, as the dispersion forces that have long been suspected to be important can now be modeled.

In the group 2 dihalides, a consensus has been reached that their bent geometries is the result of involvement of the (*n*-1)d-orbitals and polarization of the core electrons by the highly electronegative halides.[158] Also, when the potential energy surfaces have been calculated, there is a very small difference in energy between the bent and linear geometries. To some extent, these explanations can be extended to the group 2 molecules in this study. The d-orbitals have a high degree of overlap with those of the occupied valence shell. In addition, the core electrons for group 2 are more energetically accessible than are those in most other elements in the rest of the periodic table. The ligands used (cyclopentadienyl and substituted alkyls) are not as electronegative as the halides, however, and are unlikely to polarize the core as readily. They do have large interacting ligands that are affected by dispersion forces.

APPENDICES

Supplementary Material

SYNTHESIS OF IMIDAZOLIUM FUNCTIONALIZED SILANE-, SILOXANE-, AND SILSESQUIOXANE-BASED IONIC LIQUIDS

Introduction

Ionic liquids are salts that melt at temperatures of 100°C or less and have received interest from the green chemistry community as an alternative to organic solvents.[186] Ionic liquids are unique in that it is simple to tune their properties by substituting different cations or anions into the specific ionic liquid. They can be used as a medium for biphasal catalysis[187] or even to change the reaction pathway of a catalyst or reaction.[188] Methylimidazole is one of the common cations used in ionic liquids. It is often used because a cation is formed when a carbon chain is added to the nitrogen, and the selection of the carbon chain will alter the properties of the ionic liquid. Recently there has been interest in incorporating ionic liquids onto silicon surfaces.[189] Silsesquioxanes are molecular mimics of silicon surfaces that allow the reactions to be done on a molecular level rather than on a bulky surface. These are used to take advantage of the tunability of ionic liquids and retain the catalytic ability of a silicon surface in a liquid form.

Experimental

General considerations and instrumentation

All chemicals were used as bought from Gelest, Alfa Aesar, Strem, and Fisher. NMR spectra were obtained for all compounds on Bruker 300 or 400 MHz spectrometers. Fluorescence measurements were taken on an ISS PCI spectrofluorometer and UV/Vis measurements were

taken on a Varian Cary 100 UV/Vis dual beam spectrophotometer in the Vanderbilt Chemistry Department Instrumental Lab. Mass spectrometry was performed by Andrzej Balinski on a Voyager DE-STR MALDI-TOF-MS.

Poly(silsesquioxanes)

(Chloropropyl)(Isobutyl)$_7$silsesquioxane (2)

Allyl substituted poly(isobutyl)silsesquioxane (**1**) (4. 017 g, 4.684 mmol) was added to a flask equipped with a gas inlet, septum, and stirbar. The flask was evacuated and filled with nitrogen before dry THF (20 mL) was added by cannulation. A catalytic amount of $TiCl_4$ (0.1 mL, 0.9 mmol) was injected into the flask before a slight excess of $LiAlH_4$ (3mL of 1M in diethyl ether) was carefully added. The mixture was allowed to react overnight. The mixture was then cooled to -78 °C for half an hour. After the mixture was cooled it was opened to air and $CuCl_2$ (1.268 g, 9.431 mmol) was added. It was allowed to react at -78 °C for an hour before warming to room temperature. The mixture was then diluted with ether (30 mL), washed with HCl twice and sodium bicarbonate, and then dried with magnesium sulfate before the solvent was removed under reduced pressure for near quantitative yield. This is a modified literature preparation.[190]

***N,N*(n-propyl substituted(isobutyl)silsesquioxane)methylimidazole chloride (3)**

All of the previous product (**2**) was dissolved in toluene with an excess of 1-methylimidazole and refluxed for a week. The solvent was then removed by reduced pressure for near quantitative yield. This is a modified literature preparation .[189]

Na[Eu(1-(2-Naphthoyl)-3,3,3-trifluoroacetone)$_4$]

1-(2-Naphthoyl)-3,3,3-trifluoroacetone (HNTA) (0.8719 g, 3.275 mmol) was dissolved in ethanol with NaOH (3.4 mL of 1.007 M) and allowed to deprotonate. Then $EuCl_3$ (0.2479 g, 0.9597 mmol) dissolved in 10 mL ethanol was added and the mixture was allowed to react overnight at 50 °C. The solvent was then removed at reduced pressure, and yielded a slightly yellow solid. This solid was washed with $CHCl_3$ for near quantitative yield. This was done according to the literature preparation .[189]

[*N*,*N*((n-propyl)$_1$(Isobutyl)$_7$silsesquioxane)methylimidazole] [Eu(1-(2-Naphthoyl)-3,3,3-trifluoroacetone)$_4$] (4)

The propylmethylimidazole substituted silsesquioxane (0.905 g, 0.927 mmol) (**3**) was dissolved in toluene. $Eu(NTA)_4$ (1.03 g, 0.853mmol) was dissolved in $CHCl_3$ and allowed to react at room temperature for 24 h. The liquid was filtered and then the solvent was removed under reduced pressure to yield a slightly yellow powder. This is a modified literature preparation. [189]

Hexasilsesquioxane

(Chloropropyl)$_6$hexasilsesquioxane

DMSO (4.0 mL, 54 mmol) was dissolved in 35 mL chloroform. This was slowly added to a solution of chloropropyltrichlorosilane (4.2 mL, 27 mmol) in 40 mL of chloroform. The mixture was stirred and allowed to react for 24 hours. The product was washed with water, dried with $MgSO_4$ and the solvent removed under reduced pressure.[191]

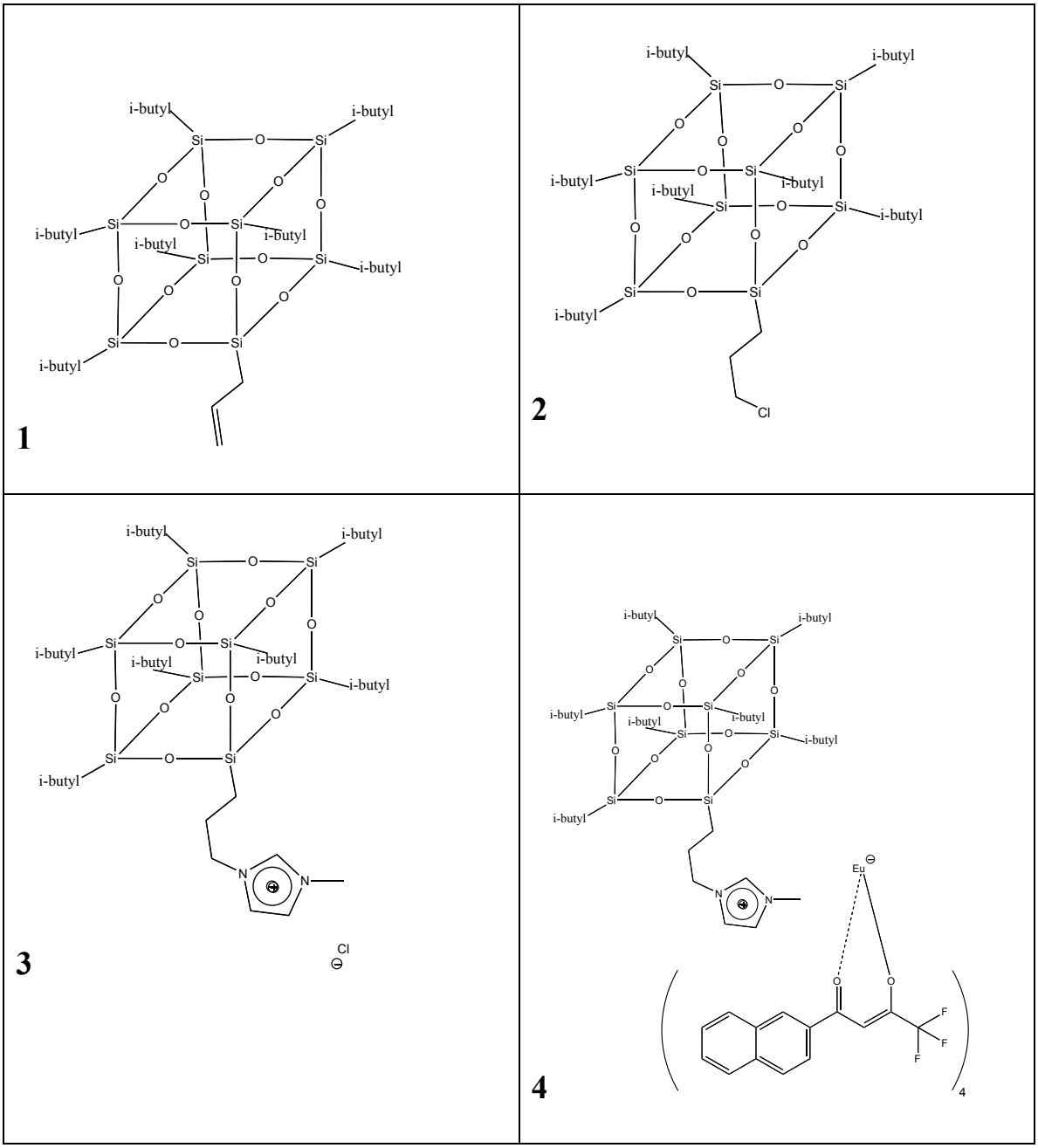

Figure 1. The Poly(silsesquioxanes): **1** Allyl substituted polyisobutylsilsesquioxane, **2**(Chloropropyl)(Isobutyl)$_7$-silsesquioxane, **3** *N,N*((n-propyl)$_1$(Isobutyl)$_7$silsesquioxane)methylimidazole chloride, **4** [*N,N*((n-propyl)$_1$(Isobutyl)$_7$silsesquioxane)methylimidazole] [Eu(1-(2-Naphthoyl)-3,3,3-trifluoroacetone)$_4$]

***N,N*((n-propyl)$_6$hexasilsesquioxane)methylimidazole chloride**

(Chloropropyl)$_6$hexasilsesquioxane (5.7 g, 9.0 mmol) was added to a roundbottom flask with 1-methylimidazole (4.3 mL, 54 mmol) and toluene and refluxed overnight. The solvent was then removed under reduced pressure.[189]

Silanes

***N,N*(n-propylmethyldimethoxysilane)methylimidazole chloride**

3-chloropropylmethyldimethoxysilane (3.92mL, 22.1mmol) was added to a roundbottom flask with 1-methylimidazole (1.79 mL, 22.6mmol) and toluene and refluxed overnight. The solvent was then removed under reduced pressure. The syntheses of the other five silanes were conducted in the same manner with the amounts below.[189]

Table 1. Reagents and amounts used in the substituted silane preparations

Silane	Amount Silane used	Amount methyl imidazole used
p-(chloromethyl)phenyltrimethyloxylsilane	4.5 mL, 21 mmol	1.55 mL, 19.5 mmol
3-chloropropyldimethylmethoxysilane	3.0 mL, 17 mmol	1.34 mL, 16.9 mmol
3-chloropropyltrimethoxysilane	3.0 mL, 16 mmol	1.35 mL, 17.0 mmol
chloromethyltrimethylsilane	3.5mL, 25 mmol	1.93 mL, 24.3mmol
3-chloropropyltrimethylsilane	3.4mL, 20 mmol	1.63 mL, 20.5 mmol

[*N,N*(silane)methylimidazole] [Ln(NTA)$_4$]

The selected methylimidazolsilane chloride was dissolved in 10 mL toluene. An equimolar amount of Na[Ln(NTA)$_4$] was dissolved in 10 mL $CHCl_3$ and allowed to react at room

temperature for 24 h. The liquid was filtered and then the solvent was removed under reduced pressure. Amounts are in Table 5 below.[189]

Table 2. Reagents and amounts used in the lanthanide NTA reactions

$[Ln(NTA)_4]^-$	Amount used	[*N,N*(silane)methylimidazole]Cl	Amount used
Sm	0.0887 g, 0.0732 mmol	p-(chloromethyl)phenyltrimethyloxylsilane	0.0186 g, 0.0566 mmol
Sm	0.0903 g, 0.0746 mmol	3-chloropropyltrimethoxysilane	0.0265 g, 0.0944 mmol
Sm	0.1060 g, 0.08752 mmol	Chloromethyltrimethylsilane	0.0184 g, 0.0899 mmol
Sm	0.0973 g, 0.0803 mmol	3-chloropropyldimethylmethoxysilane	0.0214 g, 0.0860 mmol
Sm	0.0905 g, 0.0747 mmol	3-chloropropylmethyldimethoxysilane	0.0208 g, 0.0791 mmol
Eu	0.0993 g, 0.0819 mmol	3-chloropropyltrimethylsilane	0.0199 g, 0.0855 mmol
Eu	0.0957 g, 0.0789 mmol	3-chloropropylmethyldimethoxysilane	0.0211 g, 0.0803 mmol
Yb	0.0842 g, 0.0682 mmol	3-chloropropyltrimethylsilane	0.0172 g, 0.0739 mmol
Yb	0.0955 g, 0.0774 mmol	3-chloropropylmethyldimethoxysilane	0.0205 g, 0.0780 mmol

Tetravinyltetramethylcyclotetrasiloxane

Tetravinyltetramethylcyclotetrasiloxane (3.0 mL, 14 mmol) was added to a flask equipped with a gas inlet, septum, and stirbar. The flask was evacuated and filled with nitrogen before dry THF (20 mL) was added by cannulation. A catalytic amount of $TiCl_4$ (0.1 mL, 0.9 mmol) was injected into the flask before a slight excess of $LiAlH_4$ (9.5 mL of 1M in diethylether) was carefully added. The mixture was allowed to react for 3 h. The mixture was then cooled to -78 °C for half an hour. After the mixture was cooled it was opened to air and $CuCl_2$ (10.8g, 80.1 mmol) was added. It was allowed to react at -78°C for an hour before warming to room temperature. The mixture was then diluted with ether (30 mL), washed with HCl twice and sodium

bicarbonate, and then dried with magnesium sulfate before the solvent was removed under reduced pressure for near quantitative yield. This is a modified literature preparation.[190]

Results

Silanes

Six different silanes were chosen as prototypes of cyclotetrasiloxane and poly(silsesquioxanes). They were allowed to react with 1-methylimidazole to produce viscous liquids (with the exception of the phenyl-substituted which was a solid) and NMR was used to confirm the additions. All of them were then allowed to react with Na[Sm(1-(2-naphthoyl)-3,3,3-trifluoroacetone)$_4$] (Na[Sm(NTA)$_4$]) and selected ones were allowed to react with Na[Eu(NTA)$_4$] and Na[Yb(NTA)$_4$]. Initial characterization with was conducted with UV/Vis and spectrofluorometry. Some of the compounds, such as [*N,N*(n-propylmethyl dimethoxysilane)-methylimidazole][Sm(NTA)$_4$] and [*N,N*(n-propyltrimethoxysilane) methylimidazole]-[Sm(NTA)$_4$], did not fluoresce at all, while [*N,N*(n-propyltrimethylsilane) methylimidazole]-[Sm(NTA)$_4$] and [*N,N*(n-propyltrimethylsilane)methylimidazole] [Eu(NTA)$_4$] had the sharp peaks characteristic of lanthanides. The spectrum for Na[Eu(NTA)$_4$] was also taken as a comparison, and was comparable in intensity to [*N,N*(n-propyltrimethylsilane)-methylimidazole][Eu(NTA)$_4$].

Cyclotetrasiloxane

The initial anti-Markonikov addition produced a green gel that could not be further purified. Methylimidazole was added to the green gel in an attempt to continue the synthesis but no further reaction occurred.

Poly(silsesquioxanes)

Initial attempts to synthesize and characterize the polysilsesquioxanes proved difficult, as the resonances of interest in their NMR spectra were small compared to the isobutyl peaks. After the addition of $Na[Eu(NTA)_4]$, a MALDI spectrum was taken to examine the connectivity[192]. Only peaks from the $Eu(NTA)_4^-$ anion were visible. MALDI analysis was run on the silsesquioxanes as received; they appeared to be impure as all the major peaks were above 912.57 m/z for a compound of 857.56 g/mol (See Table 3). Furthermore, the peaks appeared regularly as if it had polymerized. Enquiries were made to Gelest about the purity of the sample, which were not answered. A literature preparation[191] was then attempted to make the silsesquioxanes. After this the product was allowed to react with methylimidazole and produced a solid product that would not dissolve.

Table 3. Major peaks from MALDI-TOF-MS of allyl substituted Poly(Isobutylsilsesquioxane) (**1**)

Mass (m/z)	% intensity
609.89	15
912.57	100
945.15	17
1357.9	60
1802.87	20
2247.8	6
2692.17	3
3133.86	small

Discussion

The silanes reacted well with the methylimidazole. When they were allowed to react with the lanthanide containing anion, however, there were mixed results of quenching and florescence. None of the larger siloxane molecules were viable. The reactions either did not work or the

starting material was impure. Since it was the siloxanes and polysilsesquioxanes that were the silicon surface analogues, this project is being put aside for now.

Future Work

Due to the fact that the larger surface analogues did not work this project will be discontinued for the near future. One of the things that should still be done is to take more of the spectrofluorometer measurements to finish the possible combinations to determine if there are trends in which compounds fluoresce or extinguish. Other lanthanides that fluoresce within the detection limits of the instrument could also be used to examine these trends.

Since the poly(silsesquioxanes) that were commercially available were evidently impure, and the literature preparation used in the synthesis of them was not reproducible, another synthetic method would have to be developed to continue this project, along with another method to characterize these compounds.

REFERENCES

(1) Engerer, L. K.; Hanusa, T. P. *J.Org. Chem.* **2010**, *76*, 42.

(2) Engerer, L. K.; Carlson, C. N.; Hanusa, T. P.; Brennessel, W. W.; Young, V. G. *Organometallics* **2012**, *31*, 6131.

(3) Ma, J. C.; Dougherty, D. A. *Chem. Rev.* **1997**, *97*, 1303.

(4) Meyer, E. A.; Castellano, R. K.; Diederich, F. *Angew. Chem., Int. Ed.* **2003**, *42*, 1210.

(5) Kim, D.; Hu, S.; Tarakeshwar, P.; Kim, K. S.; Lisy, J. M. *J. Phys. Chem. A* **2003**, *107*, 1228.

(6) Bartoli, S.; Roelens, S. *J. Am. Chem. Soc.* **2002**, *124*, 8307.

(7) Sarri, P.; Venturi, F.; Cuda, F.; Roelens, S. *J. Org. Chem.* **2004**, *69*, 3654.

(8) Araki, K.; Shimizu, H.; Shinkai, S. *Chem. Lett.* **1993**, *2*, 205.

(9) Arduini, A.; Pochini, A.; Secchi, A. *Eur. J. Org. Chem.* **2000**, 2325.

(10) Matthews, S. E.; Schmitt, P.; Felix, V.; Drew, M. G. B.; Beer, P. D. *J. Am. Chem. Soc.* **2002**, *124*, 1341.

(11) Matthews, S. E.; Rees, N. H.; Felix, V.; Drew, M. G. B.; Beer, P. D. *Inorg. Chem.* **2003**, *42*, 729.

(12) Ferdani, R.; Barbour, L. J.; Gokel, G. W. *J. Supramol. Chem.* **2002**, *2*, 343.

(13) Choi, H. S.; Suh, S. B.; Cho, S. J.; Kim, K. S. *Proc. Nat. Acad. Sci. U.S.A.* **1998**, *95*, 12094.

(14) Clegg, W.; Dale, S. H.; Hevia, E.; Hogg, L. M.; Honeyman, G. W.; Mulvey, R. E.; O'Hara, C. T. *Angew. Chem., Int. Ed.* **2006**, *45*, 6548.

(15) Priyakumar, U. D.; Punnagai, M.; Krishna Mohan, G. P.; Sastry, G. N. *Tetrahedron* **2004**, *60*, 3037.

(16) Dinadayalane, T. C.; Hassan, A.; Leszczynski, J. *J. Mol. Struct.* **2010**, *976*, 320.

(17) Vijay, D.; Sastry, G. N. *Phys. Chem. Chem. Phys.* **2008**, *10*, 582.

(18) Dougherty, D. A. *Science (Washington, D. C.)* **1996**, *271*, 163.

(19) Nakamura, R. L.; Anderson, J. A.; Gaber, R. F. *J. Biol. Chem.* **1997**, *272*, 1011.

(20) Dougherty, D. A.; Lester, H. A. *Angew. Chem., Int. Ed.* **1998**, *37*, 2329.

(21) De Wall, S. L.; Meadows, E. S.; Barbour, L. J.; Gokel, G. W. *Proc. Nat. Acad. Sci., U.S.A.* **2000**, *97*, 6271.

(22) Amicangelo, J. C.; Armentrout, P. B. *J. Phys. Chem. A* **2000**, *104*, 11420.

(23) Sunner, J.; Nishizawa, K.; Kebarle, P. *J. Phys. Chem.* **1981**, *85*, 1814.

(24) Macias, A. T.; Norton, J. E.; Evanseck, J. D. *J. Am. Chem. Soc.* **2003**, *125*, 2351.

(25) Feller, D. *Chem. Phys. Lett.* **2000**, *322*, 543.

(26) Choi, H. S.; Kim, D.; Tarakeshwar, P.; Suh, S. B.; Kim, K. S. *J. Org. Chem.* **2002**, *67*, 1848.

(27) Gokel, G. W.; De Wall, S. L.; Meadows, E. S. *Eur. J. Org. Chem.* **2000**, 2967.

(28) Hu, J.; Barbour, L. J.; Gokel, G. W. *Chem. Commun.* **2001**, 1858.

(29) Hu, J.; Barbour, L. J.; Gokel, G. W. *J. Am. Chem. Soc.* **2001**, *123*, 9486.

(30) Chmely, S. C.; Carlson, C. N.; Hanusa, T. P.; Rheingold, A. L. *J. Am. Chem. Soc.* **2009**, *131*, 6344.

(31) Armentrout, P. B.; Rodgers, M. T. *J.Phys. Chem. A* **2000**, *104*, 2238.

(32) Amicangelo, J. C.; Armentrout, P. B. *Int. J. Mass Spec.* **2001**, *212*, 301.

(33) Gren, C. K.; Hanusa, T. P.; Rheingold, A. L. *Organometallics* **2007**, *26*, 1643.

(34) Cabarcos, O. M.; Weinheimer, C. J.; Lisy, J. M. *J. Chem. Phys.* **1999**, *110*, 8429.

(35) Te Velde, G.; Bickelhaupt, F. M.; Baerends, E. J.; Fonseca Guerra, C.; Van Gisbergen, S. J. A.; Snijders, J. G.; Ziegler, T. *J. Comput. Chem.* **2001**, *22*, 931.

(36) Guerra, C. F.; Snijders, J. G.; Te Velde, G.; Baerends, E. J. *Theor. Chem. Acc.* **1998**, *99*, 391.

(37) ADF2008.01; SCM; Theoretical Chemistry; Vrije Universiteit; Amsterdam; The Netherlands; (http://www.scm.com).

(38) Becke, A. D. *Phys. Rev. A* **1988**, *38*, 3098.

(39) Lee, C.; Yang, W.; Parr, R. G. *Phys. Rev. B* **1988**, *37*, 785.

(40) Miehlich, B.; Savin, A.; Stoll, H.; Preuss, H. *Chem. Phys. Lett.* **1989**, *157*, 200.

(41) Zheng, X.; Wang, X.; Yi, S.; Wang, N.; Peng, Y. *J. Comput. Chem.* **2010**, *31*, 1458.

(42) Yuan, X.-L.; Zhang, H.; Xie, F.-J. *THEOCHEM* **2009**, *900*, 103.

(43) Wang, Y.; Xu, Z.; Gao, Y.; Zhang, L.; Li, H. *J. Phys. Chem. A* **2009**, *113*, 7097.

(44) Zajac, M.; Hrobarik, P.; Magdolen, P.; Foltinova, P.; Zahradnik, P. *Tetrahedron* **2008**, *64*, 10605.

(45) Wu, R.; McMahon, T. B. *J. Am. Chem. Soc.* **2008**, *130*, 12554.

(46) Polfer, N. C.; Oomens, J.; Dunbar, R. C. *ChemPhysChem* **2008**, *9*, 579.

(47) Li, Q.; Li, W.; Cheng, J.; Gong, B.; Sun, J. *THEOCHEM* **2008**, *867*, 107.

(48) Jover, J.; Bosque, R.; Sales, J. *Dalton Trans.* **2008**, 6441.

(49) Hallowita, N.; Carl, D. R.; Armentrout, P. B.; Rodgers, M. T. *J. Phys. Chem. A* **2008**, *112*, 7996.

(50) Escudero, D.; Frontera, A.; Quinonero, D.; Deya, P. M. *Chem. Phys. Lett.* **2008**, *455*, 325.

(51) Morris, J. J.; Noll, B. C.; Honeyman, G. W.; O'Hara, C. T.; Kennedy, A. R.; Mulvey, R. E.; Henderson, K. W. *Chem.--Eur. J.* **2007**, *13*, 4418.

(52) Parkhots, O. P.; Ivashin, N. V. *Opt. Spectrosc.* **2006**, *101*, 215.

(53) Liu, F.; Qian, P.; Yan, S.; Bu, Y. *THEOCHEM* **2006**, *760*, 209.

(54) Cheng, J.; Zhu, W.; Tang, Y.; Xu, Y.; Li, Z.; Chen, K.; Jiang, H. *Chem. Phys. Lett.* **2006**, *422*, 455.

(55) Ruan, C.; Yang, Z.; Hallowita, N.; Rodgers, M. T. *J. Phys. Chem. A* **2005**, *109*, 11539.

(56) Reddy, A. S.; Sastry, G. N. *J. Phys. Chem. A* **2005**, *109*, 8893.

(57) Frontera, A.; Garau, C.; Quinonero, D.; Ballester, P.; Costa, A.; Deya, P. M. *Internet Electron. J. Mol. Des.* **2005**, *4*, 264.

(58) Sousa, S. F.; Fernandes, P. A.; Ramos, M. J. *J. Phys. Chem. A* **2007**, *111*, 10439.

(59) As an example, geometry optimization (ADF2009) of $[K(C_6H_6)]^+$ under D_{6h} symmetry with the TZ2P basis set on an 8-core 2.8 GHz machine required 38 s with the PBE

functional. Starting from the same geometry, optimization with the B3LYP functional required 56 m 32 s, i.e., slower by a factor of 89.

(60) Perdew, J. P.; Burke, K.; Ernzerhof, M. *Phys. Rev. Lett.* **1996**, *77*, 3865.

(61) Tao, J.; Perdew, J. P.; Staroverov, V. N.; Scuseria, G. E. *Phys. Rev. Lett.* **2003**, *91*, 146401.

(62) Staroverov, V. N.; Scuseria, G. E.; Tao, J.; Perdew, J. P. *J. Chem. Phys.* **2003**, *119*, 12129.

(63) Hoyau, S.; Norrman, K.; McMahon, T. B.; Ohanessian, G. *J. Am. Chem. Soc.* **1999**, *121*, 8864.

(64) Curutchet, C.; Bofill, J. M.; Hernández, B.; Orozco, M.; Luque, F. J. *J. Comp. Chem.* **2003**, *24*, 1263.

(65) Krossing, I.; Reisinger, A. *Angew. Chem. Int. Ed.* **2003**, *42*, 5725.

(66) Lau, J. K.-C.; Wong, C. H. S.; Ng, P. S.; Siu, F. M.; Ma, N. L.; Tsang, C. W. *Chem–Eur. J.* **2003**, *9*, 3383.

(67) Dunbar, R. C.; Petrie, S. *Astrophys. J.* **2002**, *564*, 792.

(68) Stanger, A. *J. Phys. Chem. A* **2008**, *112*, 12849.

(69) Soncini, A.; Havenith, R. W. A.; Fowler, P. W.; Jenneskens, L. W.; Steiner, E. *J. Org. Chem.* **2002**, *67*, 4753.

(70) A somewhat more sophisticated model involving the cosine of the theta angle was also explored, but it did not provide appreciably better correlation with the binding energy.

(71) Sauer, J.; Deininger, D. *J. Phys. Chem.* **1982**, *86*, 1327.

(72) Soteras, I.; Orozco, M.; Luque, F. J. *Phys. Chem. Chem. Phys.* **2008**, *10*, 2616.

(73) Hinchliffe, A.; Soscún M, H. J. *J. Mol. Struct.* **1993**, *300*, 1.

(74) Moszynski, R.; Wormer, P. E. S.; Jeziorski, B.; van der Avoird, A., *J. Chem. Phys.* **1995**, *103*, 8058.

(75) Hunter, C. A.; Low, C. M. R.; Rotger, C.; Vinter, J. G.; Zonta, C. *Proc. Natl. Acad. Sci. U.S.A.* **2002**, *99*, 4873.

(76) Amunugama, R.; Rodgers, M. T. *Int. J. Mass Spectrom.* **2003**, *227*, 339.

(77) Suresh, C. H.; Gadre, S. R. *J Phys Chem A* **2007**, *111*, 710.

(78) Marshall, M. S.; Steele, R. P.; Thanthiriwatte, K. S.; Sherrill, C. D. *The J. Phys. Chem. A* **2009**, *113*, 13628.

(79) Monillas, W. H.; Theopold, K. H.; Yap, G. P. A. *CSD Communication* **2007**, *CCDC 667985*.

(80) Daniele, S.; Drost, C.; Gehrhus, B.; Hawkins, S. M.; Hitchcock, P. B.; Lappert, M. F.; Merle, P. G.; Bott, S. G. *J. Chem. Soc., Dalton Trans.* **2001**, 3179.

(81) Evans, W. J.; Rego, D. B.; Ziller, J. W. *Inorg. Chem.* **2006**, *45*, 3437.

(82) Zuniga, M. F.; Deacon, G. B.; Ruhlandt-Senge, K. *Inorg. Chem.* **2008**, *47*, 4669.

(83) Khan, H. M.; Grauffel, C.; Broer, R.; MacKerell, A. D.; Havenith, R. W. A.; Reuter, N. *J. Chem. Theory Comput.* **2016**.

(84) Rapp, C.; Goldberger, E.; Tishbi, N.; Kirshenbaum, R. *Proteins* **2014**, *82*, 1494.

(85) Cassani, M. C.; Duncalf, D. J.; Lappert, M. F. *J. Am. Chem. Soc.* **1998**, *120*, 12958.

(86) Fässler, T. F.; Hoffmann, R.; Hoffmann, S.; Wörle, M. *Angew. Chem. Int. Ed.* **2000**, *39*, 2091.

(87) F.Dornhaus, M. B. *CSD Communication* **2012**, *CCDC 884771*.

(88) Fang, M.; Bates, J. E.; Lorenz, S. E.; Lee, D. S.; Rego, D. B.; Ziller, J. W.; Furche, F.; Evans, W. J. *Inorg. Chem.* **2011**, *50*, 1459.

(89) McNerney, B.; Whittlesey, B.; Krempner, C. *Eur. J. Inorg. Chem.* **2011**, *2011*, 1699.

(90) Camp, C.; Pécaut, J.; Mazzanti, M. *J. Am. Chem. Soc.* **2013**, *135*, 12101.

(91) Huang, Y.-L.; Lu, D.-Y.; Yu, H.-C.; Yu, J.-S. K.; Hsu, C.-W.; Kuo, T.-S.; Lee, G.-H.; Wang, Y.; Tsai, Y.-C. *Angew. Chem. Int. Ed.* **2012**, *51*, 7781.

(92) Hitchcock, P. B.; Lappert, M. F.; Protchenko, A. V. *J. Am. Chem. Soc.* **2001**, *123*, 189.

(93) Cubero, E.; Luque, F. J.; Orozco, M. *Proc. Nat. Acad. Sci.* **1998**, *95*, 5976.

(94) Meier, R. M.; Hanusa, T. P. In *PATAI'S Chemistry of Functional Groups*; John Wiley & Sons, Ltd: 2011, p 43.

(95) Layfield, R. A. *Chem. Soc. Rev.* **2008**, *37*, 1098.

(96) Haaland, A. *Inorg. Nucl. Chem. Lett.* **1979**, *15*, 267.

(97) Haaland, A.; Lusztyk, J.; Brunvoll, J.; Starowieyski, K. B. *J. Organomet. Chem.* **1975**, *85*, 279.

(98) Shannon, R. D. *Acta Crystallogr., Sect A* **1976**, *32*, 751.

(99) Crisp, J. A.; Meier, R. M.; Overby, J. S.; Hanusa, T. P.; Rheingold, A. L.; Brennessel, W. W. *Organometallics* **2010**, *29*, 2322.

(100) Gritzo, H.; Schaper, F.; Brintzinger, H. H. *Acta Crystallogr., Sect. E: Struct. Rep. Online* **2004**, *E60*, m1108.

(101) Ferguson, I. T. *Phys. Stat. Sol. (c)* **2007**, *4*, 389.

(102) Gupta, S.; Kang, H.; Kane, M. H.; Park, E.-H.; Ferguson, I. T. *Phys. Stat. Sol. (c)* **2008**, *5*, 1740.

(103) Qi, Y.; Musante, C.; Lau, K. M.; Smith, L.; Odedra, R.; Kanjolia, R. *J. Electron. Mater.* **2001**, *30*, 1382.

(104) Cheng, A. T.; Su, Y. K.; Lai, W. C. *Phys. Stat. Sol. (c)* **2008**, *5*, 1685.

(105) Solomon, S. A.; Muryn, C. A.; Layfield, R. A. *Chem. Commun.* **2008**, 3142.

(106) Walczak, K.; Friedrich, J.; Dolg, M. *Chem. Phys.* **2010**, *376*, 36.

(107) Chai, J.; Zhu, H.; Roesky, H. W.; Yang, Z.; Jancik, V.; Herbst-Irmer, R.; Schmidt, H.-G.; Noltemeyer, M. *Organometallics* **2004**, *23*, 5003.

(108) Layfield, R. A.; Humphrey, S. M. *Angew. Chem., Int. Ed.* **2004**, *43*, 3067.

(109) Layfield, R. A.; Buehl, M.; Rawson, J. M. *Organometallics* **2006**, *25*, 3570.

(110) Bond, A. D.; Layfield, R. A.; MacAllister, J. A.; McPartlin, M.; Rawson, J. M.; Wright, D. S. *Chem. Commun.* **2001**, 1956.

(111) Alvarez, C. S.; Bashall, A.; McInnes, E. J. L.; Layfield, R. A.; Mole, R. A.; McPartlin, M.; Rawson, J. M.; Wood, P. T.; Wright, D. S. *Chem—Eur. J.* **2006**, *12*, 3053.

(112) Gren, C. K.; Hanusa, T. P.; Rheingold, A. L. *Main Group Chem.* **2009**, *8*, 225.

(113) Kralik, M. S.; Stahl, L.; Arif, A. M.; Strouse, C. E.; Ernst, R. D. *Organometallics* **1992**, 3617.

(114) Elschenbroich, C. *Organometallics*; 3rd. ed.; VCH Publishers: Weinheim, 2006, p. 440.

(115) Jochmann, P.; Spaniol, T. P.; Chmely, S. C.; Hanusa, T. P.; Okuda, J. *Organometallics* **2011**, *30*, 5291.

(116) Layfield, R. A. In *PATAI'S Chemistry of Functional Groups*; John Wiley & Sons, Ltd: 2011, p 721.

(117) Williams, R. A.; Tesh, K. F.; Hanusa, T. P. *J. Am. Chem. Soc.* **1991**, *113*, 4843.

(118) Perrin, D. D.; Armarego, W. L. F. *Purification of Laboratory Chemicals*; 3rd ed.; Pergamon Press: New York, 1988.

(119) Fraenkel, G.; Chow, A.; Winchester, W. R. *J. Am. Chem. Soc.* **1990**, *112*, 1382.

(120) Carlson, C. N.; Hanusa, T. P.; Brennessel, W. W.; Young, J., V. G. *J. Organomet. Chem.* **2003**, *683*, 191.

(121) Evans, D. F. *J. Chem. Soc.* **1959**, 2003.

(122) Loeliger, J.; Scheffold, R. *J. Chem. Educ.* **1972**, *49*, 646.

(123) Grant, D. H. *J. Chem. Educ.* **1995**, *72*, 39.

(124) Sur, S. K. *J. Magn. Reson.* **1989**, *82*, 169.

(125) Lindoy, L. F.; Katovic, V.; Busch, D. H. *J. Chem. Educ.* **1972**, *49*, 117.

(126) A. Altomare, M. C. B., M. Camalli, G. Cascarano, C. Giacovazzo, A. Guagliardi, A. G. G. Moliterni, G. Polidori, R. Spagna *J. Appl. Cryst.* **1998**, *32*, 115.

(127) *SHELXTL*, 6.1; Bruker Analytical X-Ray Systems, Madison, WI.: 2000.

(128) ADF2012.01; SCM; Theoretical Chemistry; Vrije Universiteit; Amsterdam; The Netherlands; (http://www.scm.com).

(129) Grimme, S.; Antony, J.; Ehrlich, S.; Krieg, H. *J. Chem. Phys.* **2010**, *132*, 154104/1.

(130) Grimme, S.; Ehrlich, S.; Goerigk, L. *J. Comput. Chem.* **2011**, *32*, 1456.

(131) Almenningen, A.; Samdal, S.; Haaland, A. *J. Chem. Soc., Chem. Commun.* **1977**, 14.

(132) Almenningen, A.; Haaland, A.; Samdal, S. *J. Organomet. Chem.* **1978**, *149*, 219.

(133) Andersen, R. A.; Boncella, J. M.; Burns, C. J.; Blom, R.; Haaland, A.; Volden, H. V. *J. Organomet. Chem.* **1986**, *312*, C49.

(134) Andersen, R. A.; Blom, R.; Burns, C. J.; Volden, H. V. *J. Chem. Soc., Chem. Commun.* **1987**, 768.

(135) Wharton, L.; Berg, R. A.; Klemperer, W. *J. Chem. Phys.* **1963**, *39*, 2023.

(136) Wang, S. G.; Schwarz, W. H. E. *J. Chem. Phys.* **1998**, *109*, 7252.

(137) Gole, J. L.; Siu, A. K. Q.; Hayes, E. F. *J. Chem. Phys.* **1973**, *58*, 857.

(138) Rittner, E. S. *J. Chem. Phys.* **1951**, *19*, 1030.

(139) Guido, M.; Gigli, G. *J. Chem. Phys.* **1976**, *65*, 1397.

(140) Bytheway, I.; Gillespie, R. J.; Tang, T.-H.; Bader, R. F. W. *Inorg. Chem.* **1995**, *34*, 2407.

(141) Kaupp, M.; Schleyer, P. v. R.; Stoll, H.; Preuss, H. *J. Am. Chem. Soc.* **1991**, *113*, 6012.

(142) Koput, J.; Roszczak, A. *The J. of Phys. Chem. A* **2004**, *108*, 9267.

(143) Varga, Z.; Lanza, G.; Minichino, C.; Hargittai, M. *Chem.—Eur. J.* **2006**, *12*, 8345.

(144) Hollis, T. K.; Burdett, J. K.; Bosnich, B. *Organometallics* **1993**, *12*, 3385.

(145) Timofeeva, T. V.; Lii, J.-H.; Allinger, N. L. *J. Am. Chem. Soc.* **1995**, *117*, 7452.

(146) Eisenschitz, R.; London, F. *Z. Phys.* **1930**, *60*, 491.

(147) Klimeš, J.; Michaelides, A. *J. Chem. Phys.* **2012**, *137*, 120901.

(148) Dinadayalane, T. C.; Gorb, L.; Simeon, T.; Dodziuk, H. *Int. J. Quant. Chem.* **2007**, *107*, 2204.

(149) Kristyán, S.; Pulay, P. *Chem. Phys. Lett.* **1994**, *229*, 175.

(150) Cohen, A. J.; Mori-Sánchez, P.; Yang, W. *Chem. Rev.* **2012**, *112*, 289.

(151) Riley, K. E.; Pitoňák, M.; Jurečka, P.; Hobza, P. *Chem. Rev.* **2010**, *110*, 5023.

(152) Johnson, E. R.; Mackie, I. D.; DiLabio, G. A. *J. Phys. Org. Chem.* **2009**, *22*, 1127.

(153) van Santen, J. A.; DiLabio, G. A. *J. Phys. Chem. A* **2015**, *119*, 6703.

(154) Zhao, Y.; Truhlar, D. G. *Chem. Phys. Lett.* **2011**, *502*, 1.

(155) Zhao, Y.; Truhlar, D. G. *Acc. Chem. Res.* **2008**, *41*, 157.

(156) Grimme, S.; Antony, J.; Ehrlich, S.; Krieg, H. *J. Chem. Phys.* **2010**, *132*, 154104.

(157) Grimme, S. *WIREs Comput. Mol. Sci.* **2011**, *1*, 211.

(158) Iron, M. A.; Oren, M.; Martin, J. M. L. *Mol. Phys.* **2003**, *101*, 1345.

(159) Eaborn, C.; B. Hitchcock, P. *Chem. Commun.* **1997**, 1961.

(160) Dave, L. D.; Evans, D. F.; Wilkinson, G. *J. Chem. Soc. (Resumed)* **1959**, 3684.

(161) Harrison, P. G.; Zuckerman, J. J. *J. Am. Chem. Soc.* **1969**, *91*, 6885.

(162) Harrison, P. G.; Zuckerman, J. J. *J. Am. Chem. Soc.* **1970**, *92*, 2577.

(163) Cradock, S.; Duncan, W. *J. Chem. Soc., Faraday Trans. 2.* **1978**, *74*, 194.

(164) Baxter, S. G.; Cowley, A. H.; Lasch, J. G.; Lattman, M.; Sharum, W. P.; Stewart, C. A. *J. Am. Chem. Soc.* **1982**, *104*, 4064.

(165) Almlöf, J.; Fernholt, L.; Fægri, J. K.; Haaland, A.; Schilling, B. E. R.; Seip, R.; Taugbøl, K. *Acta Chem. Scand.* **1983**, *37a*, 131.

(166) Dory, T. S.; Zuckerman, J. J. *J. Organomet. Chem.* **1984**, *264*, 295.

(167) Armstrong, D. R.; Duer, M. J.; Davidson, M. G.; Moncrieff, D.; Russell, C. A.; Stourton, C.; Steiner, A.; Stalke, D.; Wright, D. S. *Organometallics* **1997**, *16*, 3340.

(168) Heeg, M. J.; Janiak, C.; Zuckerman, J. J. *J. Am. Chem. Soc.* **1984**, *106*, 4259.

(169) Jutzi, P.; Holtmann, U.; Kanne, D.; Krüger, C.; Blom, R.; Gleiter, R.; Hyla-Kryspin, I. *Chem. Ber.* **1989**, *122*, 1629.

(170) Sitzmann, H.; Boese, R.; Stellberg, P. *Z. Anorg. Allg. Chem.* **1996**, *622*, 751.

(171) Constantine, S. P.; Hitchcock, P. B.; Lawless, G. A. *Organometallics* **1996**, *15*, 3905.

(172) Constantine, S. P.; Hitchcock, P. B.; Lawless, G. A.; De Lima, G. M. *Chem. Commun.* **1996**, 1101.

(173) Burkey, D. J.; Hanusa, T. P.; Huffman, J. C. *Inorg. Chem.* **2000**, *39*, 153.

(174) Becke, A. D. *Phys. Rev. A* **1988**, *38*, 3098.

(175) Perdew, J. P. *Phys. Rev. B* **1986**, *33*, 8822.

(176) Austin, A.; Petersson, G. A.; Frisch, M. J.; Dobek, F. J.; Scalmani, G.; Throssell, K. *J. Chem.Theory Comp.* **2012**, *8*, 4989.

(177) Smith, J. D.; Hanusa, T. P. *Organometallics* **2001**, *20*, 3056.

(178) Williams, R. A.; Hanusa, T. P.; Huffman, J. C. *Organometallics* **1990**, *9*, 1128.

(179) Labouille, S.; Clavaguéra, C.; Nief, F. *Organometallics* **2013**, *32*, 1265.

(180) Raju, R. K.; Bengali, A. A.; Brothers, E. N. *Dalton Trans.* **2016**, *45*, 13766.

(181) Hughes, T. F.; Harvey, J. N.; Friesner, R. A. *Phys. Chem. Chem. Phys.* **2012**, *14*, 7724.

(182) Bader, R. F. W. *Atoms in Molecules - A Quantum Theory*; Oxford University Press: New York, 1994.

(183) Tassell, M. J.; Kaltsoyannis, N. *Dalton Trans.* **2010**, *39*, 6719.

(184) J. Bridgeman, A. *J. Chem. Soc., Dalton Trans.* **1997**, 2887.

(185) Bytheway, I.; Popelier, P. L. A.; Gillespie, R. J. *Can. J. Chem.* **1996**, *74*, 1059.

(186) Holbrey, J. D.; Seddon, K. R. *Clean Tech. Environ. Policy* **1999**, *1*, 223.

(187) Picquet, M.; Poinsot, D.; Stutzmann, S.; Tkatchenko, I.; Tommasi, I.; Wasserscheid, P.; Zimmermann, J. *ChemInform* **2004**, *35*.

(188) Daguenet, C.; Dyson, P. J. *Organometallics* **2006**, *25*, 5811.

(189) Bruno, S. M.; Ferreira, R. A. S.; Almeida Paz, F. A.; Carlos, L. D.; Pillinger, M.; Ribeiro-Claro, P.; Gonçalves, I. S. *Inorg. Chem.* **2009**, *48*, 4882.

(190) Sato, F. M., Yoshikuni; Sato, Masao *Chem. Lett.* **1978**, *7*, 833.

(191) Bassindale, A. R.; MacKinnon, I. A.; Maesano, M. G.; Taylor, P. G. *Chem. Commun.* **2003**, 1382.

(192) Anderson, S. E.; Mitchell, C.; Haddad, T. S.; Vij, A.; Schwab, J. J.; Bowers, M. T. *Chem. Mater.* **2006**, *18*, 1490.